COLLISION-INDUCED ADSORPTION OF THE FIRST OVERTONE BANDS OF H_2 AND D_2

MAHMOUD HASAN ABU-KHARMA

Collision-induced absorption of the first overtone bands of H_2 and D_2

by

©Mahmoud Hasan Abu-Kharma
B.Sc., M.Sc. The University of Jordan
M.Sc. Memorial University of Newfoundland

A thesis submitted to the School of Graduate
Studies in conformity with the requirements for the
Degree of Doctor of Philosophy

Department of Physics and Physical Oceanography
Memorial University of Newfoundland
1 July 2005

St. John's Newfoundland Canada

Your file Votre référence
ISBN: 978-0-494-15656-8
Our file Notre référence
ISBN: 978-0-494-15656-8

To everyone who has helped on this journey...

Abstract

Enhancement spectra of the collision-induced absorption (CIA) of H_2 in its first overtone region 7500 - 9500 cm^{-1} in binary mixtures H_2 - N_2 and H_2 - CO were studied at 298 K for base densities of H_2 in the range 89 - 145 amagat and for partial densities of N_2 and CO in the range 19 - 392 amagat. The observed spectra consist of the quadrupolar double transitions: $Q_2(J)$ (H_2) + $S_0(J)$, $O_0(J)$ and $Q_0(J)$ (N_2/CO), $O_2(J)$ (H_2) + $Q_0(J)$ (N_2/CO) and $S_2(J)$ (H_2) + $Q_0(J)$ (N_2/CO) with $J = 0$ to 4 for H_2 and $J = 1$ to 25 for N_2/CO. Enhancement absorption profiles of H_2-N_2 and H_2-CO were modelled by a total of 434 components of quadrupolar double transitions. The observed spectra agree with theoretical spectra and confirm that the isotropic overlap induction is absent in the 2 - 0 band of H_2 unlike in the CIA spectra of the fundamental band of H_2. The present analysis also confirms that there is no contribution from the electric dipole of CO to the induction mechanism in H_2 - CO mixtures.

CIA spectra in the first overtone region from 5250 to 7250 cm^{-1} of pure D_2 were studied at 77, 201 and 298 K. The observed spectra were modelled by a total of 92, 214 and 267 components of double vibrational transitions respectively. Enhancement spectra of the CIA in the first overtone region 5000 to 7000 cm^{-1} of D_2 in D_2 - N_2 were studied at 298 K for a base density of D_2 of 73 amagat and for partial densities of N_2 in the range 150 - 370 amagat. The observed spectra were modelled with a total of 1176 components of double vibrational transitions. Enhancement spectra of the CIA in the first overtone region 5500 to 6750 cm^{-1} of D_2 in the D_2-Ar, D_2-Kr and D_2-Xe binary mixtures were studied at room temperature for base densities of D_2 in the range 55 to 251 amagat and for partial densities of Ar, Kr and Xe in the range 46 to 384 amagat. The observed spectra consist of the following quadrupolar transitions: $O_2(3)$, $O_2(2)$, $Q_2(J)$, $J = 1$ to 5 and $S_2(J)$, $J = 0$ to 5 of D_2.

The observed spectra confirm that the isotropic overlap interaction does not contribute to the absorption of the first overtone band, unlike in the CIA spectra of the

fundamental band. The binary and ternary absorption coefficients were determined from the integrated absorption coefficients of the band. Profile analysis of the observed spectra was carried out using the Birnbaum-Cohen line shape function for each component of the band and the characteristic half-width parameters δ_1 and δ_2 for the transitions were determined.

Acknowledgements

In the name of Allah, the Beneficent, the Merciful. Praise and thanks be to Allah almighty for His help to complete this program successfully.

It is with great pleasure that I express my gratitude and thanks to my supervisor, Professor S. P. Reddy, for his guidance and assistance throughout all stages of the work presented in this thesis. I thank Drs. M. Clouter and G. Varghese for the helpful discussions during this work and the preperation of the thesis.

I am also grateful to the head, faculty and staff of the Physics and Physical Oceanography Department who helped me in different ways in acheive this goal. Many thanks are extended to my friends and colleagues in the department for their help in computer programming. Special thanks are also extended to Jason Mercer and Cliff Stamp who helped in solving computer problems during this work.

I also acknowledge all the services rendered by various members of the technical services group. I wish particularly to thank W. Holly, R. Guest and W. Kieley for their assistance in supplying liquid nitrogen and building some of special tools needed for the research.

Finally, I wish to express my sincere appreciation to my wife, daughters, sons, brothers here in St. John's and in Jordan and all the family members for their support, encouragement and patience. Without their support this work would not have progressed so well.

Financial support for this work was provided by Natural Sciences and Engineering Research Council of Canada (NSERC) research grant received by Professor S. Paddi Reddy, and also in the form of a graduate fellowship offered by Memorial University of Newfoundland.

Contents

List of Figures

List of Tables

Chapter 1

Introduction

Symmetric diatomic molecules such as H_2, D_2 and N_2 do not have transition electric-dipole moments in their ground electronic states and are therefore forbidden to absorb or emit dipole radiation. However, a transient electric dipole moment can be induced in a pair -or more- of colliding homonuclear molecules due to intermolecular interaction [1] and therefore they will be active in the infrared region. This phenomenon led to the formulation of the theory of collision induced absorption (CIA). CIA of the fundamental band of gaseous hydrogen was first identified by Welsh et al. [2] in 1949 soon after the discovery of this phenomenon in compressed O_2 and N_2 in the fundamental bands by the same authors [3]. Since 1949, the phenomenon of CIA has been extensively studied experimentally in many gases, mixtures of gases [2–15], solids [16–18] and liquids [17–21]. Along with the experimental results, theoretical aspects of CIA were given by van Kranendonk [22–27], Poll and Hunt [28], Poll [29], Birnbaum and Cohen [30], Birnbaum et al. [31], Lewis [32], Frommhold [33] and Tabisz and Neuman [34].

Welsh [1] has reviewed the experimental work done until 1971 on the translational, rotational and vibrational CIA spectra of H_2. The induced vibrational spectra of the

isotopomers H_2, D_2 and HD have been reviewed in detail by Reddy in 1985 [35]. More comprehensive reviews were also done by other authors such as Frommhold in 1993 [33]. For reviews of the theory of CIA the reader is referred to van Kranendonk [27], Lewis [32], Frommhold [33], Tabisz and Neuman [34] and references therein.

This thesis will begin with an introducting survey of the previous studies of H_2 and D_2 in this chapter, then chapter two will discuss the experimental setup, isothermal data and the method used to calculate the gas density in amagat, spectral calibration. procedure and data acquisition. Chapter three presents the theoretical background needed for this research. Chapters four to seven describe the different experiments performed and the results obtained. Finally chapter eight summarizes the conclusions of this work. The constants used in this study are listed in appendices A.1 and A.2, along with part of the calculations needed in appendices B, C and D.

1.1 Collision-induced absorption applications in astrophysics

CIA has been used to determine the composition of many stellar bodies and to study the force of interaction between colliding molecules. The rotational-vibrational bands of the CIA spectra of pure gases and gaseous mixtures such as H_2, H_2-He and H_2-N_2 are of considerable interest in astrophysics, especially for spectral studies of planetary atmospheres [36–42]. CIA provides the thermal opacity of the giant planets. Also, CIA is expected to have played a major role in the formation of these planets by controlling the rate of cooling of the protoplanetary material and the resultant contraction to their present sizes. CIA from H_2 and N_2 in Titan's atmosphere may be

primarliy responsible for the warm surface and the increase of atmospheric temperature with depth. CIA is the major source of the infrared opacity of dense planetary atmospheres and cool stars. For more details about the role of CIA in planetary atmospheres, see Refs. [36, 41, 42] and the references therein. It is known that the H_2 molecule occupies a unique position in molecular physics because of its simplicity and suitability for both theoretical and experimental studies over a wide range of experimental conditions. Moreover, hydrogen is a major component of the outer planets and cool stars.

1.2 Collision-induced absorption of H_2

Researchers continue to study experimentally and theoretically the infrared spectra and the different bands of H_2 and its isotopomers in the pure gases and in H_2-foreign gas binary mixtures over a wide range of temperatures and pressures [36–47].

The CIA spectrum of H_2 in the first overtone band in the pure gas was observed in 1951 by Welsh et al. [6] who identified the spectrum as consisting of single vibrational transitions ($\Delta v = v' - v'' = 2 \leftarrow 0$) and double vibrational transitions wherein the transition $\Delta v = 1 \leftarrow 0$ occurs in each of the molecules in the pair. The first overtone band of H_2 has been further investigated under different experimental conditions by Welsh and co-workers [48–51]. The CIA spectra of the first overtone band of H_2 in H_2-Ar and H_2-N_2 in the temperature range 85 - 116 K have been investigated by McKellar and Welsh [49]. Silvaggio et al. [52], Reddy and his collaborators [14, 53–58] and McKellar [59] have been studying the fundamental, first and the second overtone bands of pure H_2 and H_2-foreign gases mixtures at different temperatures and pressures. McKellar and Clouter [21] studied the fundamental band of H_2 and

D_2 liquids in the regions 4000 to 5000 cm^{-1} and 2900 to 3600 cm^{-1}, respectively. Gustafsson et al. [45] reported the collision-induced absorption spectra of H_2-H_2 at temperatures of 297.5 K and 77.5 K in the frequency range 1900 to 2260 cm^{-1} at gas densities ranging from 51 to 610 amagat. McKellar [46, 47, 60] studied the infrared spectra of H_2-Ar, HD-Ar, D_2-Ar, CO_2-H_2, H_2-Kr and D_2-Kr. Enhancements of CIA spectra of the first overtone band of H_2 in binary mixtures H_2-Kr and H_2-Xe at room temperature have been studied in our laboratory by Prasad et al. [57] for base densities of H_2 in the range of 30 - 57 amagat and for partial densities of Kr and Xe in the range 50 - 250 amagat for each of Kr and Xe, and the binary, ternary and quarternary absorption coefficients of the band have been determined. The spectra were interpreted in terms of the quadrupolar induction mechanism. Also, Stamp et al. have investigated the first overtone CIA spectra of pure hydrogen at 77, 201 and 295 K [58].

1.3 Collision-induced absorption of D_2

The infrared spectrum of D_2 induced by intermolecular forces has been studied under a variety of experimental conditions and many of its properties have been determined. CIA of the fundamental band of gaseous deuterium was investigated at room temperature up to 250 atm by Reddy and Cho [8] and at a density of 11 amagat in the range 24 K to 77.3 K by Watanabe and Welsh [10, 61]. Soon after, the fundamental and the overtone bands of D_2 and the binary mixtures of D_2 were investigated under different experimental conditions by Reddy and co-workers [9, 11, 12, 15, 55]. In addition. the same band was studied in D_2-He, D_2-Ar and D_2-N_2 at pressures up to 1200 atm at room temperature by Pai et al. [9]. Russell et. al. [12] studied the fundamental

band of D_2 in D_2-He and D_2-Ne mixtures at 273 K, 195 K and 77 K at different densities. Recently Varghese et al. [62] studied the fundamental band of D_2 in D_2-N_2 and D_2-CO mixtures.

The CIA spectrum of D_2 in the pure gas, D_2-Ar and D_2-N_2 binary mixtures in the first overtone band was investigated at room temperature by Reddy and Kuo [11], who identified the spectrum of D_2-N_2 as consisting of single transition quadrupolar lines $Q_2(J)$ where $J = 1, 2$ and $S_2(J)$ where $J = 0$ to 4, and double vibrational transitions $Q_1(J)$ of D_2+$Q_1(J)$ of N_2 and $Q_1(J)$ of D_2+$S_1(J)$ of N_2. A special feature of the spectra was the absence of the isotropic overlap contribution. Enhancements of CIA spectra of the first overtone band of D_2 in binary mixtures D_2-N_2, D_2-Ar, D_2-Kr and D_2-Xe at room temperature have been studied in our laboratory by Abu-Kharma et al. [63] for base densities of D_2 in the range of 55 to 251 amagat and for partial densities of Ar, Kr and Xe in the range 46 to 384 amagat for each of N_2, Ar, Kr and Xe. Binary, ternary and quaternary absorption coefficients of the band have been determined. The spectra of D_2-N_2 mixtures were interpreted in terms of the quadrupolar induction mechanism, and the observed spectra are formed by transitions of the following types:

1. $Q_2(J)$ of D_2+$O_0(J)$, $Q_0(J)$ and $S_0(J)$ of N_2,

2. $O_2(J)$ of D_2+$Q_0(J)$ of N_2,

3. $S_2(J)$ of D_2+$Q_0(J)$ of N_2, and

4. $X_1(J)$ of D_2+$X_1(J)$ of N_2, where X is Q, O and S transition.

The spectra of D_2 mixed with rare gases are simpler and form only the following 13 components: $O_2(2)$, $O_2(3)$, $Q_2(J)$ (J = 1 to 5) and $S_2(J)$ (J = 0 to 5) of D_2.

1.4 The present study

In the present work the CIA spectra of the first overtone band of H_2 in the binary mixtures of H_2-N_2 and H_2-CO at room temperature were investigated for the first time. The first overtone band of pure D_2 at 77 K, 201 K and at 298 K was studied, and the first overtone band of D_2 in the binary mixtures of D_2-N_2, D_2-Ar, D_2-Kr and D_2-Xe at room temperature were also studied.

Chapter 2

Experimental setup

The infrared spectra of the collision-induced absorption of H_2 in H_2-N_2 and H_2-CO mixtures, pure D_2 and binary mixtures D_2-N_2, D_2-Ar, D_2-Kr and D_2-Xe in the first overtone region were studied for total gas pressures up to 850 atm at room temperature. The experimental setup consisted of a 2 m transmission-type absorption cell, a high-pressure gas handling system, an infrared spectrometer and a microprocessor-controlled stepping motor. In the present chapter, a brief description of the apparatus, the experimental setup and the procedure will be presented.

2.1 The absorption cell

A two meter transmission-type absorption cell constructed of stainless steel was used to contain the experimental gases. It was designed for experiments at room temperature and at lower temperatures down to 77 K and at high pressures [55].

Several factors were taken into consideration in the design of the absorption cell. Firstly, high transmission was achieved by using a polished stainless steel light guide with an aperture 1.0 cm×0.5 cm, which reduces the quantity of the gas needed. The cell withstood high pressures, up to 2.0×10^4 psi. Secondly, sapphire windows (2.54

cm in diameter and 1 cm thick) were used to transmit IR radiation and to withstand the high pressure inside the cell. Thirdly, frost on the windows at low temperatures was prevented by providing each window with a vacuum housing heated electrically. Fourthly, the stainless steel bellows B_i ($i = 1$ to 2) were provided at each end of the cell to prevent the cracking of the cell due to the thermal contraction while cooling. Finally, the cell was insulated by evacuating chamber I around it; this also decreased the amount of coolant used in chamber II, see Fig. 2.1.

A cross section of the cell is shown schematically in Fig. 2.1 and the construction details were described by Gillard [55]. The cell mainly consists of the cell body B, a two meter long stainless steel tube 7.63 cm in diameter with a central bore of 2.54 cm. A polished stainless steel light guide L constructed in five sections with an outer diameter 2.54 cm was inserted inside the central bore. Both the entrance and the exit windows W_1 are synthetic sapphire discs 1.0 cm thick and 2.54 cm in diameter. Both of them were cemented to stainless steel window seats S with aperture 1.02 cm$\times$0.51 cm. Frosting of cell windows at temperature below room temperatures was prevented by providing each end of the cell with a vacuum housing 10 cm long and 10.5 cm in diameter.

2.2 Gas handling system

The gas-handling system used in the present investigation is shown schematically in Fig. 2.2. C_i ($i = 1$ to 3) are thermal compressors made from stainless steel with different capacities, thus allowing higher pressures to be attained. These compressors withstood more than 1.5×10^4 psi. The compressors are used to increase the density of the gas in the cell to the required value in each step of the experiment. In order to

do so, the compressor C_1 and the coil trap L_1 were immersed in liquid nitrogen, while both of them were connected to the gas cylinder. The trap was used to eliminate traces of water vapour, carbon dioxide, or other impurities. Then, the cylinder valve and the valve between the trap and the compressor were closed, the compressor was allowed to warm up, and the gas was allowed into the cell. If more pressure was needed, two compressors were immersed in liquid nitrogen at the same time, the gas cylinder was opened to both of them, after closing the valve of the gas cylinder, one of them is warmed to room temperature while the second compressor is still in liquid nitrogen, after closing the valve between the two compressors, the last compressor was allowed to warm up, so the gas pressure was increased more than in the previous stage, to achieve higher pressure, the last step was repeated several times until the desired pressure was reached. The Aminco stainless steel fittings and capillary tubes were used to transfer the gas into the cell. These connections withstood pressures up to 6×10^4 psi, while the gas valves were suitable up to 3×10^4 psi. The pressure was measured with Ashcroft-type Bourdon tube gauges (G), which were calibrated against mirror test gauges, which in turn were calibrated with a dead-weight pressure gauges. The ultra high purity grade hydrogen and research grade nitrogen and carbon monoxide used in the experiments were supplied by Matheson of Canada Ltd. .

2.3 Isothermal data of gases

In the present experiments the density of H_2 and D_2 in amagat[1] was obtained directly using the pressure-density calibration curves, Fig. 2.3 [64, 65]. The density of a gas expressed in amagat is directly related to the number density (i.e. the number of

[1]amagat is the ratio of the density at a given temperature and pressure to its density at standard temperature and pressure (S.T.P.)

molecules per unit volume). The partial densities of the component gases of a gas mixture (i.e. N_2, CO, Ar, Kr and Xe) were calculated by an interpolation method described by Reddy and Cho [8]. The base density ρ_a of H_2 or D_2 was obtained directly as mentioned before. The partial density, ρ_b, of the foreign gas was determined by using the iteration of the following equation

$$\rho_b = \frac{1}{1+\beta'}[(\rho_a)_p + \beta'(\rho_b)_p] - \rho_a, \tag{2.3.1}$$

where $\beta' = \rho'_b/\rho_a$ is the approximate ratio of densities, ρ'_b is the approximate density of the foreign gas which is obtained on the assumption that the partial pressures of the component gases of the mixture are additive. The quantities $(\rho_a)_p$ and $(\rho_b)_p$ are the densities of H_2 or D_2 and the foreign gas, respectively at the total pressure of the mixture. The density at total pressure of N_2 was taken from the isothermal data given in Refs. [66, 67] and for CO, Ar, Kr and Xe was taken from the isothermal data given in Refs. [68–71], respectively, see Figs. 2.4 and 2.5.

2.4 Removal of water vapour from the optical path

The atmospheric water vapour absorbs radiation in the region 8700-8900 cm^{-1} which overlaps with the hydrogen spectra in the first overtone region 7500-9500 cm^{-1}, and in the region 5250-5450 cm^{-1} which overlaps the higher wavelength wing of the first overtone band of deuterium 5500-7000 cm^{-1}. In order to remove the water vapour from the optical path of the radiation, the source and the spectrometer were housed in an airtight Plexiglas box as shown in Fig. 2.6. Dry nitrogen evaporating from a 200 litre container of liquid nitrogen was flushed through the housing reducing the intensity of water vapour absorption to an acceptable and stable level during the experiment.

2.5 Spectral calibration

The hydrogen and deuterium spectra were recorded as intensities versus drum number of the spectrometer. To convert the drum numbers into wave numbers (cm^{-1}) a least squares fit to a suitable order polynomial was determined. The emission lines of mercury (Hg) [72] and absorption peaks of atmospheric water vapour [73, 74] in the region of hydrogen and deuterium first overtone band were measured as a function of the drum reading, and the wave number was plotted against the drum reading which forms the calibration curve.

2.6 The spectrometer and the optical system

The optical setup is shown in Fig. 2.6. The source of continuous infrared radiation is a General Electric FFJ. 600 W Quartzline projection lamp S enclosed in a water cooled brass jacket designed in our laboratory. The power for the lamp S was supplied by a Variac (W10MT3A Autotransformer supplied by General Radio USA). The output voltage of the Variac was stabilized by Sorensen Power Supply (AC Regulator ACR1000) which was adjusted at 90 volts and 4.1 amps to bring the signal to the required intensity. A concave M_1 mirror was used to focus the radiation at the cell window; M_2 also is a concave mirror used to focus the radiation at the entrance slit of the spectrometer. The radiation enters a Perkin-Elmer Model 112 double-pass prism spectrometer. The light beam is dispersed by an LiF prism, reflected back by a Littrow mirror to complete the first pass through the prism and brought to a focus. This light is chopped by a tuning fork chopper at 260 Hz and sent back through the prism for a second pass. The rotation of the Littrow mirror allows different frequencies of the second pass radiation to fall on the internal or the external uncooled PbS

detector. The rotation of the prism was controlled by the stepper driver built in the Memorial University Electrical workshop, with steps of 10 cm^{-1}. The slit width was choosen according to the different experiments, for example in the H_2-N_2 and H_2-CO experiments the slit width was maintained at 60 μm, which gave a spectral resolution of 26 cm^{-1} at the origin of the first overtone band of H_2 (8087 cm^{-1}).

2.7 Signal detection

The PbS detector is a photoconductive device whose resistance varies with the incident light intensity upon its surface. The output voltage (signal) from the detector is proportional to the light intensity when it is supplied with a constant current. This signal is sent to a lock-in amplifier, SR510, supplied by Stanford Research System with a built-in preamplifier. The output signal is passed to a Dekavider, DV412, supplied by Electro-Measurement Inc. for attenuation. The attenuated signal was sent to a microprocessor-controlled analog-to-digital converter (ADC). The transmitted data from the ADC are stored and analyzed by the computer. For additional information the reader is refered to Ref. [75].

2.8 Procedure

After checking the chopper, the stepper driver and the detector, the transmitted intensity through an empty cell was recorded as a function of the drum number using a Hg source. The known wavenumbers of the water vapour peaks and the emission lines of Hg were compared with the drum number, and subsequantly used to calibrate the experimental profiles. The source cooling system and the stability of the transmitted intensity of the IR source were then checked. The transmitted intensity

from an empty cell was recorded against the drum number. The flushing with dry nitrogen causes the water vapour absorption to decrease. When the level of water vapour absorption has reached a minimum and was stable, a number of traces were recorded. This step was repeated once with the cell filled with the base gas (i.e. H_2 or D_2), and a second time with the cell filled with the mixture (i.e. the base gas + the foreign gas). The number of traces needed to be averaged depends on the noise of the signal. The average of the traces was determined in each case.

To study a pure gas spectrum, the profiles of the base gas is reduced from the profiles of the empty cell, then it is calibrated in the desired region of study. But in the case of a mixture, the profiles of the mixture were reduced from the profiles of the base gas. An example of this process is given in Fig. 2.7.

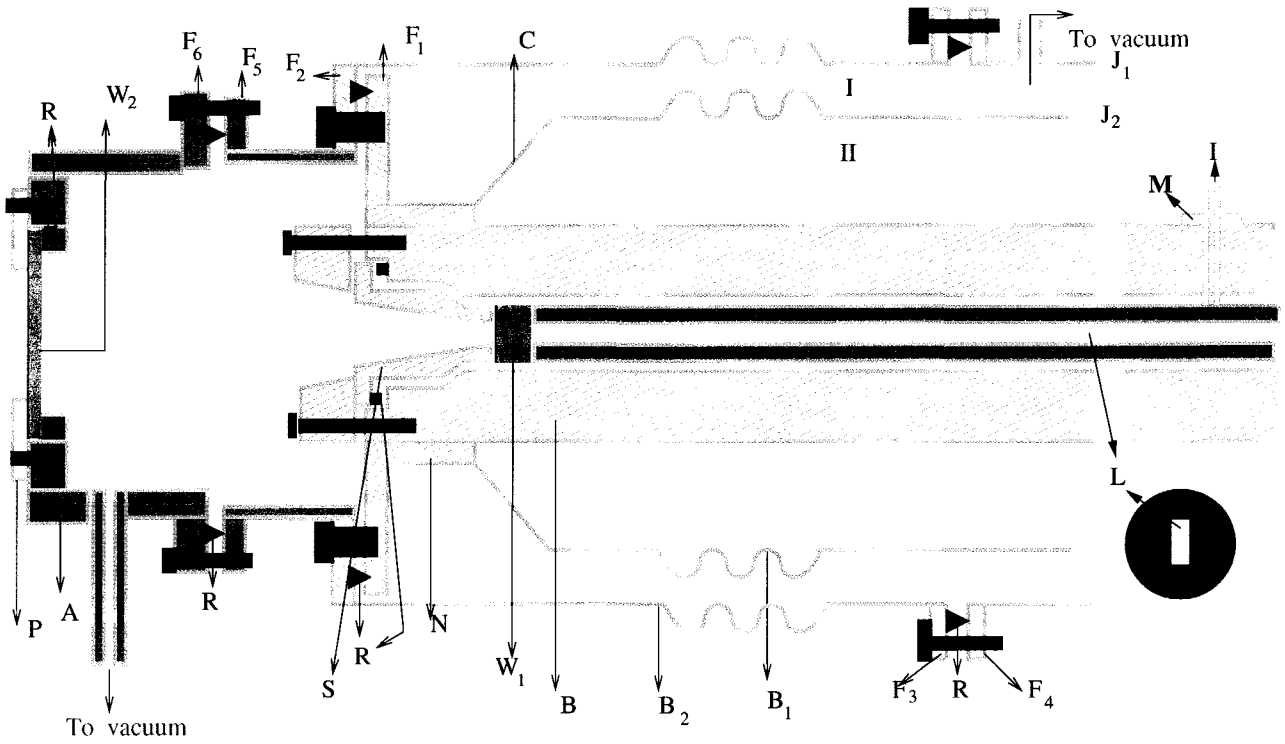

Figure 2.1: A cross sectional view of one end of the absorption cell. B: the cell body, L: polished light guide, W_i: sapphire window, R: O rings, I: a gas inlet of a stainless steel capillary tube, M: Aminco fitting, F: flange, B_i: Bellows, I (J_1) and II (J_2) chambers, where J_1 is a vacuum jacket.

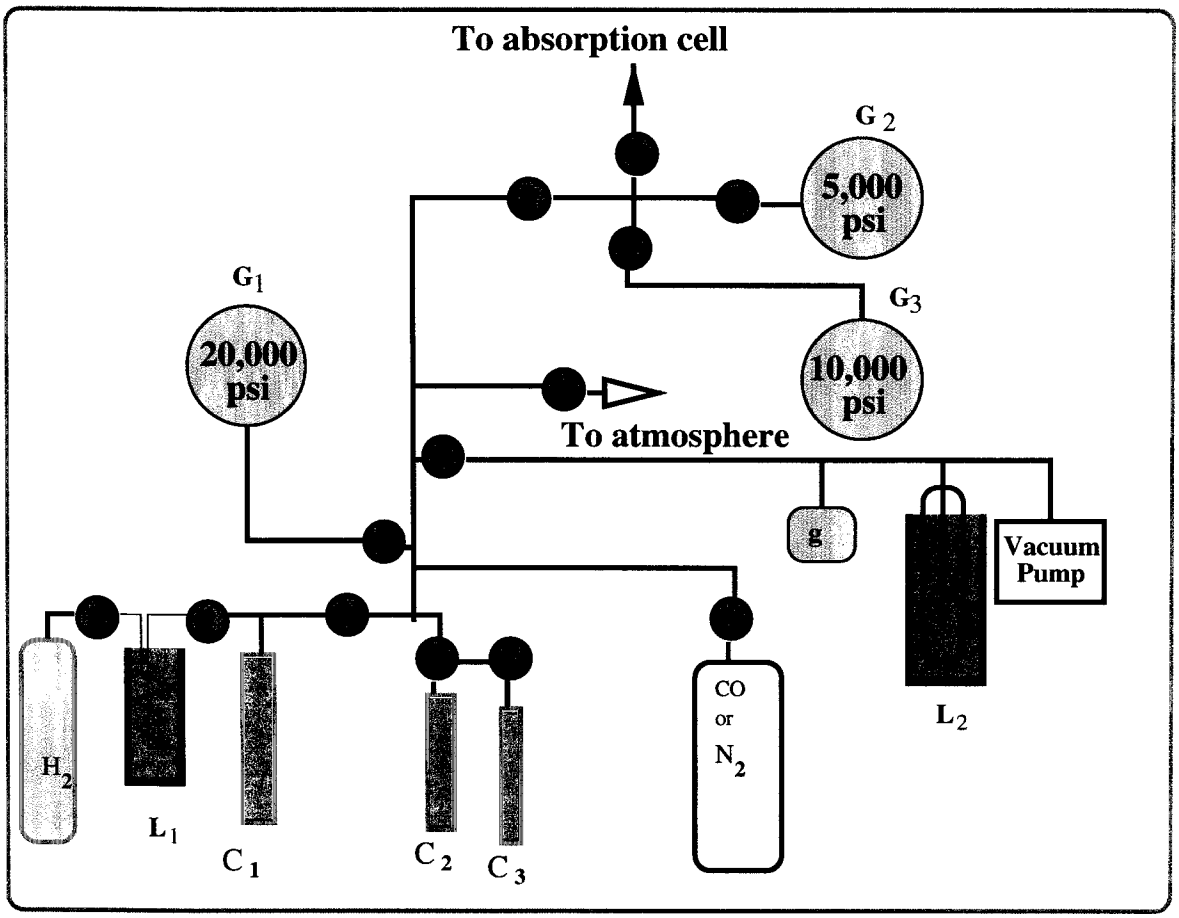

Figure 2.2: The gas handling system, where C_i represents thermal compressors, G's are the Ashcroft-type Bourdon tube gauges, g is the vacuum gauge, L's are the liquid nitrogen traps and the circles are gas valves.

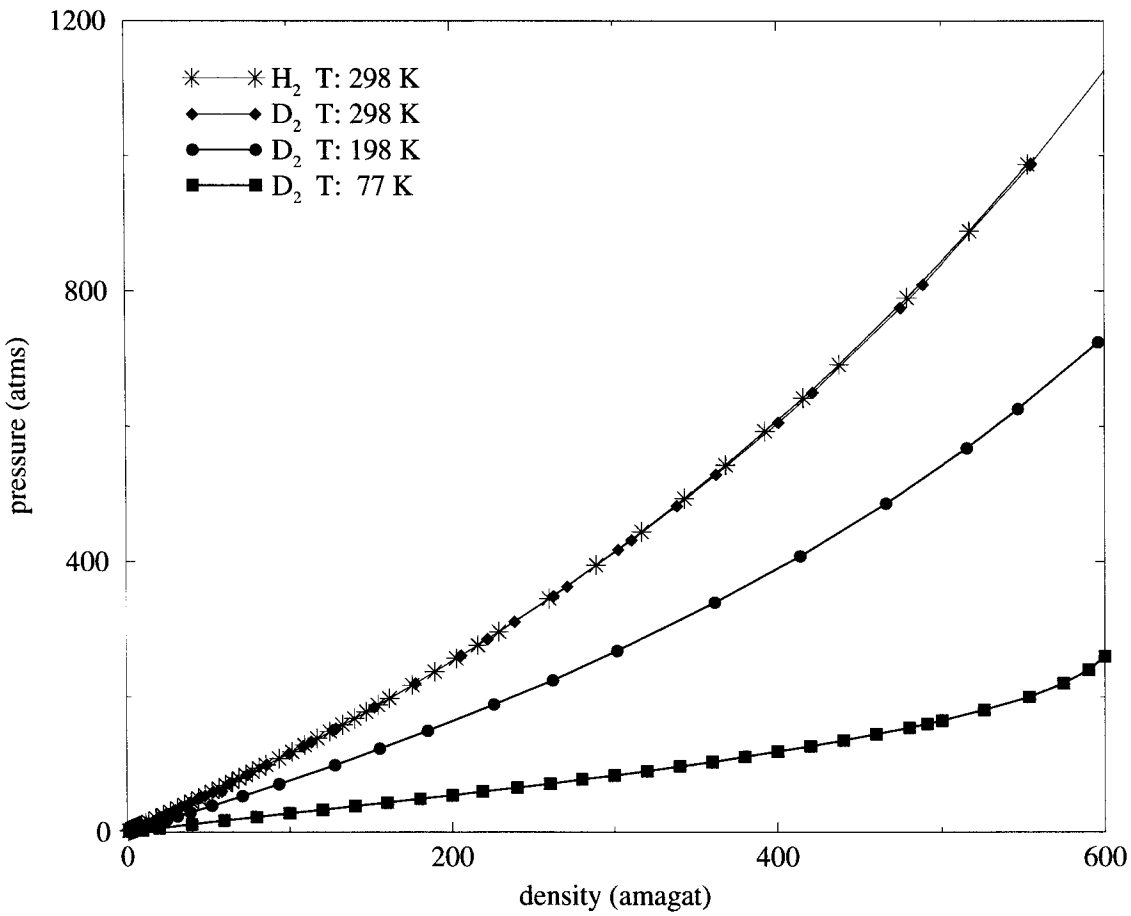

Figure 2.3: The pressure-density calibration curves of H_2 at 298 K and D_2 at 77, 198 and 298 K.

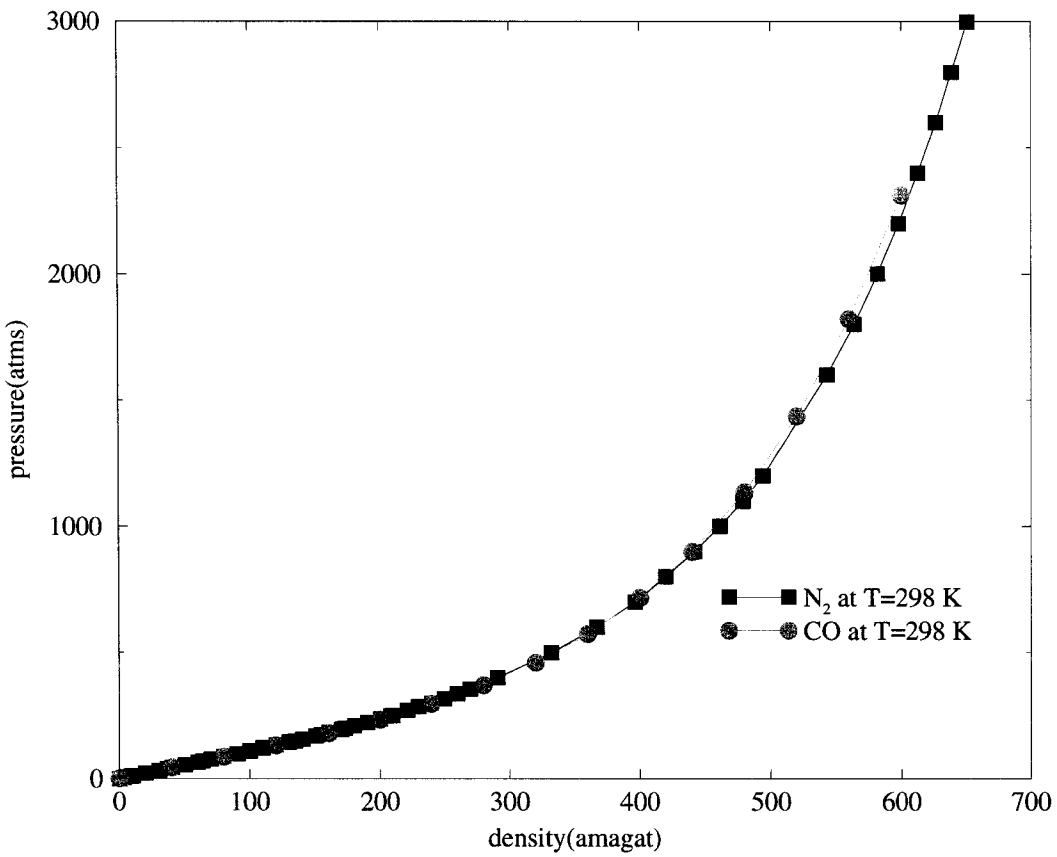

Figure 2.4: The density-pressure calibration curves of N_2 and CO at 298 K.

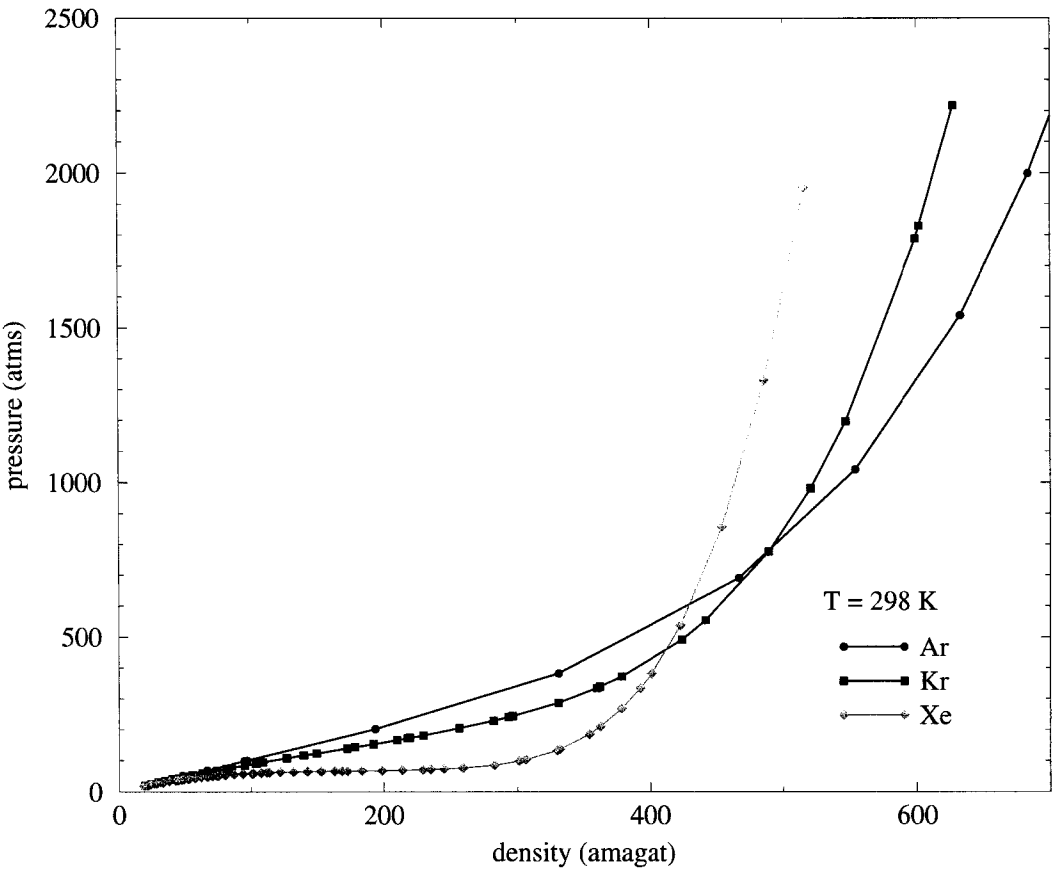

Figure 2.5: The pressure-density calibration curves of Ar, Kr and Xe at 298 K.

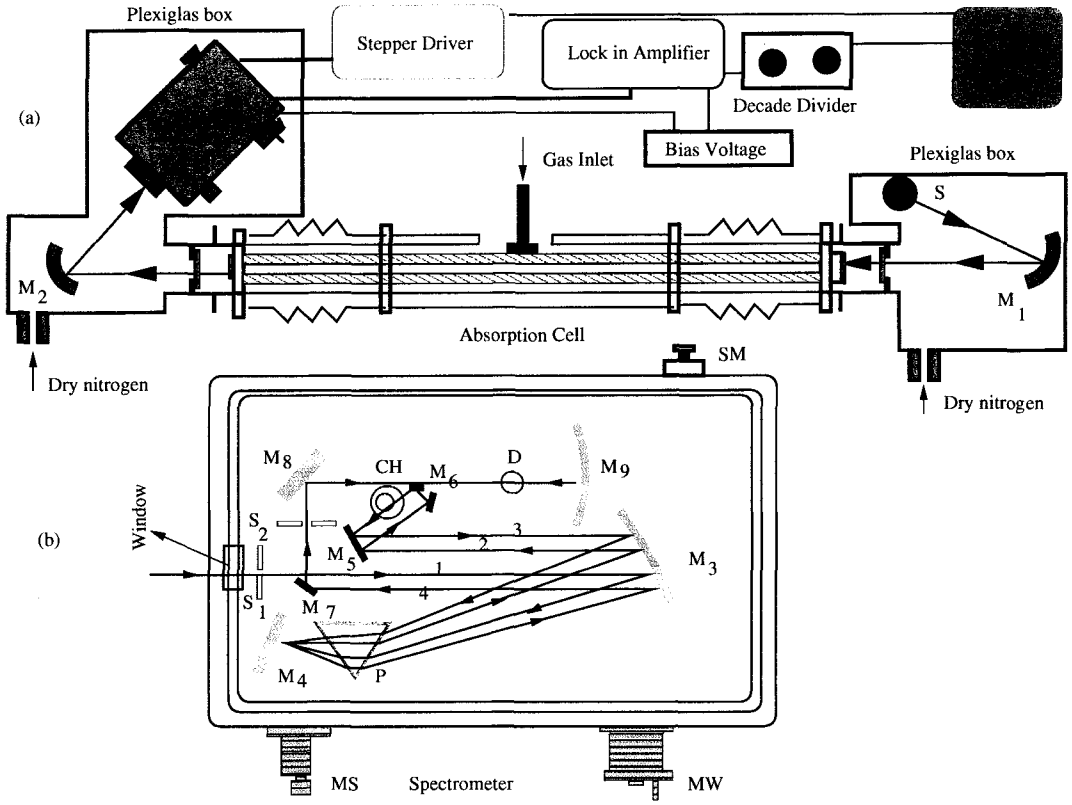

Figure 2.6: (a) A schematic diagram of the experimental setup. S: source of radiation, M_1 and M_2:spherical mirrors. (b) Path of the monochromatic radiation inside the spectrometer, S_1 and S_2: slits, M_3 and M_9: parabolic mirror, M_4: Littrow mirror, P: prism, M_5, M_6, M_7 and M_8: plane mirrors, CH: tuning fork chopper, D: PbS detector, SM: stepping motor.

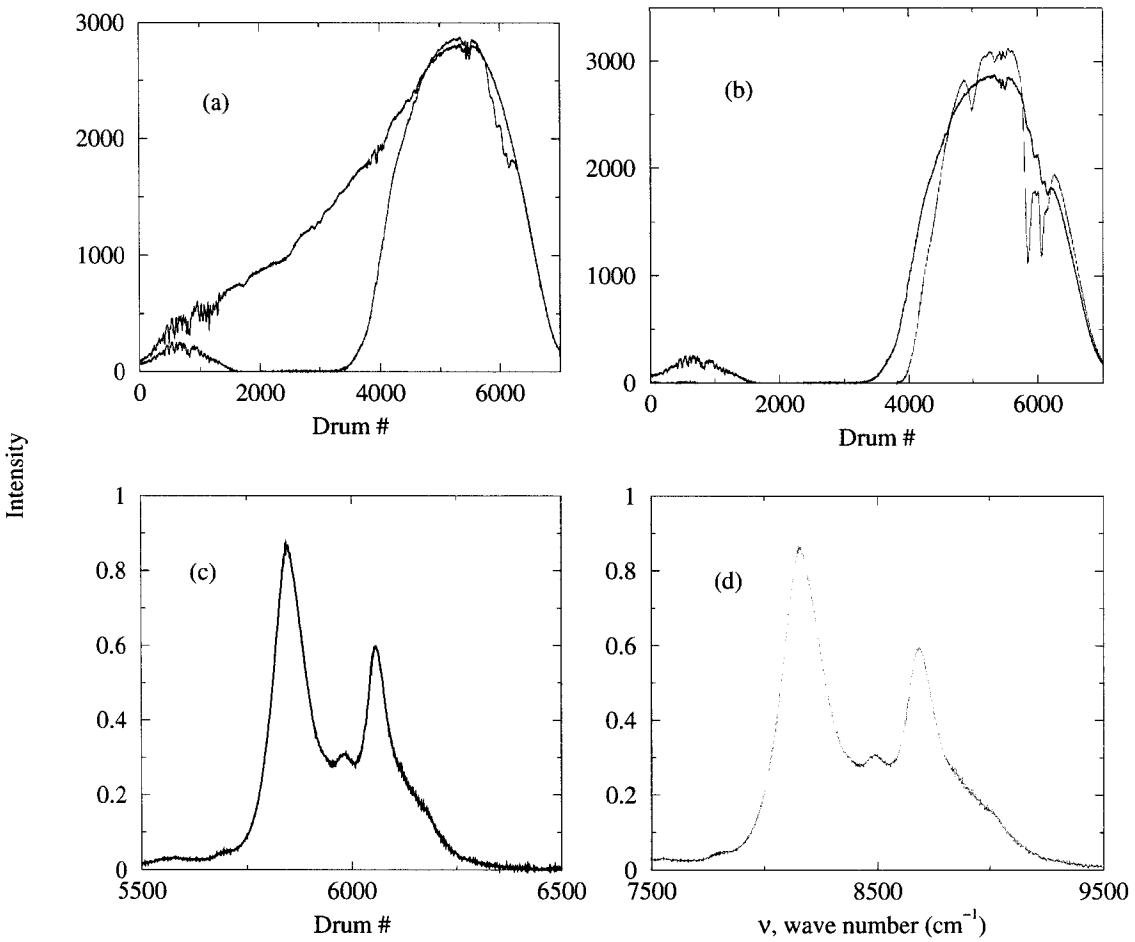

Figure 2.7: (a)- shows two traces: the black curve represents the average of the intensity versus the drum number of the spectrometer for the empty cell, while the red curve represents the base gas in this example H_2; (b)- shows two traces, the black curve represents intensity versus the drum number for the base gas H_2 while the blue curve represents the mixture of H_2 and N_2; (c)- represents the reduced trace of the traces in b; (d)- the experimental profile.

Chapter 3

Theory

This chapter describes the theory used in the analysis in the present investigation. First, a theoretical description of the energy levels in the fundamental and the first overtone bands of H_2, D_2, N_2 and CO is given. Then, the transition intensity corresponding to each possible transition is determined. After that, a brief description of the theory of collision-induced absorption is provided. Finally, the theory of the line shape function and the non-linear fitting of the experimental data is presented.

3.1 Vibrational and rotational energy of levels

The energy of the vibrational levels and the band centers in the ground electronic state $^1\Sigma_g^+$ were calculated using the vibrational term

$$G_0(v) = \omega_e(v+1) - \omega_e x_e(v+1)^2 + \omega_e y_e(v+1)^3 + \omega_e z_e(v+1)^4, \qquad (3.1.1)$$

where v is the vibrational quantum number, ω_e is the vibrational frequency, $\omega_e x_e$, $\omega_e y_e$ and $\omega_e z_e$ are the anharmonicities and their values are given in Appendix A.1. The energy of the rotational levels in each vibrational state were calculated using the rotational term

$$F_v(J) = B_v J(J+1) - D_v J^2(J+1)^2 + H_v J^3(J+1)^3 + L_v J^4(J+1)^4 + \cdots, \quad (3.1.2)$$

where J is the rotational quantum number and B_v is a rotational constant of a molecule in level v which is given by

$$B_v = B_e - \alpha_e \left(v + \frac{1}{2}\right) + \gamma_e \left(v + \frac{1}{2}\right)^2 + \delta_e \left(v + \frac{1}{2}\right)^3 + \cdots, \tag{3.1.3}$$

where α_e, γ_e and δ_e are small constant terms that correct for the vibration-rotation interaction of a particular vibrational state ($\alpha_e \gg \gamma_e \gg \delta_e$). D_v and H_v are the stretching constants ($B_v \gg D_v \gg H_v \gg L_v$), and are represented by the following equations

$$D_v = D_e + \beta_e \left(v + \frac{1}{2}\right) + \epsilon_e \left(v + \frac{1}{2}\right)^2 + \kappa_e \left(v + \frac{1}{2}\right)^3 + \cdots, \tag{3.1.4}$$

where ($\beta_e \gg \epsilon_e \gg \kappa_e$) and

$$H_v = H_e - \eta_e \left(v + \frac{1}{2}\right) + \zeta_e \left(v + \frac{1}{2}\right)^2 + \xi_e \left(v + \frac{1}{2}\right)^3 + \cdots, \tag{3.1.5}$$

($\eta_e \gg \zeta_e \gg \xi_e$) where β_e, ϵ_e, δ_e, H_e, η_e, ζ_e are small correction terms. The vibrational and rotational energy levels of pure H_2, D_2, N_2 and CO in their ground electronic states were calculated using the molecular constants given by McKellar and Oka, and Huber and Herzberg [76, 77] and listed in Appendicies B.1, B.4 and B.5. While B.2 and B.3 give the possible transitions in the fundamental and the first overonebands and their transitions frequencies, respectively. The molecular constants are listed in Appendix A.2. The $O_1(J)$ ($\Delta J = J'$ - $J'' =$ - 2), $Q_1(J)(\Delta J = 0)$ and $S_1(J)(\Delta J = 2)$ transitions in the fundamental band were calculated using the following equation (where J' is the upper rotational state and J'' is the lower rotational state, the subscript 1 means the transition from the lower vibrational level $v'' = 0$ to the upper level $v' = 1$)

$$\nu_{O,Q,S} = \nu_{10} + F'_{v=1}(J') - F''_{v=0}(J''), \tag{3.1.6}$$

where $\nu_{10} = \mathrm{Q}_1(0)$ (in cm^{-1}) is the fundamental band center. The transitions $\mathrm{O}_1(0)$, $\mathrm{Q}_1(J)$ and $\mathrm{S}_1(J)$ can be determined by solving equations 3.1.2 to 3.1.6, the transition $\mathrm{O}_1(J)$ is given by:

$$\begin{aligned}\nu_O &= \nu_{10} + 2(B_1 - 2D_1 + 4H_1) + J(-B_0 - 3B_1 + 12D_1 - 36H_1) \\ &\quad + J^2(-B_0 + B_1 + D_0 - 13D_1 + 66H_1) + J^3(2D_0 + 6D_1 - H_0 - 63H_1) \\ &\quad + J^4(D_0 - D_1 - 3H_0 + 33H_1) - 3J^5(H_0 + 3H_1) + J^6(-H_0 + H_1), \quad (3.1.7)\end{aligned}$$

the $\mathrm{Q}_1(J)$ is given by:

$$\begin{aligned}\nu_Q &= \nu_{10} + J(-B_0 + B_1) + J^2(-B_0 + B_1 + D_0 - D_1) \\ &\quad + J^3(2D_0 - 2D_1 - H_0 + H_1) + J^4(D_0 - D_1 - 3H_0 + 3H_1) \\ &\quad - 3J^5(H_0 - H_1) + J^6(-H_0 + H_1), \quad (3.1.8)\end{aligned}$$

and the $\mathrm{S}_1(J)$ is given by:

$$\begin{aligned}\nu_S &= \nu_{10} + 6(B_1 - 6D_1 + 36H_1) + J(-B_0 + 5B_1 - 60D_1 + 540H_1) \\ &\quad + J^2(-B_0 + B_1 + D_0 - 37D_1 + 558H_1) + J^3(2D_0 - 10D_1 - H_0 + 305H_1) \\ &\quad + J^4(D_0 - D_1 - 3H_0 + 93H_1) - 3J^5(H_0 - 5H_1) + J^6(-H_0 + H_1). \quad (3.1.9)\end{aligned}$$

The possible transitions $\mathrm{O}_1(J)$, $\mathrm{Q}_1(J)$ and $\mathrm{S}_1(J)$ for $J = 0$ to 5 in the fundamental bands of H_2 and D_2 were calculated using equations 3.1.7, 3.1.8 and 3.1.9 respectively: these values are listed in Appendix B.2. In the same manner the $\mathrm{O}_2(J)$, $\mathrm{Q}_2(J)$ and $\mathrm{S}_2(J)$ (where the subscript 2 = $\Delta\nu = \nu' - \nu''$) transitions in the first overtone band were determined using

$$\nu_{O,Q,S} = \nu_{20} + F'_{v=2}(J') - F''_{v=0}(J''), \quad (3.1.10)$$

where $\nu_{20} = Q_2(0)$ (in cm^{-1}) is the center of the first overtone band. The transition $O_2(J)$ is given by:

$$\begin{aligned}\nu_O &= \nu_{20} + 2(B_2 - 2D_2 + 4H_2) + J(-B_0 - 3B_2 + 12D_2 - 36H_2) \\ &\quad + J^2(-B_0 + B_2 + D_0 - 13D_2 + 66H_2) + J^3(2D_0 + 6D_2 - H_0 - 63H_2) \\ &\quad + J^4(D_0 - D_2 - 3H_0 + 33H_2) - 3J^5(H_0 + 3H_2) \\ &\quad + J^6(-H_0 + H_2), \end{aligned} \tag{3.1.11}$$

$Q_2(J)$ is given by:

$$\begin{aligned}\nu_Q &= \nu_{20} + J(-B_0 + B_2) + J^2(-B_0 + B_2 + D_0 - D_2) \\ &\quad + J^3(2D_0 - 2D_2 - H_0 + H_2) + J^4(D_0 - D_2 - 3H_0 + 3H_2) \\ &\quad - 3J^5(H_0 - H_2) + J^6(-H_0 + H_2), \end{aligned} \tag{3.1.12}$$

and $S_2(J)$ is given by:

$$\begin{aligned}\nu_S &= \nu_{20} + 6(B_2 - 6D_2 + 36H_2) + J(-B_0 + 5B_2 - 60D_2 + 540H_2) \\ &\quad + J^2(-B_0 + B_2 + D_0 - 37D_2 + 558H_2) + J^3(2D_0 - 10D_2 - H_0 + 305H_2) \\ &\quad + J^4(D_0 - D_2 - 3H_0 + 93H_2) - 3J^5(H_0 - 5H_2) + J^6(-H_0 + H_2). \end{aligned} \tag{3.1.13}$$

The possible transitions $O_2(J)$, $Q_2(J)$ and $S_2(J)$ in the first overtone bands of H_2 and D_2 were calculated using equations 3.1.11, 3.1.12 and 3.1.13 respectively, and are listed in Appendix B.3.

3.2 Induced dipole moments

Symmetric diatomic molecules such as H_2, D_2 and N_2 have no permanent electric-dipole moments in their ground electronic states becuase of their charge symmetry.

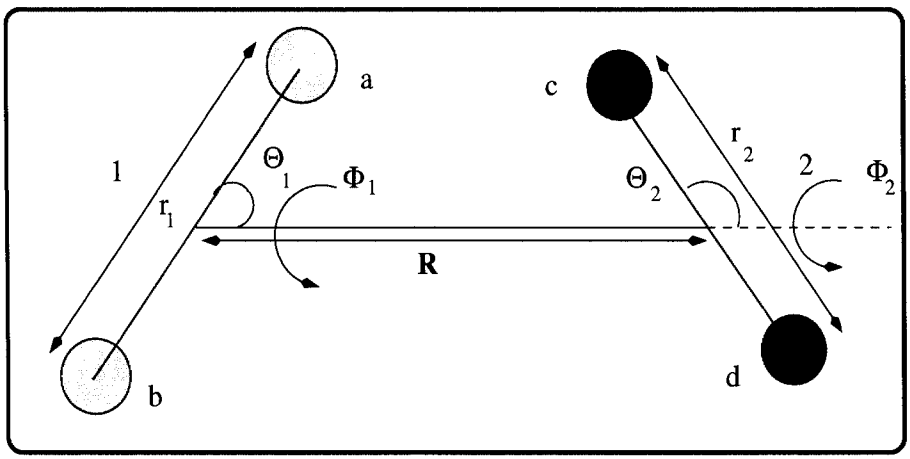

Figure 3.1: Coordinates in the two molecule system: $r_1 = r_{ab}$, $r_2 = r_{cd}$, $\omega_1 = \theta_1, \phi_1$ and $\omega_2 = \theta_2, \phi_2$.

Consequently, these molecules are forbidden to absorb or emit dipole radiation. However, transient electric dipole moments μ_{ind} can be induced in a pair or more of colliding molecules. Considering only the binary collisions, the total induced electrical dipole moment $\vec{\mu}_{ind}$ [22] of an interacting molecular-pair is represented by a sum of terms which has the form

$$\vec{\mu}_{ind}(\mathbf{R}; \omega_1, \omega_2; r_1, r_2) = \vec{\mu}_{ov} + \vec{\mu}_q + \vec{\mu}_h + \vec{\mu}_{th} + \cdots , \tag{3.2.1}$$

where μ_{ind} is a function of the intermolecular separation $\mathbf{R}$, internuclear separations r_1 and r_2, and their orientations $\omega_1(\theta_1, \phi_1)$, and $\omega_2(\theta_2, \phi_2)$ with respect to the z-axis chosen along $\mathbf{R}$, see Fig. 3.1. The first term $\vec{\mu}_{ov}$ is a short range electron-overlap induced moment. The induced dipole moment $\vec{\mu}_{ov}$ contains an isotropic part directed along the z axis, i.e., the intermolecular axis, and an anisotropic part which can have any direction.

(i) The isotropic part:

This part can be represented by an exp-7 model; a short range part varying exponentially with **R** together with a long range part an R^{-7} dispersion contribution. This contibutes to collision induced absorption of the fundamental bands and the second overtone bands. It is found that the isotropic overlap induction does not contribute to the first overtone CIA band. The rotational selection rule in this case is: $\Delta J = J'$ - $J'' = 0$, which gives rise to Q_{ov} transitions.

(ii) Anisotropic part:

This part can be represented by an exp-4 model; a short range part varying exponentially with **R** together with a long range part an R^{-4} contribution. This contributes to pure translational CIA spectra in the far infrared region and also contributes some intensity to the rotational and vibrational bands. The rotational selection rule is: $\Delta J = J'$ - $J'' = 0, \pm 2$ giving rise to O(ΔJ= -2), Q($\Delta J = 0$) and S(ΔJ= 2) transitions. In the overlap induction mechanism, the model used is the exp-4 model which results from an adequate approximation, where the long-range part of the isotropic component and the short-range parts of the anisotropic components neglected.

The second term $\overrightarrow{\mu}_q$ in equation (3.2.1) is a long-range quadrupole-induced and angle-dependent moment varying as R^{-4} which results from the interactions of permanent molecular quadrupole moments i.e. the quadrupole induction mechanism, which are responsible for the O, Q and S-branches. This term consists of two contributions:

a) The first term arises from the isotropic component of the polarizability of a colliding pair of molecules, and contributes to the following transitions:
$O_{\Delta v}(J) + Q_0(J)$, $Q_{\Delta v}(J) + Q_0(J)$, $S_{\Delta v}(J) + Q_0(J)$, $Q_{\Delta v}(J) + O_0(J)$,
$Q_{\Delta v}(J) + S_0(J)$, $O_{\Delta v}(J) + Q_{\Delta v}(J)$, $Q_{\Delta v}(J) + Q_{\Delta v}(J)$ and $S_{\Delta v}(J) + Q_{\Delta v}(J)$.

b) The second term arises from the anistropic component of the polarizability

which contributes a small amount to the previous transitions and gives rise to the transitions: $S_{\Delta v}(J) + S_0(J)$ and $S_{\Delta v}(J) + S_{\Delta v}(J)$.

The selection rule for these transitions is $\Delta J = J' - J'' = 0, \pm 2$.

The third term $\overrightarrow{\mu}_h$ in equation (3.2.1) is an intermediate range hexadecapole-induced, and angle-dependent moment and is proportional to R^{-6}. The selection rule for these transitions is $\Delta J = J' - J'' = 0, \pm 2, \pm 4$, which gives rise to the Q, O, S, M and U transitions respectively. This model of the induced dipole when combined with appropriate pair distribution functions allows the integrated absorption coefficient to be calculated and will be discussed in the following section. These induced electric dipole moments and the higher degree moments interact with the electromagnetic waves produced by an appropriate radiation source, so the colliding molecules absorb radiation in the near infra-red region (i.e. vibration-rotation region) as mentioned earlier.

3.3 Absorption coefficients

The intensity of radiation $I(\nu)$ transmitted through a cell of length l filled with the absorbing gas is given by

$$I(\nu) = I_0(\nu)e^{-\alpha(\nu)l}, \tag{3.3.1}$$

where $I_0(\nu)$ is the intensity of radiation transmitted through the empty cell and $\alpha(\nu)$ is the absorption coefficient at a given wave number ν in (cm^{-1}). For binary gas mixtures, the intensity is given by

$$I_2(\nu) = I_1(\nu)e^{-\alpha_{en}(\nu)l}, \tag{3.3.2}$$

where $I_1(\nu)$ and $I_2(\nu)$ are the intensities of radiation transmitted by the cell containing the base gas of density ρ_a and the binary mixture of density $(\rho_a + \rho_b)$, respectively, and $\alpha_{en}(\nu)$ is the enhancement absorption coefficient[1], which can be expressed as

$$\alpha_{en}(\nu) = (1/l)ln[I_1(\nu)/I_2(\nu)]. \tag{3.3.3}$$

The area of the enhancement absorption profiles gives the integrated absorption coefficient $\int \alpha(\nu)_{en}\, d\nu$ for the band. The integrated absorption coefficient can be expanded in terms of the densities ρ_a and ρ_b as

$$\begin{aligned}\int \alpha_{en}(\nu)d\nu = {} & \alpha_{ab}\rho_a\rho_b + \alpha_{2ab}\rho_a^2\rho_b + \alpha_{a2b}\rho_a\rho_b^2 \\ & + \alpha_{3ab}\rho_a^3\rho_b + \alpha_{2a2b}\rho_a^2\rho_b^2 + \alpha_{a3b}\rho_a\rho_b^3 + \cdots .\end{aligned} \tag{3.3.4}$$

Equation 3.3.4 can be rewritten in the form:

$$\begin{aligned}[1/(\rho_a\rho_b)]\int \alpha_{en}(\nu)d\nu = {} & [\alpha_{ab} + \alpha_{2ab}\rho_a + \alpha_{3ab}\rho_a^2 + \cdots] \\ & + [\alpha_{a2b} + \alpha_{2a2b}\rho_a + \cdots]\rho_b + \alpha_{a3b}\rho_b^2 + \cdots ,\end{aligned} \tag{3.3.5}$$

where ρ_a is the base density and ρ_b is the density of the foreign gas in the mixture in amagat units. α_{ab} is the binary absorption coefficient resulting from collisions of the type $a-b$, and α_{a2b}, and α_{2ab} are the ternary absorption coefficients resulting from collisions of the type $a-b-b$ and $a-a-b$, respectively, and α_{3ab}, α_{2a2b} and α_{a3b} are the quarternary absorption coefficients resulting from collisions of the type $a-a-a-b$, $a-a-b-b$ and $a-b-b-b$, respectively. To compare the experimental results with theoretical calculations it is more useful to use the absorption coefficient. The integrated dimensionless absorption coefficient can be represented by the following

[1]It is the additional absorption caused by the addition of the the perturbing gas to an absorption cell containing the base gas.

equation,

$$c\int \widetilde{\alpha}_{en}(\nu)d\nu = \widetilde{\alpha}_{ab}\rho_a\rho_b n_0^2 + \widetilde{\alpha}_{2ab}\rho_a^2\rho_b n_0^3 + \widetilde{\alpha}_{a2b}\rho_a\rho_b^2 n_0^3 + \widetilde{\alpha}_{3ab}\rho_a^3\rho_b n_0^4 + \widetilde{\alpha}_{2a2b}\rho_a^2\rho_b^2 n_0^4 + \widetilde{\alpha}_{a3b}\rho_a\rho_b^3 n_0^4 + \cdots \tag{3.3.6}$$

where c is the speed of light, and the absorption coefficient is given by

$$\widetilde{\alpha}_{en}(\nu) \equiv \alpha_{en}(\nu)/\nu, \tag{3.3.7}$$

and n_0 is Loschmidt's number[2] (2.68676×10^{19} cm^{-3}). The absorption coefficients $\widetilde{\alpha}_{ab}(cm^6 s^{-1})$, $\widetilde{\alpha}_{2ab}$ and $\widetilde{\alpha}_{a2b}(cm^9 s^{-1})$, and $\widetilde{\alpha}_{3ab}$, $\widetilde{\alpha}_{2a2b}$ and $\widetilde{\alpha}_{a3b}(cm^{12} s^{-1})$, are related to α_{ab}, α_{2ab}, α_{a2b}, α_{3ab}, α_{2a2b} and α_{a3b} by the following terms:

$$\widetilde{\alpha}_{ab}(\nu) = \left(\frac{c}{n_0^2}\right)\frac{\alpha_{ab}(\nu)}{\overline{\nu}}, \tag{3.3.8}$$

$$\widetilde{\alpha}_{2ab}(\nu) = \left(\frac{c}{n_0^3}\right)\frac{\alpha_{2ab}(\nu)}{\overline{\nu}}, \tag{3.3.9}$$

$$\widetilde{\alpha}_{a2b}(\nu) = \left(\frac{c}{n_0^3}\right)\frac{\alpha_{a2b}(\nu)}{\overline{\nu}}, \tag{3.3.10}$$

$$\widetilde{\alpha}_{3ab}(\nu) = \left(\frac{c}{n_0^4}\right)\frac{\alpha_{3ab}(\nu)}{\overline{\nu}}, \tag{3.3.11}$$

$$\widetilde{\alpha}_{2a2b}(\nu) = \left(\frac{c}{n_0^4}\right)\frac{\alpha_{2a2b}(\nu)}{\overline{\nu}}, \tag{3.3.12}$$

and

$$\widetilde{\alpha}_{a3b}(\nu) = \left(\frac{c}{n_0^4}\right)\frac{\alpha_{a3b}(\nu)}{\overline{\nu}}, \tag{3.3.13}$$

where $\overline{\nu}$ is the the weighted mean wavenumber of the band and is given by

$$\overline{\nu} = \frac{\int \alpha_{en}(\nu)d\nu}{\int \alpha_{en}(\nu)\nu^{-1}d\nu}. \tag{3.3.14}$$

[2]the number of molecules in 1 cm^3 of an ideal gas at 0°C and 1 atmosphere of pressure; Avogadro's number divided by 22,414.

3.4 The quadrupole-induced binary absorption coefficients in CIA

The basic theory of collision-induced absorption in gases has been developed by Van Kranendonk [22–27], with additional aspects given by Mizushima [78, 79], Poll, Hunt, Lewis and others [28, 32, 80–84]. A brief review of the theory is presented here. The integrated dimensionless absorption coefficient has been the focus of theoretical work; it is possible to calculate this and to compare it with the experimental results. The integrated binary absorption coefficient of a specific order Lth multipole-induced transition[3] is given by (see Reddy [35])

$$\begin{aligned} \widetilde{\alpha}_{Lm}(\nu) &= (1/\rho^2) \int \frac{\alpha_m(\nu)}{\nu} d\nu \\ &= \frac{4\pi^3 e^2}{3hc} n_0^2 a_0^5 \left(\frac{a_0}{\sigma}\right)^{2L+1} \widetilde{J}_L X_{Lm}, \end{aligned} \tag{3.4.1}$$

where the quantity X_{Lm} is given by

$$\begin{aligned} X_{Lm} = P_{J_1} P_{J_2} [& C(J_1\ L\ J_1'; 00)^2 < v_1 J_1 \mid Q_{L_1} \mid v_1' J_1' >^2 \\ & \times C(J_2\ 0\ J_2'; 00)^2 < v_2 J_2 \mid \alpha_2 \mid v_2' J_2' >^2 \\ & + C(J_2\ L\ J_2'; 00)^2 < v_2 J_2 \mid Q_{L_2} \mid v_2' J_2' >^2 \\ & \times C(J_1\ 0\ J_1'; 00)^2 < v_1 J_1 \mid \alpha_1 \mid v_1' J_1' >^2] + Y_{Lm}, \end{aligned} \tag{3.4.2}$$

and

$$\widetilde{J}_L(T) = 4\pi(L+1) \int_0^\infty x^{-2(L+2)} g_0(x) x^2 dx, \tag{3.4.3}$$

where x denotes the separation between the centers of mass of the colliding pair of molecules in atomic units, m indicates all the quantum numbers characterizing the transition, ρ is the gas density in amagat, e is the electron charge, n_0 is the Loschmidt number, a_0 is the Bohr radius, h is the Planck constant and c is the speed

[3] L takes values 2, 4, 6, etc. for quadropole 2^2, hexadecapole 2^4 induction etc.

of light. The intermolecular potential $V(x)$ can be fairly accurately represented by the Lennard-Jones 12-6 potential

$$V(x) = 4\epsilon(x^{-12} - x^{-6}), \tag{3.4.4}$$

where σ is the intermolecular separation corresponding to $V(\sigma) = 0$, $x = R/\sigma$ with R the intermolecular separation, and ϵ the depth of the potential well. $\widetilde{J}_L = J_q$ represents the average dependence of the square of the induced dipole moment on R, and is expressed as

$$J_q(T) = 12\pi \int_0 x^{-6} g_0(x) dx; \tag{3.4.5}$$

g_0 is the low density limit of the pair correlation function which in the classical limit is given by

$$g_0(x) = e^{-V(x)/kT}. \tag{3.4.6}$$

The normalized Boltzmann factor is written as

$$P_J = \frac{g_T(2J+1)e^{-E_J/kT}}{\sum_J g_T(2J+1)e^{-E_J/kT}}, \tag{3.4.7}$$

where $g_T = 2T + 1$ is the nuclear statistical weight, where

$$T = 2I, 2I - 1, \cdots, 0. \tag{3.4.8}$$

Here I is the nuclear spin which equals to $1/2$ for H_2 and 1 for both N_2 and D_2. Thus $T = 1, 0$ for H_2 and $T = 2, 1, 0$ for N_2 and D_2. Hence $g_T = 1$ and 3 for even and odd J for H_2, and $g_T = 6$ and 3 for even and odd J for N_2 and D_2, respectively, and E_J is the rotational energy

$$E_J = F_v(J) \times hc, \tag{3.4.9}$$

where $F_v(J)$ is the rotational term value. Thus

$$\sum_{even\ J} P_J : \sum_{odd\ J} P_J = 1:3 \quad \text{for } H_2 \text{ and } \quad 2:1 \quad \text{for } N_2 \text{ and } D_2. \tag{3.4.10}$$

The squares of the Clebsch-Gordan coefficients are represented by the following equations: For the Q($\Delta J = 0, L = 0$) transitions

$$C(J\ 0\ J';00)^2 = \delta_{JJ'} = \begin{cases} 1 & \text{if } J = J' \\ 0 & \text{if } J \neq J' \end{cases}, \tag{3.4.11}$$

for the O($\Delta J = -2, L = 2$) transitions

$$C(J\ 2\ [J-2];00)^2 = \frac{3J(J-1)}{2(2J-1)(2J+1)}, \tag{3.4.12}$$

for the Q($\Delta J = 0, L = 2$) transitions

$$C(J\ 2\ J;00)^2 = \frac{J(J+1)}{(2J-1)(2J+3)}, \tag{3.4.13}$$

and for the S($\Delta J = 2, L = 2$) transitions

$$C(J\ 2\ [J+2];00)^2 = \frac{3(J+1)(J+2)}{2(2J+1)(2J+3)}. \tag{3.4.14}$$

The term Y_{Lm} in equation (3.4.2) is small compared with X_{Lm} and this term accounts for the contribution of the anistropy of the polarizability to the L-pole transitions and is given by

$$\begin{aligned} Y_{Lm} &= P_{J_1}P_{J_2}\Big[\frac{2}{9}C(J_1LJ_1';00)^2C(J_22J_2';00)^2 < v_1J_1 \mid Q_{L_1} \mid v_1'J_1' >^2 \\ &\times < v_2J_2 \mid \gamma_2 \mid v_2'J_2' >^2 + \frac{2}{9}C(J_12J_1';00)^2C(J_2LJ_2';00)^2 < v_2J_2 \mid Q_{L_2} \mid v_2'J_2' >^2 \\ &\times < v_1J_1 \mid \gamma_1 \mid v_1'J_1' >^2 - \frac{4}{15}C(J_12J_1';00)^2C(J_22J_2';00)^2 < v_1J_1 \mid Q_{L_1} \mid v_1'J_1' > \\ &\times < v_2J_2 \mid \gamma_2 \mid v_2'J_2' >< v_2J_2 \mid Q_{L_2} \mid v_2'J_2' >< v_1J_1 \mid \gamma_1 \mid v_1'J_1' > \Big], \end{aligned} \tag{3.4.15}$$

where subscripts 1 and 2 refer to the two colliding molecules 1 and 2, vJ and $v'J'$ are their initial and final vibrational and rotational quantum numbers; and $\langle|Q|\rangle$,

$\langle|\alpha|\rangle$, $\langle|\gamma|\rangle$ are the matrix elements of the 2^L-pole induction, isotropic and anisotropic polarizability, respectively. These values for H_2 and D_2 were given by Hunt et al. [84]. Since the corresponding matrix elements for N_2 and CO are not available, the $\langle|Q_2|\rangle$ and $\langle|\alpha_2|\rangle$ are assumed to be constants. The values of Q for N_2 and CO are 1.22 ea_0^2 [25] and 1.272 ea_0^2 [85], respectively, and those of α for N_2 and CO are 11.8a_0^2 [86] and 13.2 a_0^2 [87], respectively. Similarly, the corresponding matrix elements for Ar, Kr and Xe are also not available, and so the isotropic polarizability values for Ar, Kr and Xe, 11.1, 16.8 and 27.4 a_0^3 [25], respectively, were used.

3.5 Line shape functions

The dimensionless absorption coefficient $\widetilde{\alpha}(\nu)$ for the quadrupolar transitions at a wavenumber ν of a band can be represented by [35]

$$\widetilde{\alpha}(\nu) = \sum_m \frac{\widetilde{\alpha}^0_{qm} W_q(\Delta\nu)}{1 + \exp(-hc\Delta\nu/kT)}, \tag{3.5.1}$$

where $\widetilde{\alpha}^0_{qm}$ is equal to twice the maximum absorption coefficient at the molecular wavenumber ν_m, $W_q(\Delta\nu)$ with $\Delta\nu = \nu - \nu_m$ is the symmetric line shape function of the quadrupolar line, while m represents a specific transition. The factor $1 + \exp(-hc\Delta\nu/kT)$ satisfies the detailed balance condition and converts the symmetrized line shape function $W_q(\Delta\nu)$ into the observed Boltzmann-modified line shape. (see Fig 3.2). The simplest realistic approximation to $W_q(\Delta\nu)$ is

$$W_q(\Delta\nu) = \frac{1}{1 + (\Delta\nu/\delta_q)^2}, \tag{3.5.2}$$

and δ_q is the quadrupolar half-width at half-height. However, in the present analysis the Birnbaum-Cohen line shape function [30] was used because it gave an excellent

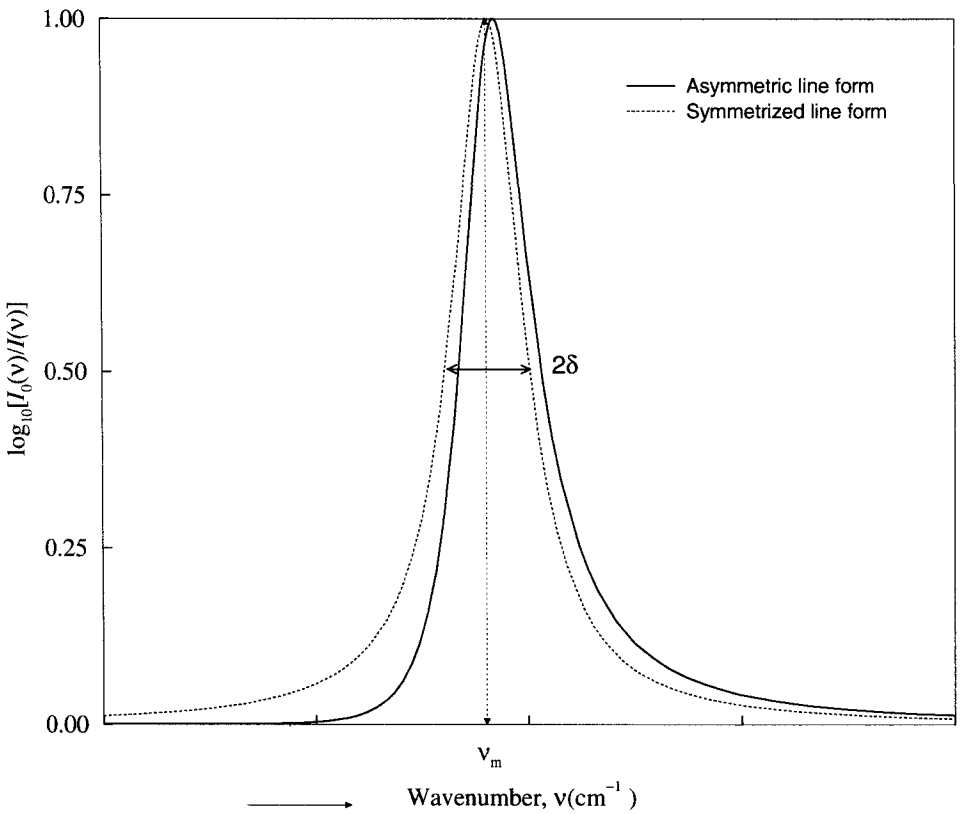

Figure 3.2: Symmetrized line shape function converts to asymmetric line shape function due to the parameter of $1+\exp(-hc\Delta\nu/kT)$ in the denominator in equation (3.5.1) and δ is the half-width at half-hight.

fit of the calculated profile with the observed profile, including the wings. Equation (3.5.1) can be modified in terms of the Birnbaum-Cohen (BC) line shape function as

$$\widetilde{\alpha}(\nu) = \sum_m \widetilde{\alpha}_{qm}^{BC} W_q^{BC}(\Delta\nu), \tag{3.5.3}$$

where $W_q^{BC}(\Delta\nu)$ is given by

$$W_q^{BC}(\Delta\nu) = \frac{1}{2\pi^2 c\delta_1} \exp\left(\frac{\delta_1}{\delta_2}\right) \exp\left(\frac{hc\Delta\nu}{2kT}\right) \frac{zK_1(z)}{1+(\Delta\nu/\delta_1)^2}, \tag{3.5.4}$$

where

$$z = \left[1 + (\Delta\nu/\delta_1)^2\right]^{1/2} \times \left[\left(\frac{\delta_1}{\delta_2}\right)^2 + \left(\frac{hc\delta_1}{2\pi kT}\right)^2\right]^{1/2}, \tag{3.5.5}$$

The function $K_1(z)$ is the modified Bessel function of the second kind of order 1, and δ_1 and δ_2 are the parameters of the line shape (or wavenumber parameters); δ_1 controls the width of the line while δ_2 affects the wing of the line. These parameters are related to the characteristic times in the dipole moment correlation function by $\tau_1 = 1/(2\pi c\delta_1)$ and $\tau_2 = 1/(2\pi c\delta_2)$ respectively [35].

3.5.1 Fitting of the experimental profiles

In order to fit the experimental profiles, the synthetic profiles should be calculated first. To calculate a synthetic profile, the Boltzmann factor is determined using equation (3.4.9), and the calculated values are listed in appendix C. Then, wavenumbers in cm^{-1} of all the possible transitions are calculated as mentioned in section 3.1 and 3.2. Also, the binary absorption coefficient resulting from the quadrupole induction mechanism in the case under study is calculated using equation (3.4.1). The total BC line shape function is determined which is the synthetic profile using equation (3.5.3). Finally. the whole synthetic spectrum with appropriate values of δ_1, δ_2 and a multiplication factor is used to fit the observed spectrum by a non linear least squares procedure.

Chapter 4

Collision-induced first overtone band of H_2 in binary mixtures H_2-N_2 and H_2-CO

Enhancement spectra of the collision-induced absorption of H_2 in its first overtone region 7500 - 9500 cm^{-1} in binary mixtures H_2 - N_2 and H_2 - CO were studied at 298 K for base densities of H_2 in the range 89 - 145 amagat and for partial densities of N_2 and CO in the range 19 - 392 amagat. The observed spectra confirm that the isotropic overlap induction is absent in the 2 - 0 band of H_2 unlike in the CIA spectra of the fundamental band of H_2. Binary and ternary absorption coefficients were determined from the integrated absorption coefficients of the band. Enhancement absorption profiles of H_2-N_2 and H_2-CO consist of a total of 434 components of quadrupolar double transitions. Profile analysis of the spectra was carried out using Birnbaum-Cohen line shape function for the individual components of the band and characteristic line shape parameters were determined from the analysis.

4.1 Introduction

CIA in compressed gases O_2 and N_2 in their fundamental bands was first identified by Crawford et al. [3] in 1949. Subsequently many studies were performed on the CIA spectra of pure H_2, pure N_2 and H_2-N_2 binary mixtures under different experimental conditions. H_2 and N_2 are major constituents of the atmospheres of several astronomical bodies such as Mars, methane dwarfs and some planetary satellites; for instance, Titan and Triton, the largest satellites of Saturn and Neptune, respectively. Reddy and Cho [8] studied the fundamental band of pure N_2 and N_2-H_2 mixtures at room temperature for densities up to 318 amagat. The CIA spectra of the first overtone and the second overtone bands of pure H_2 at 84.7 K and 85.3 K, and the first overtone band in an H_2-N_2 binary mixtures at 106.4 K for densities 7.6 (H_2) and 14.4 (N_2) amagat have been investigated by McKellar and Welsh [49]. Dore et al. [88] studied the roto-translational far infrared absorption spectra of H_2-N_2 at 91 K, 141 K, 165 K, 195 K and 298 K. New measurements were made by Codastefano and Dore [89] for the far infrared absorption of the H_2-N_2 gaseous mixtures at five different temperatures from 90 K to 298 K. McKellar [90] investigated the spectra of N_2-H_2 in the 4000 to 5000 cm^{-1} region. Stamp et al. [91] from our laboratory studied the spectra of double vibrational transitions $H_2(v = 1 \leftarrow 0)$+$N_2(v = 1 \leftarrow 0)$ in the H_2-N_2 binary mixtures in the spectral region 5900 to 7100 cm^{-1} at 201 K and 298 K for partial densities of H_2 and N_2 in the range 60 to 400 and 100 to 350 amagat, respectively. Recently, Boissoles et al. [92] studied the CIA spectra of the fundamental band of H_2 in the H_2-N_2 binary mixtures at room temperature at low pressures. In the present chapter the CIA spectra of the first overtone band in the region 7200 cm^{-1} to 9500 cm^{-1} of H_2 in binary mixtures H_2-N_2 and H_2-CO are investigated at room

temperature. Unlike the enhancement spectra of H_2-Kr or H_2-Xe in the first overtone band studied by Prasad et al. [57] the present spectra consist of a large number of double transitions of H_2 with N_2 and CO which take part in the absorption process. The absorption profiles were analyzed using Birnbaum-Cohen line shape function [30] for all the double transitions $O_2(2)$, $Q_2(J)$ and $S_2(J)$ for $J = 0$ to 3 of H_2 with the orientational transitions $Q_0(J)$ for $J = 0$ to 25 for N_2 and CO arising exclusively from the quadrupolar-induction mechanism.

4.2 Experimental details

The experimental setup and procedure in genral is described in details in chapter 2 and will not be discussed here. A two-meter transmission-type stainless steel absorption cell was used to contain the gases. A General Electric FFJ Quartzline lamp housed in a water-cooled brass jacket was used as a source of continuous infrared radiation. The spectrometer was equipped with a LiF prism, an uncooled PbS detector, and a 260 Hz tuning fork chopper driven by a Micro-Controlled Stepper Driver. A slit width maintained at 60 μm gave a spectral resolution of 26 cm^{-1} at 8087 cm^{-1}, the origin of the first overtone band of H_2. The entire optical path was boxed in a Plexiglas enclosure which was continuously flushed with dry nitrogen gas in order to decrease and maintain a constant level of water vapour absorption. Mercury emission lines and water vapour absorption peaks were used for calibration of the spectral region 7500 - 9500 cm^{-1}. Experiments were carried out with base densities of H_2 in the range 89 to 145 amagat, and the partial densities of N_2/CO in the range 19 to 392 amagat, a summary of the experimental conditions is given in Table 4.1. The wavenumbers (in cm^{-1}) of the quadrupolar transitions were calculated from the molecular constants of

Table 4.1: Summary of experimental conditions.

Base density of H_2 (amagat)	Range of partial densities of N_2 (amagat)
89	51 - 349
116	59 - 328
142	32 - 275
Base density of H_2 (amagat)	Range of partial densities of CO (amagat)
89	35 - 291
119	39 - 392
145	19 - 246

H_2 [93], N_2 [94] and CO [77], the molecular constants and the calculated wavenumbers of the quadrupolar transitions are listed in Appendicies A and B.

The base density ρ_a of H_2 was obtained from a linear least squares fit to the PVT data tabulated by McCarty et al. [95]. The isothermal data for N_2 and CO were obtained from Michels et al. [67] and Hust et al. [68], see Figs. 2.3, 2.5 and 2.6. The partial densities ρ_b of N_2 and CO in binary mixtures were calculated by the interpolation method described by Reddy and Cho [8]. For a given base density ρ_a of H_2 and a total density $(\rho_a+\rho_b)$ of the gas mixture the enhancement absorption coefficient at a given wavenumber $\nu(\mathrm{cm}^{-1})$ is expressed as

$$\alpha_{en}(\nu) = (1/l)ln[I_1(\nu)/I_2(\nu)], \tag{4.2.1}$$

where l is the sample path length of the absorption cell, and $I_1(\nu)$ and $I_2(\nu)$ are the intensities transmitted by the cell containing the base gas and the binary mixture, respectively. Absorption profiles were obtained by plotting $\log_{10}[I_1(\nu)/I_2(\nu)]$ versus ν. The areas of the enhancement absorption profiles give the integrated absorption

$\int \alpha_{en}(\nu)d\nu$ for the band. The average value of $\overline{\nu}$ for H_2-N_2 and H_2-CO are 8284 ± 22 cm^{-1} and 8267 ± 39 cm^{-1}, respectively.

The normalized rotational Boltzmann factors P_J are given in the literature, the calculated values for H_2, N_2 and CO are listed in Appendicies C.1 and C.2. The nuclear statistical weight g_T which occurs in the expression for P_J is 1 and 3 for even and odd J for H_2, and 6 and 3 for even and odd J for N_2. The matrix elements $\langle|Q|\rangle$, $\langle|\alpha|\rangle$ and $\langle|\gamma\rangle$ are the 2^L-pole induction moment, the isotropic and the anisotropic polarizability, respectively, whose values for H_2 were taken from Hunt et al. [84]. Since the corresponding matrix elements for N_2/CO are not available, the quadrupole and the isotropic polarizability values were used instead of the matrix elements. Those values are 1.22/1.272 ea_0^2 [25, 85] and 11.8/13.2 a_0^3 [86, 87], respectively.

4.3 Absorption profiles and their analysis

In the present investigation, the CIA spectra of H_2 in H_2 - N_2/CO binary mixtures were recorded at 298 K in the spectral region 7200 - 9500 cm^{-1}. The pure gas N_2 or CO does not exhibit any absorption in this region even at gas pressures up to 850 atm. Thus the spectra obtained were exclusively due to the H_2-N_2 or H_2-CO interactions. Figure 4.1 shows plots of $\log_{10}(I_1(\nu)/I_2(\nu))$ versus the wavenumber $\nu(cm^{-1})$, for three typical absorption profiles of the first overtone band of H_2 in H_2-N_2 mixtures at 298 K. The base density of H_2 is 116 amagat and partial densities of N_2 are 213, 264 and 328 amagat. The positions of the transitions $O_2(2)$, $Q_2(5)$ to $Q_2(0)$ and $S_2(0)$ to $S_2(4)$ are marked along the wavenumber axis. The Q_2 peak represents the superposition of all the Q transitions. It is clear from the profiles in Fig. 4.1 that the high wavenumber wing drops to zero giving a smooth tail, while the low wavenumber wing does not.

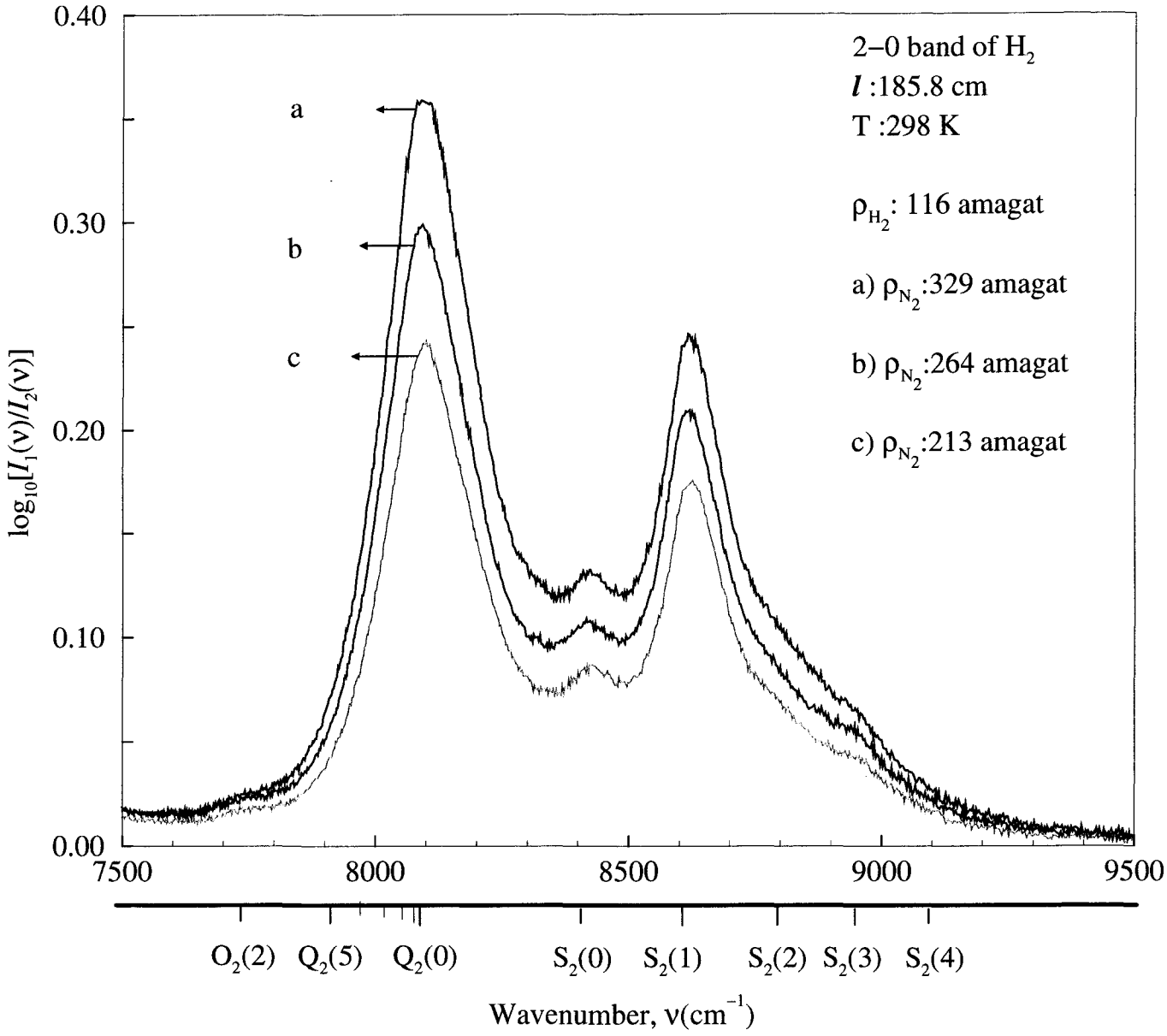

Figure 4.1: Three typical enhancement absorption profiles of the first overtone band of H_2 in H_2-N_2 mixtures at 298 K

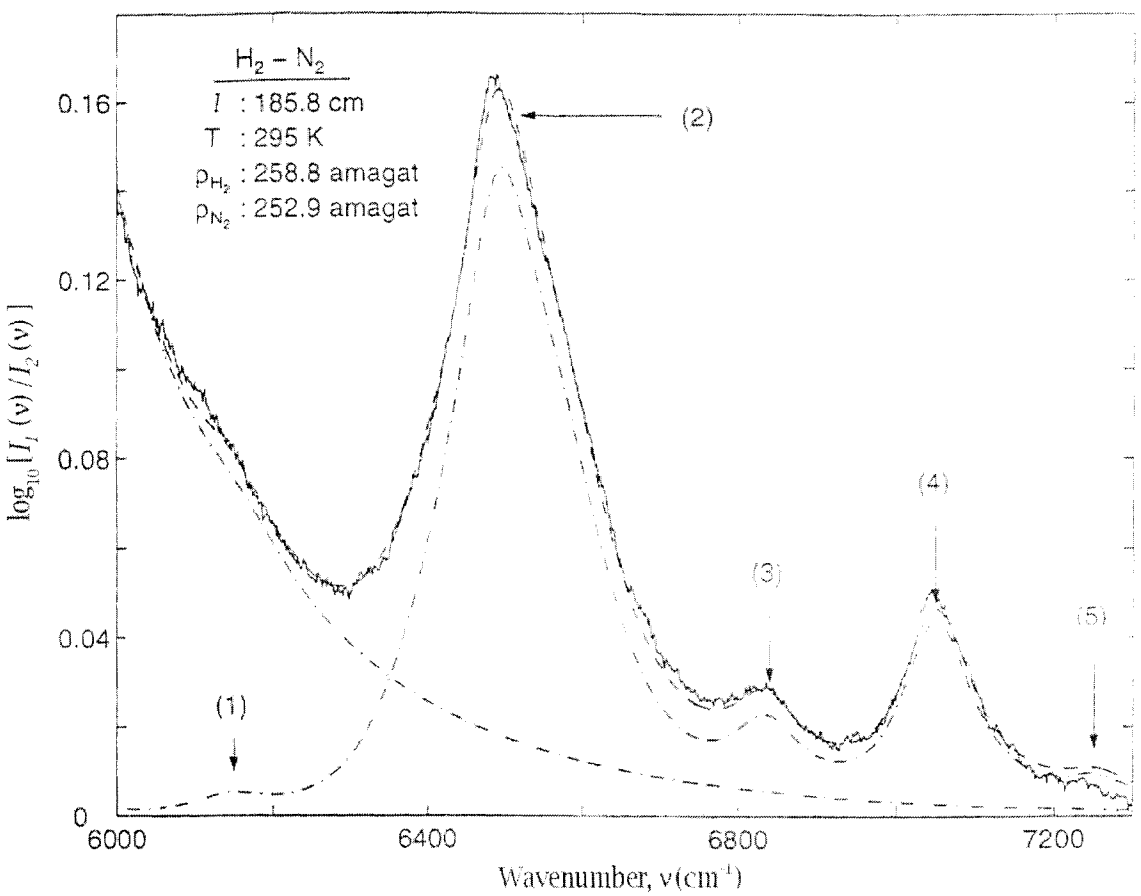

Figure 4.2: This figure is taken by permission from Ref. [90].

The discrepancy is due to the occurrence of the double vibrational transitions $S_1(J)$ of H_2 + $Q_1(J)$ of N_2, peak (5) in Fig. 4.2 does not drop to zero [91]. The profiles do not show any dip in the Q branch, unlike in the fundamental band of pure H_2. Similarly, Fig. 4.3 shows three enhancement absorption profiles for which the base density of H_2 is 89 amagat and the partial densities of the CO are 135, 211 and 291 amagat. Here, absorption in the tails is unperturbed at both ends of the profile, and again there is no sign of the dip in the Q region due to the absence of isotropic

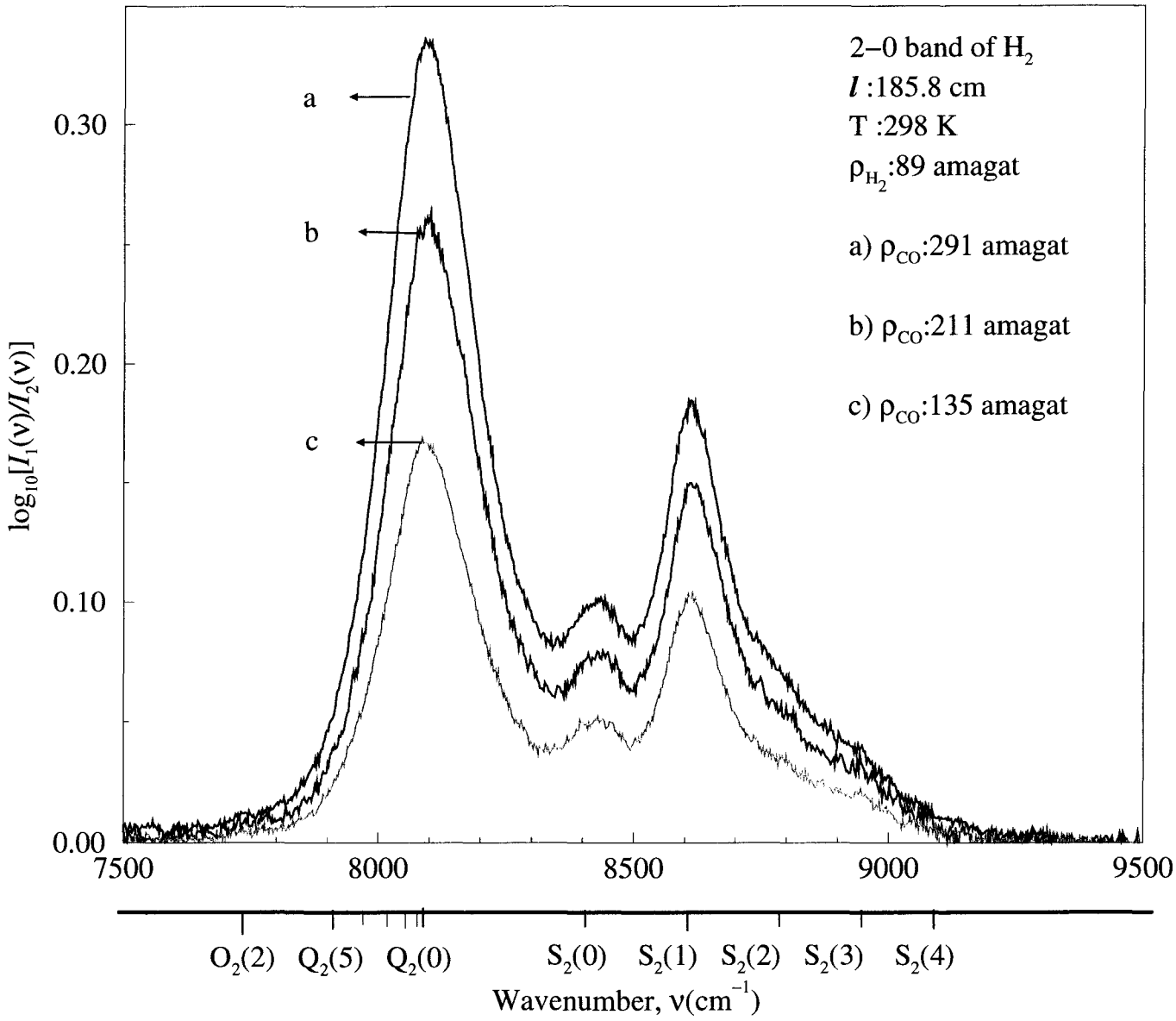

Figure 4.3: Three typical enhancement absorption profiles of the first overtone band of H_2 in H_2-CO mixtures at 298 K.

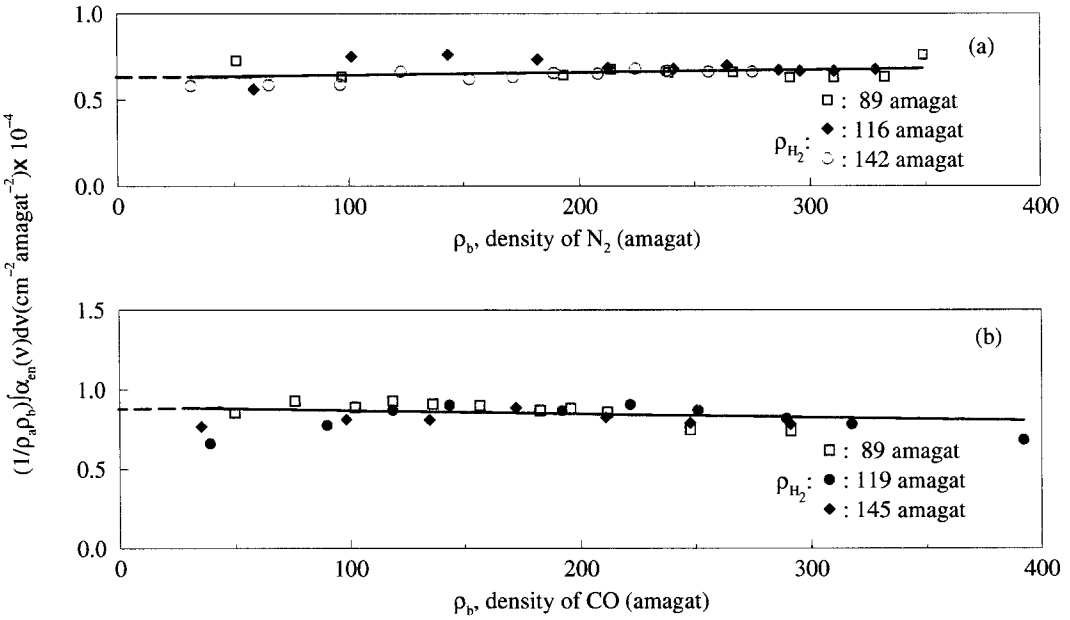

Figure 4.4: Plots of $(1/\rho_a\rho_b)\int \alpha_{en}(\nu)d\nu$ against ρ_b for the first overtone band of H_2 at 298 K in binary mixtures (a) H_2-N_2 and (b) H_2-CO.

overlap induction. These profiles also show similar peaks as in H_2-N_2 mixtures with small shifts due to the small difference between the rotational terms of N_2 and CO. Although CO has a small permanent electric dipole moment, these profiles do not exhibit any difference from the previous ones for H_2-N_2 mixture. Figure 4.4 shows plots of $(1/\rho_a\rho_b)\int \alpha_{en}(\nu)d\nu$ versus ρ_b for both H_2-N_2 and H_2-CO mixtures for three different base densities of each. The plots give straight lines in both cases, with the intercepts representing $\alpha_{ab} + \alpha_{2ab}\rho_a + \cdots$ and the slopes representing the ternary coefficients $\alpha_{a2b} + \cdots$, see equation (3.3.5). The coefficients α_{ab}, α_{2ab} and α_{a2b} were calculated and are listed in Table 4.2. It can be seen that the ternary absorption coefficients are three orders of magnitude smaller compared to the binary absorption coefficients. The quadrupolar transitions which consist of 434 in number in the first

Table 4.2: Absorption coefficients of the first overtone band of H_2 in H_2-N_2 and H_2-CO binary mixtures at room temperature.

Mixture	α_{ab} ($cm^{-2}amagat^{-2}$) $\times 10^{-5}$	$\widetilde{\alpha}_{ab}$ ($cm^6 s^{-1}$) $\times 10^{-37}$	α_{2ab} ($cm^{-2}amagat^{-3}$) $\times 10^{-8}$	$\widetilde{\alpha}_{2ab}$ ($cm^9 s^{-1}$) $\times 10^{-60}$	α_{a2b} ($cm^{-2}amagat^{-3}$) $\times 10^{-8}$	$\widetilde{\alpha}_{a2b}$ ($cm^9 s^{-1}$) $\times 10^{-60}$
H_2-N_2	6.6 ± 0.3	3.3 ± 0.1	1.9 ± 0.1	3.5 ± 0.1	1.5 ± 0.1	2.8 ± 0.1
H_2-CO	9.2 ± 0.5	4.6 ± 0.1	-8.1 ± 0.1	-15.1 ± 0.1	-2.9 ± 0.3	-5.4 ± 0.1

Table 4.3: Quadrupolar transitions of H_2-N_2 and H_2-CO at 298 K.

Transition H_2-N_2/CO	J of H_2	J of N_2/CO	Number of Components
$O_2(2) + Q_0(J)$	2	0 - 25	26
$Q_2(J) + Q_0(J)$	0 - 3	0 - 25	104
$S_2(J) + Q_0(J)$	0 - 3	0 - 25	104
$Q_2(J) + O_0(J)$	0 - 3	2 - 25	96
$Q_2(J) + S_0(J)$	0 - 3	0 - 25	104
		Total number of components	434

overtone band are listed in Table 4.3. The corresponding absorption coefficients were calculated from equation (3.4.1). Equation (3.5.3) was used to calculate the total synthetic profile. Examples of the profile analyses for H_2-N_2 and H_2-CO are shown in Figs. 4.5 and 4.6, respectively. Figure 4.5 represents the observed profile in solid line of H_2 with $\rho_a = 89$ amagat and N_2 with $\rho_b = 332$ amagat at room temperature. The dotted blue curves represent the computed individual double-transition quadrupole components, the summation of all these components gives the total synthetic profile; the dot-dashed curve is theoretical profile fitted except in the O region, due to the presence of the tail of the $S_1(J)$ of H_2 + $Q_1(J)$ of N_2 in this region and it is explained in Fig. 4.3. Similarly Fig. 4.6 represents the experimental profile of H_2 with ρ_a = 89 amagat and CO with $\rho_b = 144$ amagat at room temperature. The solid line is the experimental profile, the blue dot curves represent the individual quadrupole double transitions, the dot-dashed curve is theoretical profile fitted in all the region under study. Figure 4.7 shows an example of the lines appearing in Figs. 4.5 and 4.6. For example the transition $S_1(1)$+$Q_0(J)$ in Fig. 4.5 consists of 26 components because J of N_2/CO = 0 to 25. Eight components J=1 to 7 and $J = 20$ are shown in Fig. 4.7(a).

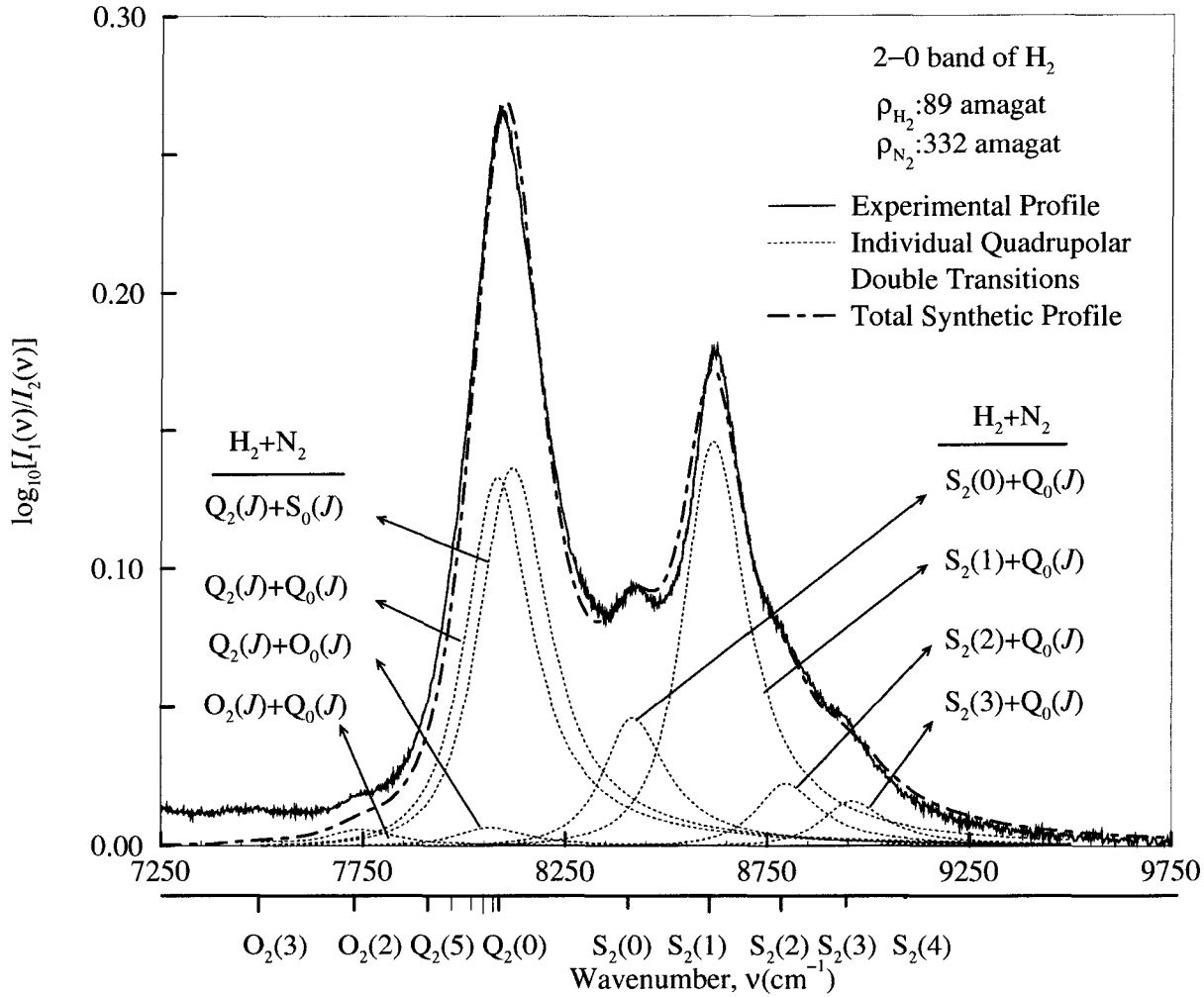

Figure 4.5: Analysis of an enhancement absorption profile of the first overtone band of H_2 in a H_2-N_2 mixture at 298 K. The solid curve is the experimental profile, the dotted curves represent the computed individual double-transition quadrupolar components and the dash-dot curve is the summation of these.

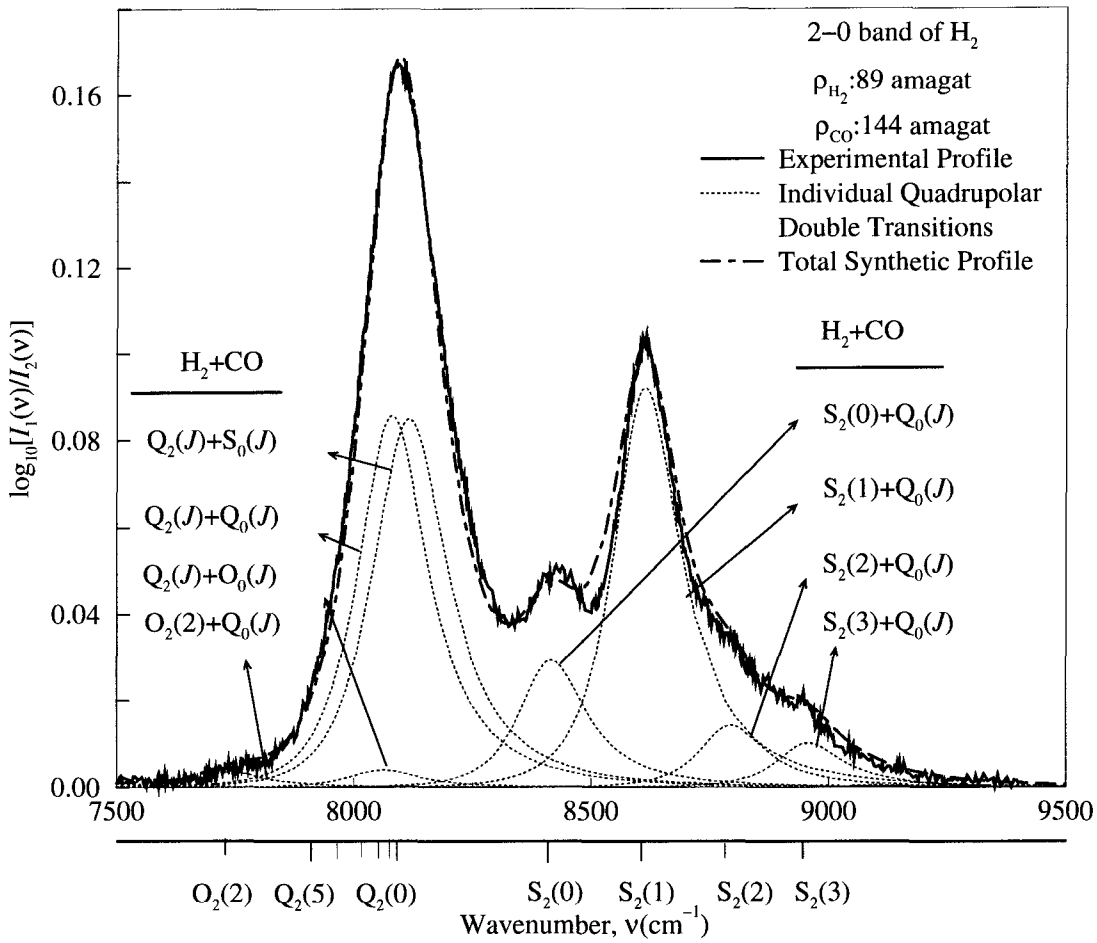

Figure 4.6: Analysis of an enhancement absorption profile of the first overtone band of H_2 in a H_2-CO mixture at 298 K.

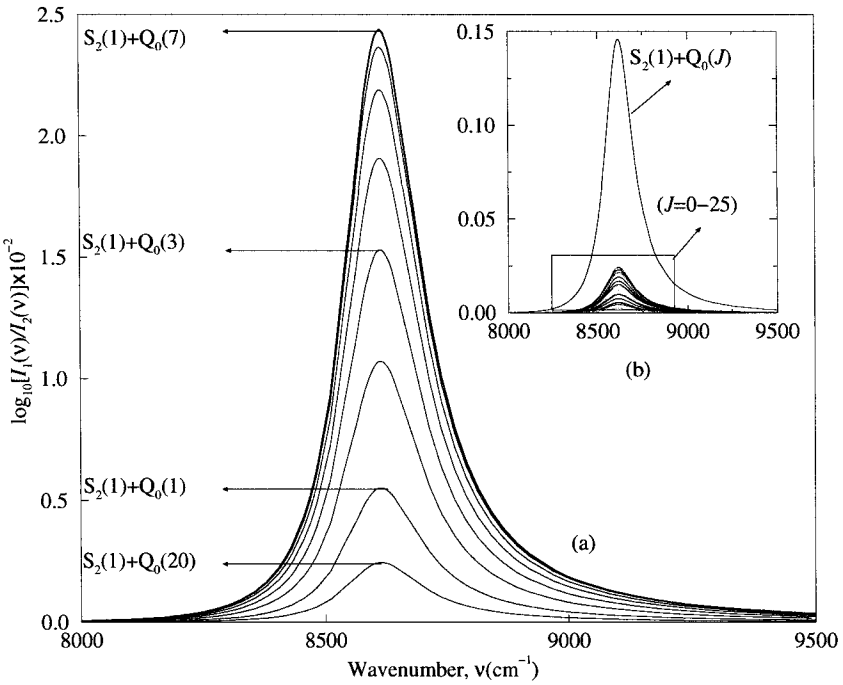

Figure 4.7: Eight components $J = 1$ to 7 and $J = 20$ are shown in (a). The summation of all the 26 components $J = 0$ to 25 which form the line $S_2(1)+Q_0(J)$ is shown in (b).

The summation of all the 26 components J=0 to 25 which form the line $S_2(1)+Q_0(J)$ is shown in Fig. 4.7(b). The component $S_2(1)+Q_0(7)$ has the maximum intensity at 298 K. A nonlinear least-squares fit was used to fit the experimental profiles. It can be seen that the agreement between the experimental profile and the synthetic profile in each case is excellent. In the H_2-N_2 binary mixtures the agreement is within 92% and this small discrepancy is due to the contribution arising from double vibrational transitions of $S_1(J)$ of $H_2+Q_1(J)$ of N_2 in the low frequency wing of the spectra [91]. In the H_2-CO binary mixtures the agreement is within 99%. Although CO has a small permanent electric dipole moment, present analysis does not indicate any detectable

contribution from the electric dipolar induction mechanism in H_2-CO mixtures. The average values of the parameters δ_1 and δ_2 of the line shape function for the best nonlinear fits for profiles of H_2-N_2 and H_2-CO and the corresponding values of τ_1 and τ_2 are given in Table 4.4.

Table 4.4: Birnbaum-Cohen line shape parameters for the first overtone band of H_2 in H_2-N_2 and H_2-CO binary mixtures.

Mixture	Number of mixtures	δ_1 (cm^{-1})	δ_2 (cm^{-1})	τ_1 ($10^{-14}s$)	τ_2 ($10^{-14}s$)
H_2-N_2	25	92 ± 4	298 ± 13	5.8 ± 0.3	1.78 ± 0.08
H_2-CO	26	94 ± 3	188 ± 5	5.6 ± 0.2	2.82 ± 0.08

4.4 Conclusions

The observed spectra confirm that the isotropic overlap induction mechanism is absent in the first overtone band of H_2 unlike the CIA spectra of its fundamental band. A total number of 434 quadrupolar transitions contribute to the CIA of the first overtone band of H_2 in each of H_2-N_2 and H_2-CO. Excellent agreement was obtained between the experimental profiles and the synthetic profiles. The line shape parameters δ_1, δ_2, τ_1 and τ_2 were determined. It is found that the ternary absorption coefficients are three orders of magnitude smaller than the binary absorption coefficients. Also, the present analysis does not indicate any detectable contribution of the permenent dipole of CO to the electric dipolar induction mechanism in H_2-CO mixtures.

Chapter 5

Collision-induced absorption in D_2 pairs in the first overtone band at 77, 201 and 298 K

CIA spectra of pure D_2 in the first overtone region from 5250 to 7250 cm^{-1}, recorded at 77, 201 and 298 K, have been analyzed. The observed spectra at 77 K, 201 K and 298 K were modeled by a total of 92, 214 and 267 components respectively of double vibrational transitions at room temperature of the type $X_2(J)+X_0(J)$ and $X_1(J)+X_1(J)$, where X is O, Q or S transitions. Profile analyses of the spectra were carried out using the Birnbaum-Cohen line shape function for the individual components of the band, and characteristic line shape parameters were determined from the analysis. The observed and fitted profiles agree well over the whole overtone band, and the agreement is better than 97% in the three cases studied. Binary and ternary absorption coefficients were determined from the integrated absorption of the band.

5.1 Introduction

CIA of the fundamental band of gaseous deuterium was originally studied by Reddy and Cho [8] and Watanabe and Welsh [61]. Later, the fundamental and the overtone bands of D_2 and the binary mixtures of D_2 were investigated under different experimental conditions by Reddy and co-workers [9, 11, 12, 15, 55]. The CIA spectra of D_2 in the pure gas and D_2-Ar and D_2-N_2 binary mixtures in the first overtone band were investigated also by Reddy and Kuo [11] who identified the spectrum of D_2-D_2 as consisting of double transitions, where the major contribution to the intensity of the absorption profiles comes from the following double transitions $Q_1(J)$+$Q_1(J)$, $Q_1(J)$+$S_1(J)$ and $Q_2(J)$+$S_0(J)$. A special feature of the spectra was the absence of the isotropic overlap contribution. Recently, the CIA spectrum of D_2 in D_2-N_2 and D_2-CO binary mixtures in the fundemental band were studied by Varghese et al. [62].

In the present chapter the investigation of the CIA spectra of the first overtone band of pure D_2 at 77, 201 and 298 K is described; and the results obtained are compared with previous studies of both D_2 and H_2 in the 1st overtone region. The spectra of pure D_2 at 298 K consist of a total 267 components of double vibrational transitions of the type $X_2(J)$+$X_0(J)$ and the type $X_1(J)$+$X_1(J)$, where X is O, Q or S transition, while it decreases to 92 components at 77 K. The possible combinations of these transitions are listed in Table 5.1. The absorption profiles were analyzed using BC line shape function [30] for all the possible transitions arising from the quadrupolar-induction mechanism.

Table 5.1: The possible quadrupolar transitions of pure D_2 at 298 K.

Transition	J of the first molecule	J of the second molecule	Number of Components[a]
$O_2(J) + Q_0(J)$	2 - 5	0 - 5	24
$Q_2(J) + Q_0(J)$[b]	0 - 5	0 - 5	35
$S_2(J) + Q_0(J)$	0 - 5	0 - 5	36
$Q_2(J) + S_0(J)$	0 - 5	0 - 5	36
$S_2(J) + S_0(J)$	0 - 4	0 - 4	25
Number of transitions			156
$O_1(2) + O_1(2)$	2	2	1
$O_1(J) + Q_1(J)$	2 - 5	0 - 5	24
$O_1(J) + S_1(J)$	2 - 4	0 - 4	15
$Q_1(J) + Q_1(J)$	0 - 5	0 - 5	20
$Q_1(J) + S_1(J)$	0 - 5	0 - 5	36
$S_1(J) + S_1(J)$	0 - 4	0 - 4	15
Number of transitions			111
Total Number of Components			267

[a]The number of components given here is for the room temperature case, this number decreases with decreasing temperature.
[b]$Q_2(0) + Q_0(0)$ is forbidden transition

5.2 Experimental details

The description of the experimental setup used for this study was already given in Chapter 2. A brief description of the experiment is given. A slit width maintained at 60 μm gave a spectral resolution of 12.5 cm^{-1} at 5868 cm^{-1}, the origin of the first overtone band of D_2. Mercury emission lines and water vapour absorption peaks were used for calibration of the spectral region 5250 - 7250 cm^{-1}. Experiments were carried out with densities in the range 118-450 amagat of D_2. The wave numbers (cm^{-1}) of the quadrupolar transitions in Appendix B were calculated from the molecular constants of D_2 [77], (Appendix A.2). The densities ρ of D_2 at temperature 201 K and 298 K were obtained from a linear least squares fit to the PVT data tabulated by A. Michels et al [64], see Fig. 2.3, while ρ at 77 K was obtained from a plot of the difference in pressure of H_2 and D_2 against density at 77, 123, 273 and 358 K, (see Ref. [55]).

For a given density ρ of D_2 the absorption coefficient at a given wavenumber $\nu(cm^{-1})$ is expressed as

$$\alpha(\nu) = (1/l)ln[I_0(\nu)/I(\nu)], \tag{5.2.1}$$

where l is the sample path length of the absorption cell, and $I_0(\nu)$ and $I(\nu)$ are the intensities transmitted by the empty cell and the cell containing the gas, respectively. Absorption profiles were obtained by plotting $\log_{10}[I_0(\nu)/I(\nu)]$ versus ν. The areas of the enhancement absorption profiles gave the integrated absorption $\int \alpha(\nu)d\nu$ for the band and it is given by

$$\int \alpha(\nu)d\nu = \alpha_1\rho^2 + \alpha_2\rho^3 + \cdots, \tag{5.2.2}$$

which can be rewritten in the form

$$(1/\rho^2)\int \alpha(\nu)d\nu = \alpha_1 + \alpha_2\rho + \cdots, \tag{5.2.3}$$

where ρ is the density of D_2 in amagat units, α_1 is the binary absorption coefficient resulting from binary collisions, and α_2 is the ternary absorption coefficient resulting from ternary collisions. The average value of $\overline{\nu}$ (equation (3.3.14)) for D_2 first overtone band is 6130 $\pm$ 7 cm^{-1}, 6114 $\pm$ 4 cm^{-1} and 6104 $\pm$ 11 cm^{-1} at 77, 201 and 298 K, respectively. The quantity g_T in equation (3.4.7) is the nuclear statistical weight, $g_T = 6$ and 3 for even and odd J for D_2. In equations (3.4.2) and (3.4.15) subscripts 1 and 2 refer to the two colliding molecules 1 and 2, vJ and $v'J'$ are their initial and final vibrational and rotational quantum numbers, and $\langle|Q|\rangle$, $\langle|\alpha|\rangle$ and $\langle|\gamma|\rangle$ are the matrix elements of the 2^L-pole inducting moment, isotropic polarizability and anisotropic polarizability respectively. These values for D_2 were given by Hunt et al. [84].

5.3 Analysis of the absorption profiles

In the present investigation the CIA spectra of the transitions of $D_2(\Delta v = 2 \longleftarrow 0)$ + $D_2(J' \longleftarrow J'')$ and $D_2(\Delta v = 1 \longleftarrow 0) + D_2(\Delta v = 1 \longleftarrow 0)$ were recorded at 77, 201 and 298 K in the spectral region 5250 - 7250 cm^{-1}. Figures 5.1, 5.2 and 5.3 show plots of $log_{10}(I_0(\nu)/I(\nu))$ versus the wavenumber $\nu(cm^{-1})$, for three representative absorption profiles of the first overtone band of D_2 at 77, 201 and 298 K respectively. The positions of the transitions $O_2(3)$, $O_2(2)$, $Q_2(5)$ to $Q_2(0)$ and $S_2(0)$ to $S_2(4)$ are marked along the wavenumber axis. The main feature of these profiles is the absence of the dip in the Q branch unlike in the fundamental band of pure D_2. Observed absorption peaks of the profiles in these figures are marked with identification numbers. There are four strong broad peaks numbered from 3 to 6, these peaks become narrower with decreasing temperature because the relative translational energy of the

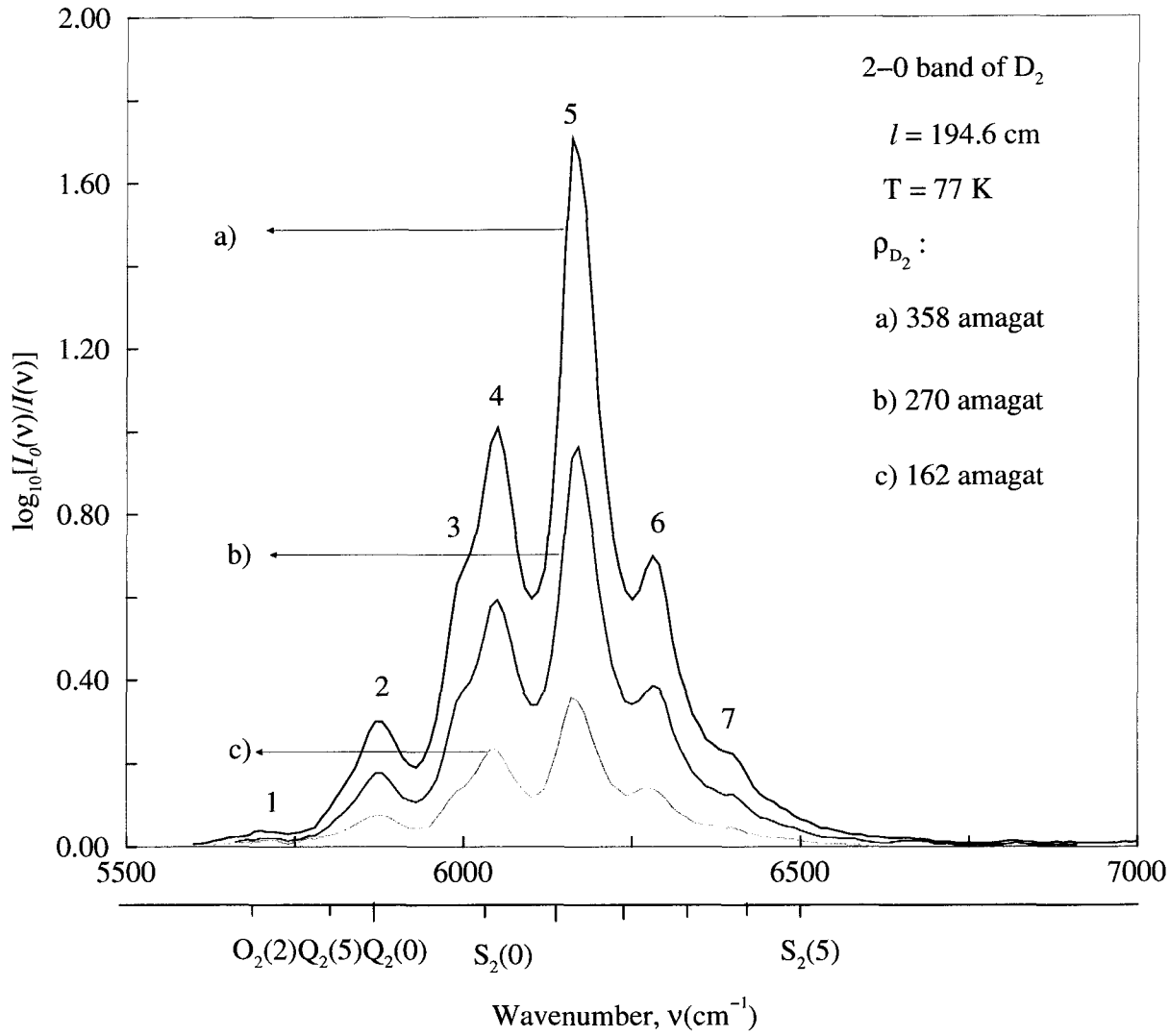

Figure 5.1: Three typical enhancement absorption profiles of the first overtone band of pure D_2 at 77 K from Ref. [55].

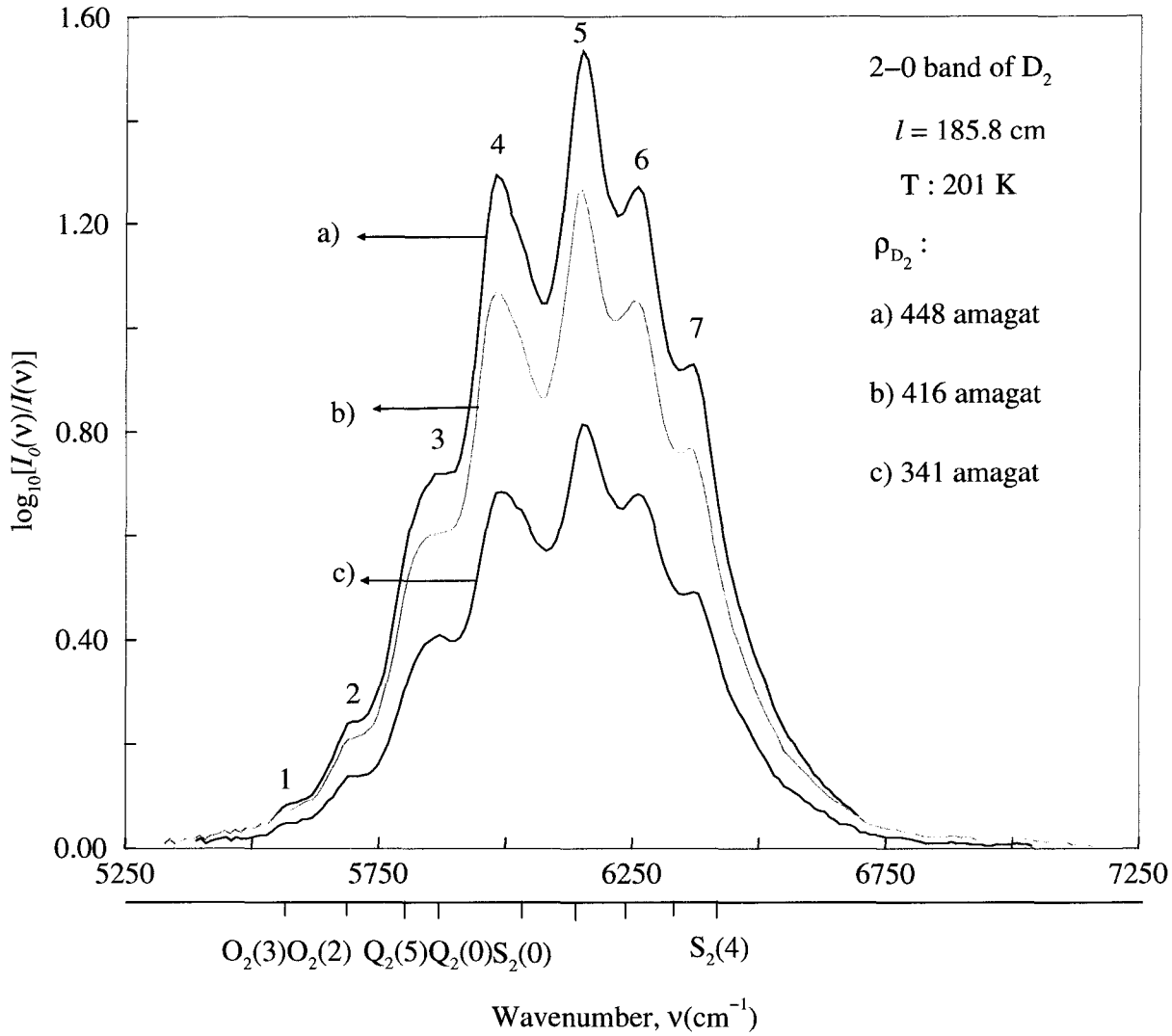

Figure 5.2: Three typical enhancement absorption profiles of the first overtone band of pure D_2 at 201 K.

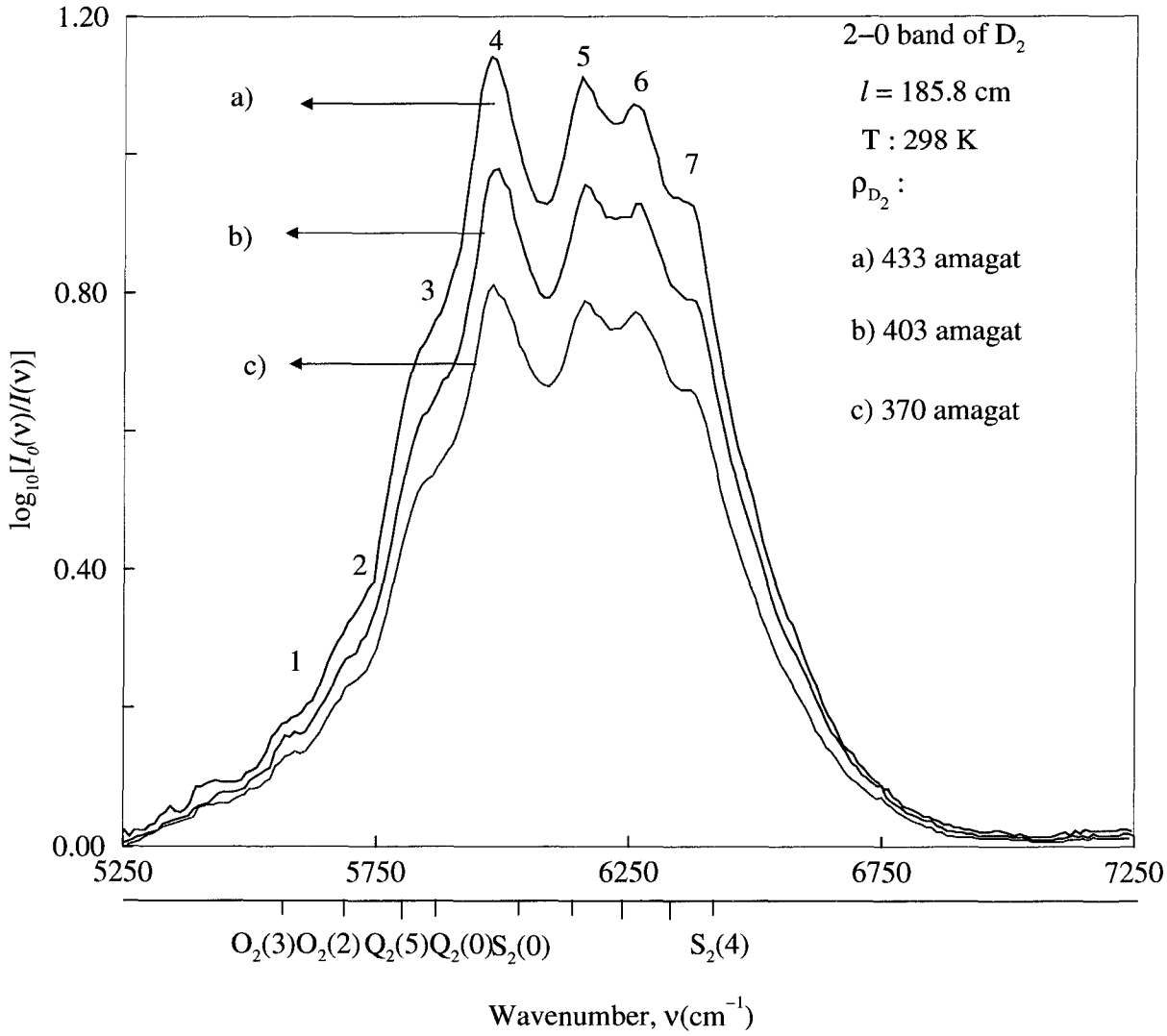

Figure 5.3: Three typical enhancement absorption profiles of the first overtone band of pure D_2 at 298 K.

colliding pair is smaller at lower temperature and hence the collision duration is relatively large. Also the intensity of peak number 5 increases rapidly with decreasing temperature, this was also observed by Gillard [55]. It is clear that none of these peaks correspond to any of the calculated single transitions. These peaks can be interpreted as a superposition of two profiles, namely, a transition of the type $X_2(J)+X_0(J)$ and the second of the type $X_1(J)+X_1(J)$, where X is $O(\Delta J = -2)$, $Q(\Delta J = 0)$ or $S(\Delta J = 2)$. All such combinations are listed in Table 5.1. For example peak four in Fig. 5.1 is formed from the following transitions: $Q_1(J)+Q_1(J)$, $S_1(J)+O_1(J)$, $Q_2(J)+Q_0(J)$, $Q_2(J)+S_0(0)$ and $S_2(0)+Q_0(J)$. While peak five is formed of the following transitions: $S_1(0)+Q_1(J)$, $Q_2(J)+S_0(1)$ $S_2(1)+Q_0(J)$. Watanabe [51] used a similar method to analyze the first overtone band of H_2. Watanabe mentioned that each of the colliding molecules simultaneously undergoes a vibrational or vibrational-orientational transition of identical energy. Figure 5.4 shows three plots of $(1/\rho^2)\int \alpha(\nu)d\nu$ versus ρ at 77, 201 and 298 K, which were used to calculate the absorption coefficients. The plots give straight lines, with the intercept representing the binary absorption coefficient α_1 and the slope representing the ternary absorption coefficient α_2. These coefficients α_1 and α_2 were determined and listed in Table 5.2 and were smaller than the corresponding values determined for H_2 at the same temperatures. It can be seen that the ternary absorption coefficients are four orders of magnitude smaller than the binary absorption coefficients, so their contribution to the absorption band is very small at the densities studied here. This result is also clear in the H_2 case. The possible transitions in the region of study 5250 to 7250 cm^{-1} with considerable intensity are listed in Table 5.1. Theoretical profiles were calculated using the same method used in Chapter 4 and described in Chapter 3. Examples of the comparison between the experimental

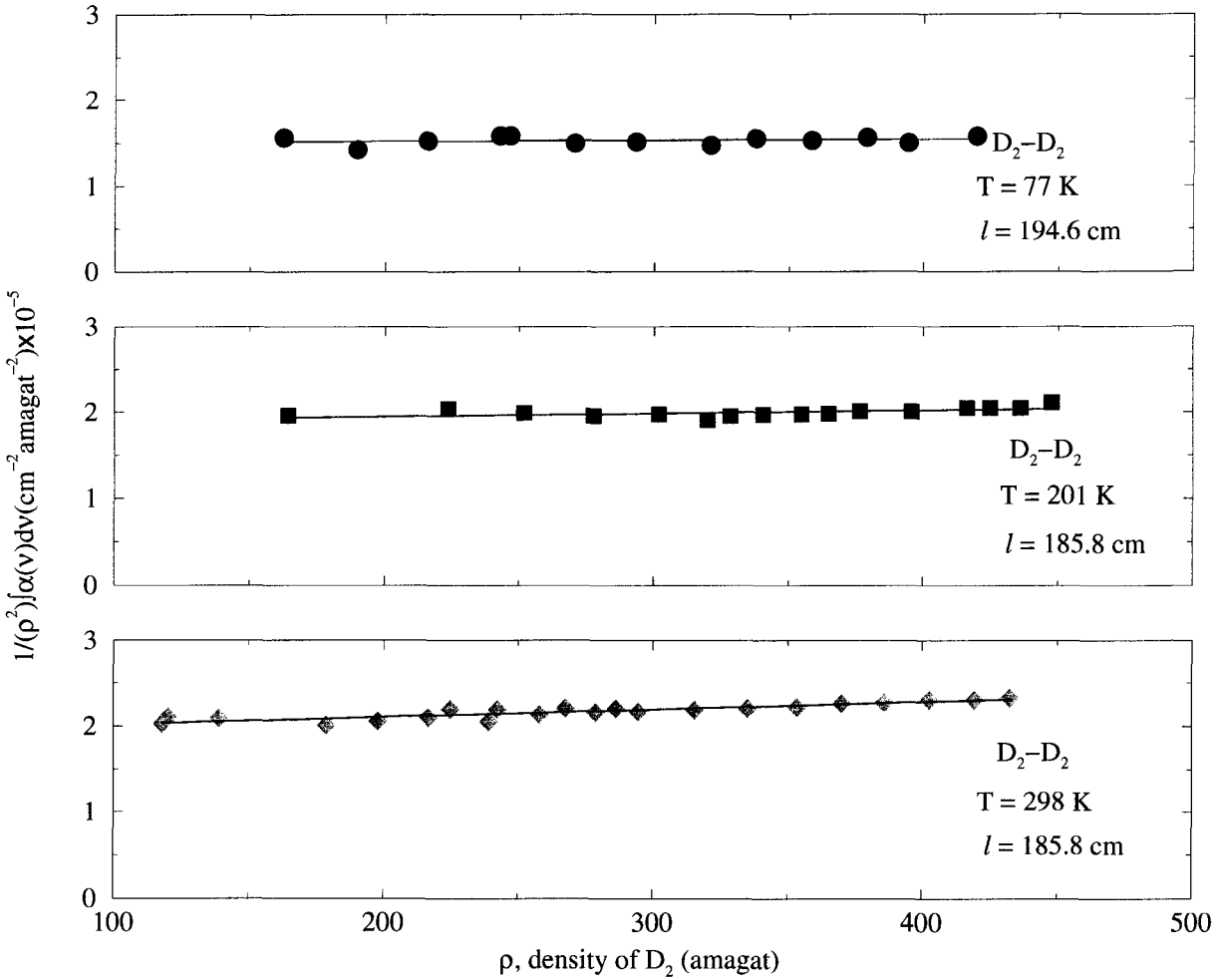

Figure 5.4: Plots of $(1/\rho^2)\int \alpha_{en}(\nu)d\nu$ against ρ for the first overtone band of D_2 at 77, 201 and 298 K.

Table 5.2: Absorption coefficients of the first overtone band of pure D_2 and pure H_2 at different temperatures.

Gas	Temperature (K)	α_1 ($cm^{-2}amagat^{-2}$) $\times 10^{-5}$	$\widetilde{\alpha}_1$ ($cm^6 s^{-1}$) $\times 10^{-37}$	$\widetilde{\alpha}_1^a$ ($cm^6 s^{-1}$) $\times 10^{-37}$	$\widetilde{\alpha}_1^b$ ($cm^6 s^{-1}$) $\times 10^{-37}$	α_2 ($cm^{-2}amagat^{-3}$) $\times 10^{-9}$	$\widetilde{\alpha}_2$ ($cm^9 s^{-1}$) $\times 10^{-60}$
D_2	77	1.50 ± 0.05^c	1.02 ± 0.03	1.04	1.17	0.73 ± 0.20	0.18 ± 0.09
D_2	201	1.88 ± 0.05	1.28 ± 0.03	1.27	1.24	3.6 ± 1.4	0.91 ± 0.04
D_2	298	1.93 ± 0.03	1.31 ± 0.02	1.18	1.30	9 ± 1	2.2 ± 0.1
D_2	298	2.10 ± 0.07^d	1.43^d	–	–	–	
H_2	77	4.31 ± 0.09^e	2.1^e	–	–	$-.03 \pm 0.3^e$	–
H_2	80	3.5^f	–	–	–	–	–
H_2	201	4.99 ± 0.08^e	2.44^e	–		1.9 ± 0.3^e	–
H_2	295	5.8 ± 0.1^{ef}	2.86^e	–	–	1.2 ± 0.3^a	–
H_2	300	6.2^f	–	–	–	–	–

[a]Experimental results from Ref. [55], the third value at 295 K.
[b]Theoretical calculations from Ref. [55].
[c]The errors quoted are standard deviations.
[d]From Ref. [11].
[e]From Ref. [96].
[f]From Ref. [6].

and the theoretical profiles at 77, 201 and 298 K are shown in Figs. 5.5, 5.6 and 5.7, respectively. It can be seen that the theoretical profiles agree very well with the experimental profiles, and the agreement is better than 97% in the three cases. Figure 5.5 shows the experimental profile of 358 amagat at 77 K which is represented by the circle symbol [55]. The dashed curve represents the computed double-transition quadrupolar components $D_2(v' = 2, J' \leftarrow v = 0, J) + D_2(v' = 0, J' \leftarrow v = 0, J)$, the dot curve represents the computed individual double-transition quadrupolar components $D_2(v' = 1, J' \leftarrow v = 0, J) + D_2(v' = 1, J' \leftarrow v = 0, J)$ and the solid curve is the summation of these, i.e., the total synthetic profile. The average values of the parameters δ_1, δ_2, τ_1 and τ_2 of the line shape function for the best fits for the profiles were determined and are given in Table 5.3. This table shows that the percentage of the contribution of the vibration - vibration transition $(v' = 1 \leftarrow v = 0) + (v' = 1 \leftarrow v = 0)$ of the two colliding molecules increases as the temperature increases, while the percentage of the contribution of the vibration - rotation and vibration - orientation $(v' = 2 \leftarrow v = 0) + (v' = 0 \leftarrow v = 0)$ decreases as the temperature increases. The percentage of the contribution of $X_1(J)+X_1(J)$ to $X_2(J)+X_0(J)$ is 65% to 35%, 69% to 31%, and 72% to 28 % at 77, 201 and 298 K, respectively. Finally Fig. 5.8 shows that δ_1 the halfwidth parameter is proportional to the square root of temperature.

5.4 Conclusions

The observed spectra confirm that the isotropic overlap induction mechanism is absent in the first overtone band of pure D_2 unlike in the CIA spectra of the fundamental band of D_2. They are formed of 267 quadrupolar transitions of the types $X_2(J)+X_0(J)$ and

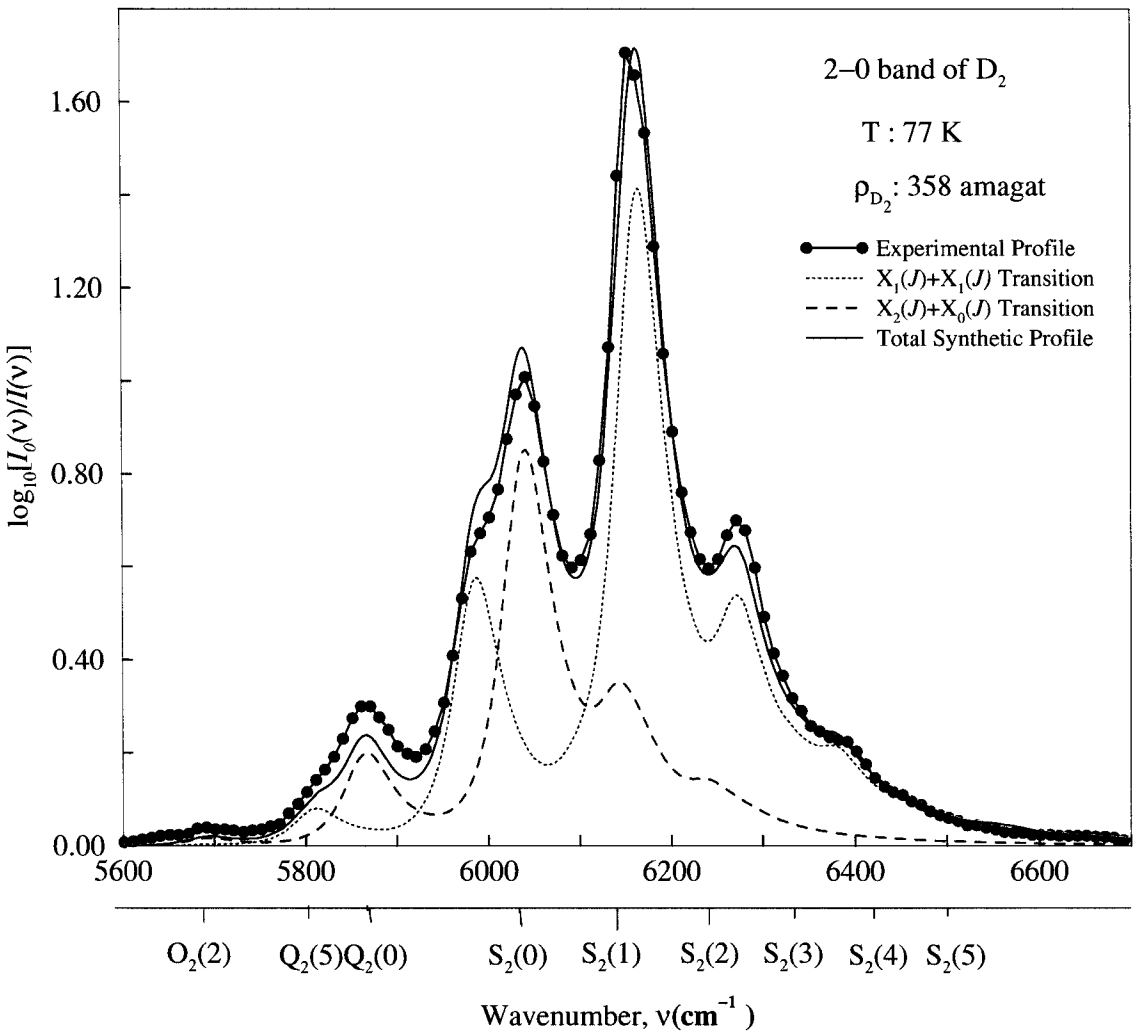

Figure 5.5: Analysis of an enhancement absorption profile of the first overtone band of D_2 at 77 K. The closed circle symbol is the experimental profile from Ref. [55], the dashed curve represents the computed double-transition quadrupolar components $D_2(v' = 2, J' \leftarrow v = 0, J) + D_2(v' = 0, J' \leftarrow v = 0, J)$, the dot curve represents the computed individual double-transition quadrupolar components $D_2(v' = 1, J' \leftarrow v = 0, J) + D_2(v' = 1, J' \leftarrow v = 0, J)$ and the solid line curve is the summation of these i.e. the total synthetic profile.

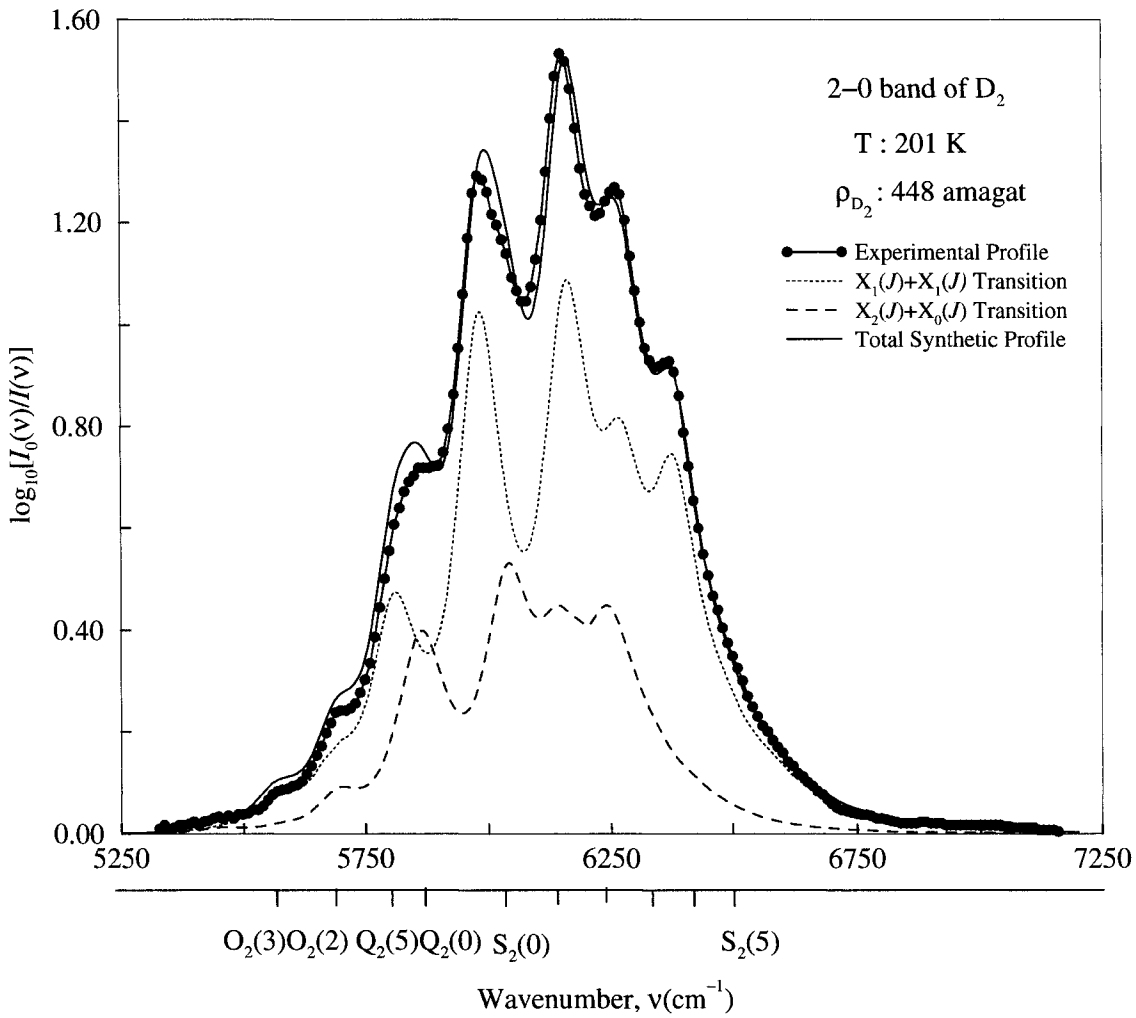

Figure 5.6: Analysis of an enhancement absorption profile of the first overtone band of D_2 at 201 K. The circle symbol is the experimental profile, the dashed curve represents the computed double-transition quadrupolar components $D_2(v' = 2, J' \leftarrow v = 0, J)$ + $D_2(v' = 0, J' \leftarrow v = 0, J)$, the dot curve represents the computed individual double-transition quadrupolar components $D_2(v' = 1, J' \leftarrow v = 0, J)$ + $D_2(v' = 1, J' \leftarrow v = 0, J)$ and the solid line curve is the summation of these i.e. the total synthetic profile.

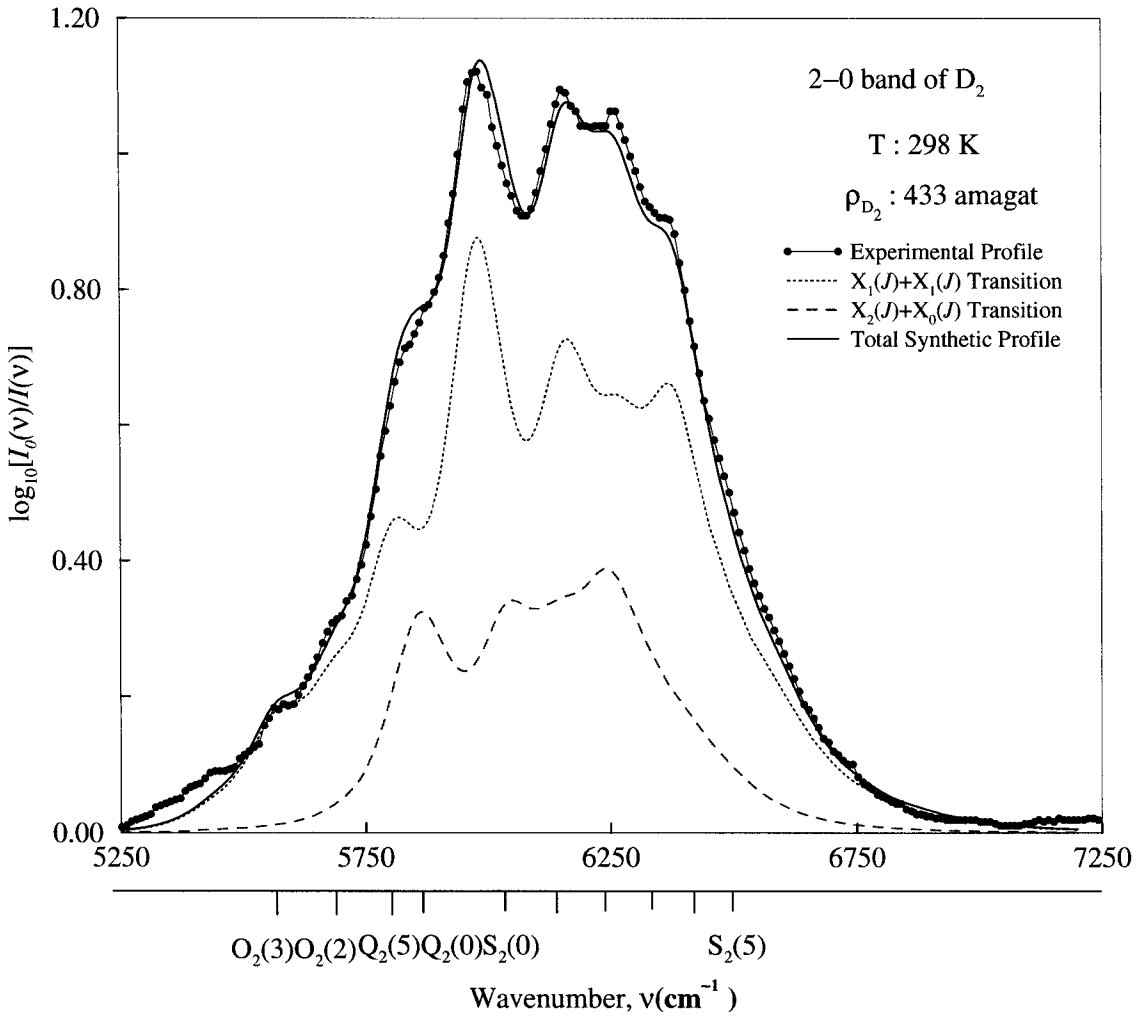

Figure 5.7: Analysis of an enhancement absorption profile of the first overtone band of D_2 at 298 K. The circle symbol is the experimental profile, the dashed curve represents the computed double-transition quadrupolar components $D_2(v' = 2, J' \leftarrow v = 0, J)$ + $D_2(v' = 0, J' \leftarrow v = 0, J)$, the dot curve represents the computed individual double-transition quadrupolar components $D_2(v' = 1, J' \leftarrow v = 0, J)$ + $D_2(v' = 1, J' \leftarrow v = 0, J)$ and the solid line curve is the summation of these i.e. the total synthetic profile.

Table 5.3: Birnbaum-Cohen line shape parameters for the first overtone band of pure D_2 at different temperatures.

Temperature	Transition	Percentage	Number of profiles	δ_1 (cm^{-1})	δ_2 (cm^{-1})	τ_1^a (10^{-14}s)	τ_2^a (10^{-14}s)
77 K	$X_1 + X_1^b$	65	13	33.6 ± 0.8^d	88 ± 5	15.8 ± 0.4	6.0 ± 0.3
	$X_2 + X_0$	35	13				
	theory/exp.^{c}	97	13				
201 K	$X_1 + X_1$	69	16	61 ± 1	150 ± 7	8.7 ± 0.1	3.5 ± 0.2
	$X_2 + X_0$	31	16				
	theory/exp.^{c}	98	16				
298 K	$X_1 + X_1$	72	22	83 ± 2	170 ± 10	6.4 ± 0.2	3.1 ± 0.2
	$X_2 + X_0$	28	22				
	theory/exp.^{c}	99	22				

[a] $\tau_i = 1/(2\pi c\delta_i)$.
[b] X could be O, Q or S transition.
[c] The theoretical to experimental ratio of the fitted area.
[d] The errors listed are standard deviations.

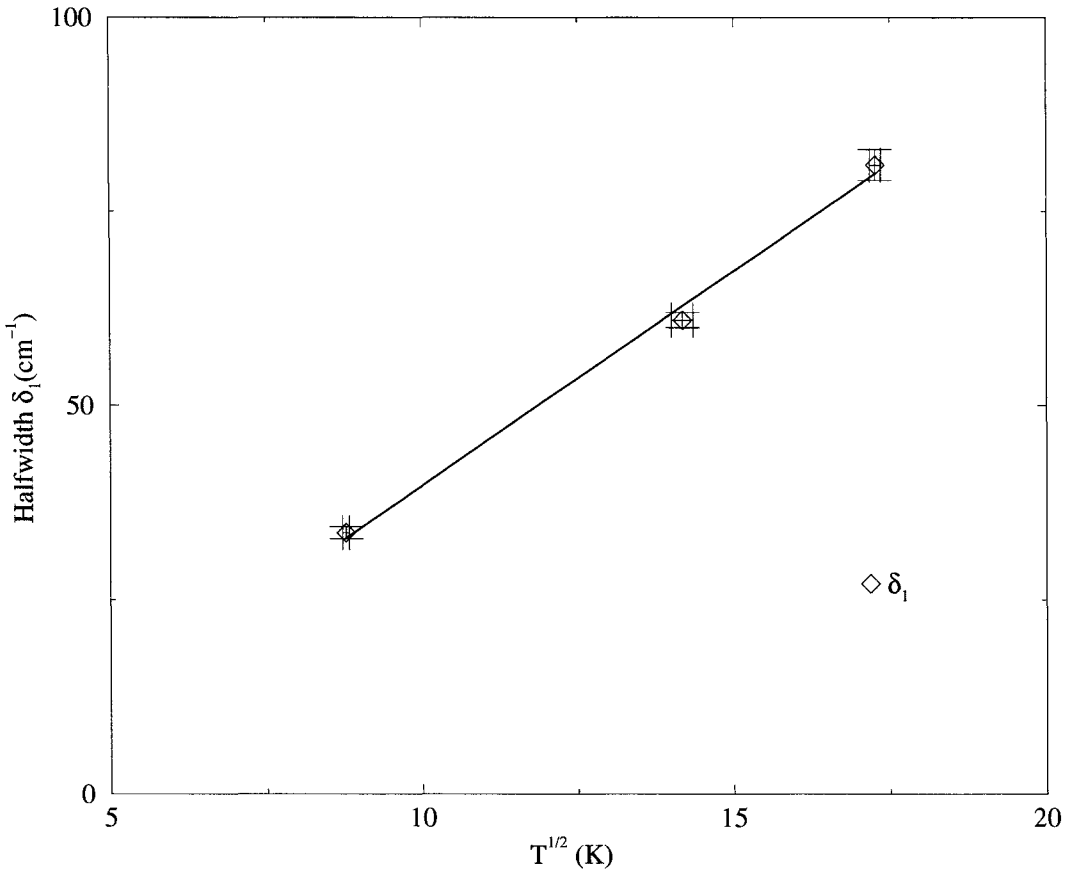

Figure 5.8: A plot of the halfwidth parameter δ_1 (cm^{-1}) versus $\sqrt{T}$. The error bars represent the maximum experimental deviations.

$X_1(J)$+$X_1(J)$, respectively, where X represents $O(\Delta J = J' - J'' = -2)$, $Q(\Delta J = 0)$ or $S(\Delta J = 2)$ transitions, at room temperature. The synthetic profiles agree well with the experimental profiles within 97%. The line shape fitting parameters δ_1, δ_2, τ_1 and τ_2 were determined. The absorption coefficients were determined and the effect of the ternary collisions is found to be smaller than the effect of the binary collisions.

Chapter 6

Analysis of the CIA spectra of the first overtone band of D_2 in D_2-N_2

Enhancement spectra of the CIA in the first overtone region 5000 to 7000 cm^{-1} of D_2 in D_2 - N_2 were studied at 298 K for a base density of D_2 of 73 amagat and for partial densities of N_2 in the range 150 - 370 amagat. The observed spectra were modeled with a total of 1176 components of double vibrational transitions. Binary and ternary absorption coefficients were determined from the integrated absorption of the band. Profile analysis of the spectra was carried out using the BC line shape function for the individual components of the band, and characteristic line shape parameters were determined from the analysis. Good agreement was obtained between the experimental and calculated spectral profiles.

6.1 Introduction

Collision-induced absorption of the fundamental band of gaseous deuterium was studied by Reddy and Cho [8] and Watanabe and Welsh [61]. Soon after, the fundamental and the 1st overtone bands of D_2 and binary mixtures of D_2 with foreign gases were investigated under different experimental conditions by Reddy and co-workers

[9, 11, 12, 15, 62]. The CIA spectrum of D_2 in the pure gas and in D_2-Ar and D_2-N_2 binary mixtures in the first overtone band was investigated also by Reddy et al. [11] who identified the enhancement spectrum of D_2-N_2 as consisting of $Q_2(J)$ of D_2 + $S_0(J)$ of N_2, $Q_1(J)$ of D_2+$Q_1(J)$ of N_2 and $Q_1(J)$ of D_2+$S_1(J)$ of N_2. Recently Varghese et al. [62] studied the fundamental band of D_2 in D_2-N_2 and D_2-CO mixtures.

In the present chapter the CIA spectra of the first overtone band of D_2 in D_2-N_2 mixtures were investigated at room temperature. The calculated spectra consist of 1176 components of double vibrational transitions of D_2 ($\Delta v = 2$) + N_2 ($\Delta v = 0$) and D_2 ($\Delta v = 1$) + N_2 (Δv=1). The Birnbaum-Cohen line shape function was used in the analysis of the absorption profile [30].

6.2 Experimental details

The experimental details were discussed in chapter 2. In this work, a slit width maintained at 60 μm gave a spectral resolution of 12.5 cm^{-1} at 5868 cm^{-1}, the origin of the first overtone band of D_2. Mercury emission lines and water vapour absorption peaks were used for the calibration of the spectral region 5000 - 7000 cm^{-1}. Experiments were carried out with a base density of 73 amagat of D_2, and partial densities of N_2 in the range 151 to 341 amagat. The wave numbers (cm^{-1}) of the quadrupolar transitions were calculated from the molecular constants of D_2 [77] and N_2 [94], Appendix B.

The base density ρ_a of D_2 was obtained from a linear least squares fit to its PVT data given by A. Michels et al. [64], Fig. 2.3. The isothermal data for N_2 was obtained from Michels et al. [67], Fig. 2.4. The partial densities ρ_b of N_2 in binary mixtures were calculated by the interpolation method described by Reddy and Cho

[8], see the previous chapters. The average value of ν for D_2-N_2 overtone band is 5902 $\pm$ 13 cm^{-1}. The normalized Boltzmann factor is

$$P_J = \frac{g_T(2J+1)e^{-E_J/kT}}{\sum_J g_T(2J+1)e^{-E_J/kT}}, \tag{6.2.1}$$

where g_T is the nuclear statistical weight, $g_T = 6$ and 3 for even and odd J for both D_2 and N_2 and E_J is the rotational energy. $\langle|Q|\rangle$, $\langle|\alpha|\rangle$ and $\langle|\gamma|\rangle$ are the matrix elements of the 2^L-pole induction, isotropic and anisotropic polarizability, respectively. These values for D_2 were given by Hunt et al. [84]. The quadrupole and the isotropic polarizability values for N_2 were set to 1.22 ea_0^2 [25] and 11.8 a_0^3 [86], respectively, as the J dependence of quantities are not available.

6.3 Absorption profiles and their analysis

In the present investigation the CIA spectra of the transitions D_2 ($v = 2 \longleftarrow 0$) + N_2 ($\Delta v = 0$) and D_2 ($v = 1 \longleftarrow 0$) + N_2 ($v = 1 \longleftarrow 0$) binary mixtures were recorded at 298 K in the spectral region 5000 - 7000 cm^{-1}. The pure gas N_2 does not exhibit any detected absorption in this region at gas pressures up to 850 atm. Figure 6.1 shows plots of $\log_{10}(I_1(\nu)/I_2(\nu))$ versus the wavenumber $\nu(cm^{-1})$, for three absorption profiles of the first overtone band of D_2 in the D_2-N_2 mixtures at 298 K. The base density of D_2 is 73 amagat with partial densities of N_2 are 234, 300 and 369 amagat. The positions of the transitions $O_2(3)$, $O_2(2)$, $Q_2(5)$ to $Q_2(1)$ and $S_2(0)$ to $S_2(5)$ are marked along the wavenumber axis. The profiles do not show any dip in the Q branch. The main feature is the high peak in the Q region, which results from the combination of all the $Q_2(J)$ transitions, with a resulting weak peak at $S_2(1)$ and a pronounced peak at $S_2(2)$. Equation (3.3.4) can be rewritten by dividing with $\rho_a\rho_b$

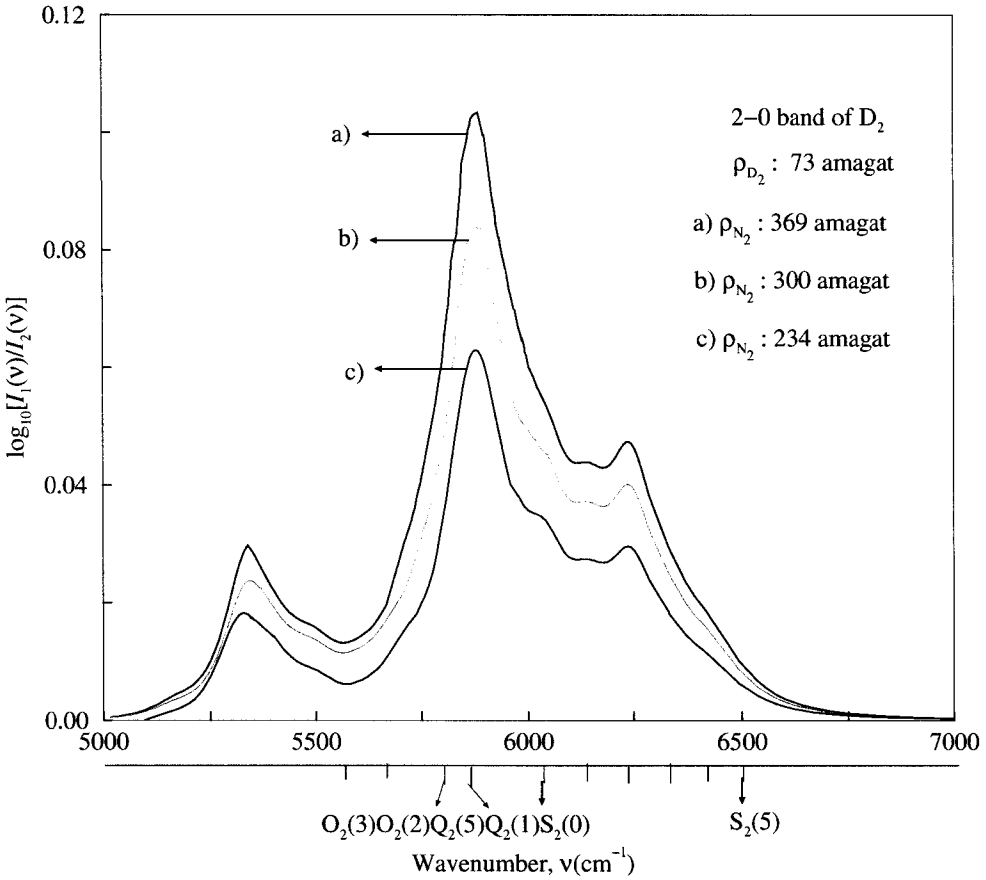

Figure 6.1: Three typical enhancement absorption profiles of the first overtone band of D_2 in D_2-N_2 mixtures at 298 K.

as

$$(1/(\rho_a\rho_b))\int \alpha_{en}(\nu)d\nu = (\alpha_{ab} + \alpha_{2ab}\rho_a) + \alpha_{a2b}\rho_b. \tag{6.3.1}$$

Figure 6.2 shows a plot of $(1/\rho_a\rho_b)\int \alpha_{en}(\nu)d\nu$ versus ρ_b for D_2-N_2 mixtures. The plot gives a straight line, with the intercept representing $\alpha_{ab}+\alpha_{2ab}\rho_a$ and the slope representing the ternary coefficient α_{a2b}. The coefficients α_{ab} and α_{a2b} were determined and listed in Table 6.1, these values agree with the results obtained by Reddy and Kuo [11]. It can be seen that the ternary absorption coefficients are three orders

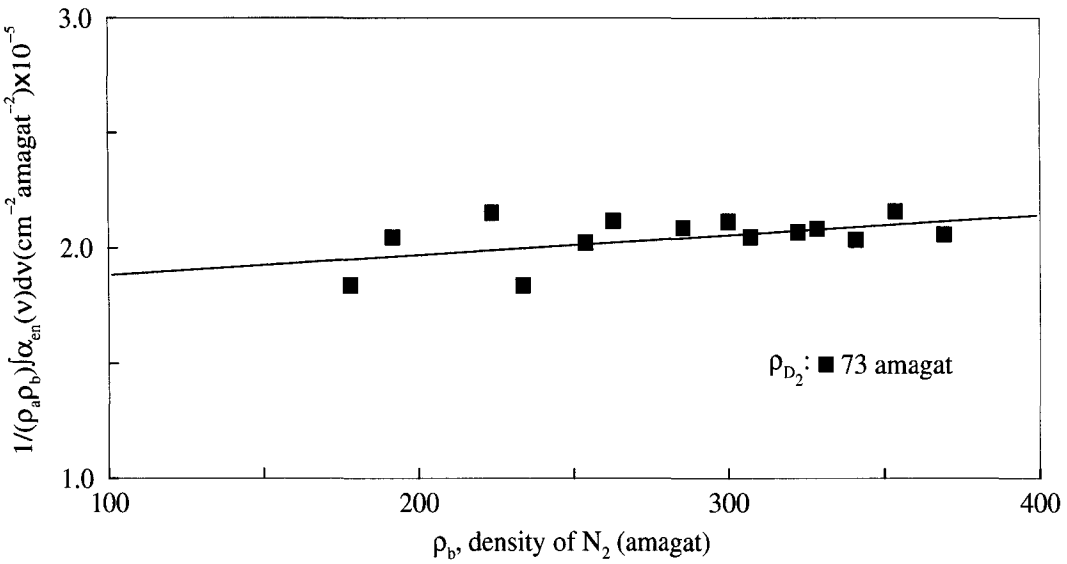

Figure 6.2: Plots of $(1/\rho_a\rho_b)\int\alpha_{en}(\nu)d\nu$ against ρ_b for the first overtone band of D_2 at 298 K in binary mixtures D_2-N_2.

of magnitude smaller compared to the binary absorption coefficients. The possible transitions in the region of study 5000 to 7000 cm^{-1} with considerable intensity (v'=2 $\leftarrow$ v=0) and (v'=1 $\leftarrow$ v=0) are listed in Table 6.2. The corresponding transition intensities calculated using equation (3.4.1) were used in equation (3.5.3) to calculate the fitted profile. An example of the comparison between the experimental and the calculated profile is shown in Fig. 6.3 The total synthetic profile is formed of two major parts and represented by the dot-dashed curve: the first one is the sum of the computed vibrational rotational transition components of $D_2(\Delta v = 2)$ + $N_2(\Delta v = 0)$ and represented by the open-circle symbols. The individual components are $O_2(J)$, $Q_2(J)$ and $S_2(J)$ of D_2 + $O_0(J)$, $Q_0(J)$ and $S_0(J)$ of N_2 and listed in Table 6.2.

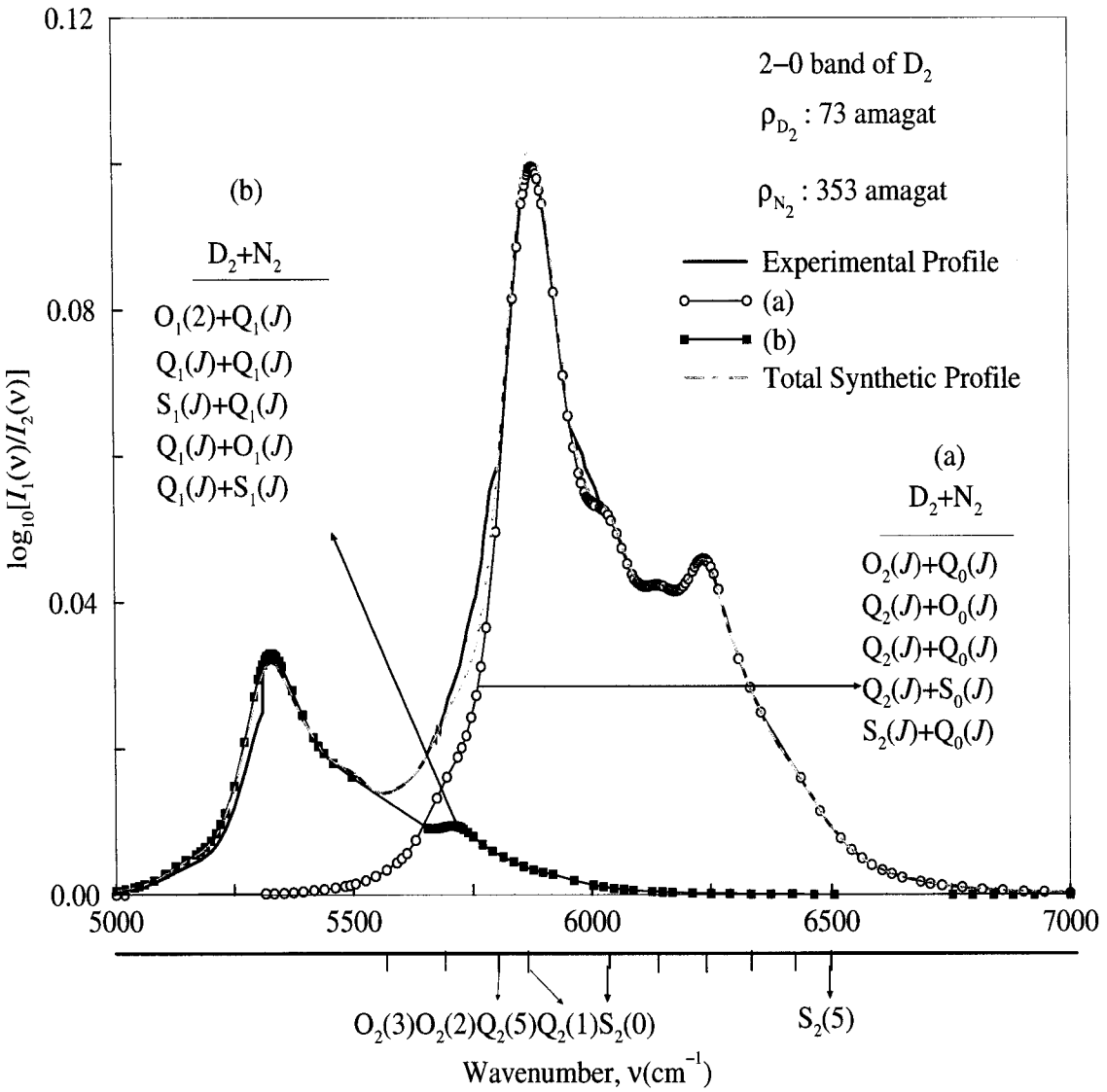

Figure 6.3: Analysis of an enhancement absorption profile of the first overtone band of D_2 in a D_2-N_2 mixture at 298 K. The solid curve is the experimental profile, the open circle symbole curve represents the computed double-transition quadrupolar components $D_2(v = 2, J' \leftarrow v = 0, J) + N_2(v = 0, J' \leftarrow v = 0, J)$, the square symbole curve represents the computed individual double-transition quadrupolar components $D_2(v = 1, J' \leftarrow v = 0, J) + N_2(v = 1, J' \leftarrow v = 0, J)$ and the dashed-dot curve is the summation of these.

Table 6.1: Absorption coefficients of the first overtone band of D_2 in D_2-N_2 binary mixtures at room temperature.

Binary absorption coefficient		Ternary absorption coefficient	
α_{ab} ($cm^{-2}amagat^{-2}$) $\times 10^{-5}$	$\widetilde{\alpha}_{ab}$ ($cm^6 s^{-1}$) $\times 10^{-37}$	α_{a2b} ($cm^{-2}amagat^{-3}$) $\times 10^{-8}$	$\widetilde{\alpha}_{a2b}$ ($cm^9 s^{-1}$) $\times 10^{-60}$
1.9 ± 0.2	1.34 ± 0.11	1.7 ± 0.2	4.45 ± 0.12
1.81 ± 0.07 [11]	1.26 [11]	$< 10^{-7}$ [11]	–

The second part is the sum of the computed double vibrational transition components $O_1(J)$, $Q_1(J)$ and $S_1(J)$ of D_2 + $O_1(J)$, $Q_1(J)$ and $S_1(J)$ of N_2 and represented by the square symbols, the total number of the different transitions which were calculated to give the total theoretical profile is 1176. It can be seen that the synthetic profile fits very well with the experimental profile and the area agrees within 98%. The average values of the parameters δ_1, δ_2, τ_1 and τ_2 of the line shape function for the best fits for profiles were determined and are given in Table 6.3.

6.4 Conclusions

The observed spectra confirm that the isotropic overlap induction mechanism is absent in the first overtone band of D_2 unlike the CIA spectra of the fundamental band of D_2. It is formed from 1176 quadrupolar transitions in the binary mixtures D_2 - N_2. Synthetic profiles agree well with the experimental profiles. The line shape parameters of the BC line shape function δ_1 and δ_2 were determined. The absorption coefficients were calculated and the ternary absorption found to be three orders of magnitude smaller than the binary absorption coefficient.

Table 6.2: The possible quadrupolar transitions of D_2 + N_2 at 298 K.

D_2 + N_2 transition	J of D_2	J of N_2	Number of Components
Double transitions with orientational transitions in N_2 ($O_0(J)$, $Q_0(J)$ and $S_0(J)$)			
$O_2(J) + Q_0(J)$	2 - 3	0 - 25	52
$Q_2(J) + O_0(J)$	1 - 4	2 -25	96
$Q_2(J) + Q_0(J)$	1 - 4	0 - 25	104
$Q_2(J) + S_0(J)$	1 - 4	0 - 25	104
$S_2(J) + S_0(J)$	0 - 5	0 - 25	156
Double vibrational transitions $O_1(J)$, $Q_1(J)$ and $S_1(J)$ of D_2 + $O_1(J)$, $Q_1(J)$ and $S_1(J)$ of N_2			
$O_1(J) + Q_1(J)$	2 - 3	0 - 25	52
$Q_1(J) + Q_1(J)$	0 - 5	0 - 25	156
$S_1(J) + Q_1(J)$	0 - 5	0 - 25	156
$Q_1(J) + O_1(J)$	0 - 5	2 - 25	144
$Q_1(J) + S_1(J)$	0 - 5	0 - 25	156
Total number of transitions			1176

Table 6.3: Birnbaum-Cohen line shape parameters for the first overtone band of D_2 in D_2-N_2 binary mixtures.

Number of mixtures	δ_1 (cm^{-1})	δ_2 (cm^{-1})	τ_1 (10^{-14}s)	τ_2 (10^{-14}s)
16	74 ± 2	178 ± 9	7.2 ± 0.2	3.0 ± 0.2

Chapter 7

Collision-induced first overtone band of D_2 in binary mixtures D_2-X, X = Ar, Kr or Xe

Enhancement spectra of the collision induced absorption in the first overtone region 5500 to 6750 cm^{-1} of D_2 in the D_2-Ar, D_2-Kr and D_2-Xe binary mixtures were studied at 298 K for base densities of D_2 in the range 55 to 251 amagat and for partial densities of Ar, Kr and Xe in the range 46 to 384 amagat. The observed spectra consist of the following quadrupolar transitions: $O_2(3)$, $O_2(2)$, $Q_2(J)$, $J = 1$ to 5 and $S_2(J)$, $J = 0$ to 5 of D_2. Binary and ternary absorption coefficients were determined from the integrated absorption coefficients of the band. Profile analyses of the spectra were carried out using the BC line shape function and characteristic line shape parameters were determined from the analyses.

7.1 Introduction

D_2 and noble gases are not active in the infrared region of the spectrum on their own. However, such molecules give rise to CIA due to transient electric moments induced in them by intermolecular interactions [1]. CIA of the fundamental and

the overtone bands of gaseous D_2 and D_2-foreign gas mixtures were studied at different experimental conditions by Reddy and coworkers [8, 9, 11, 12, 15, 62, 63]. The collision-induced fundamental infrared absorption band of D_2 was studied in D_2-He and D_2-Ar at pressures up to 1200 atm at 298 K [9]. Then, the CIA spectrum of D_2-Ar in the first overtone band was investigated also at room temperature by Reddy et al. [11] who found that the enhancement absorption profiles show only single transition quadrupolar lines $\Delta v = 2 \longleftarrow 0$. Soon after, Russell et al. [12] investigated the collision-induced fundamental band of D_2 in D_2-He and D_2-Ne mixtures at different temperatures. Recently, Varghese et al. [62] investigated the fundamental band of D_2 in D_2-N_2 and D_2-CO mixtures and Abu-Kharma et al. [63] studied the CIA spectra of the first overtone band of D_2 in D_2-N_2 at room temperature. Also, Buontempo et al. [97] studied the induced rototranslational absorption spectra of D_2 dissolved in Ar at 164 K at different densities up to 500 amagat [98]. New measurements and analysis were carried out by the same authors at 165 K and at different densities up to 650 amagat. The rototranslational absorption spectra of D_2 in D_2-He at 92 K were studied at different densities and different D_2 concentrations by Buontempo and Maselli [99].

In the present chapter the CIA spectra of the first overtone band of D_2 in the binary mixtures of D_2-Ar, D_2-Kr or D_2-Xe at room temperature and at different densities were investigated. The BC line shape function was used in the analysis of the absorption profiles. The enhancement spectra consist of double vibrational transitions of $D_2(\Delta v = 2)$+X$(\Delta v = 0)$, where X is Ar, Kr and Xe. The experimental procedure and the analysis of the enhancement profiles used in the present study are similar to those used in the previous chapters. In this study slit widths of 50/60/70 μm were

used, which gave spectral resolutions of 11/12.5/14 cm^{-1} at 5868 cm^{-1}, the origin of the first overtone band of D_2. The calibration of the spectrum in the region 5500 - 6750 cm^{-1} was performed using mercury emission lines and water vapour absorption peaks. Experiments were carried out with base densities of D_2 in the range 55 to 251 amagat, and the partial densities of Ar, Kr and Xe in the range 46 to 303 amagat. A summary of the experimental conditions under which these spectra were recorded is given in Table 7.1. The wavenumbers (cm^{-1}) of the quadrupolar transitions were calculated

Table 7.1: Summary of the experimental conditions, temperature = 298 K, the absorption path length 185.5 cm and slit width of the spectrometer 50 to 70μm.

	Range of partial densities of (amagat)	Base density of D_2 (amagat)
Ar	118 - 303	120
	137 - 242	214
	57 - 227	251
Kr	89 - 357	78
	46 - 384	119
Xe	196 - 244	55
	200 - 235	61
	195 -215	63
	146 - 237	73

from the molecular constants of D_2 [77] (Appendix A.2). The base density ρ_a of D_2 was obtained from a linear least squares fit to the PVT data tabulated by A. Michels et al. [64] (Fig. 2.3). The isothermal data for Ar, Xe were obtained from Michels et al. [69, 71] and the isothermal data for Kr was obtained from Trappeniers et al. [70] (Fig. 2.5). The partial densities ρ_b of Ar, Kr and Xe in binary mixtures were calculated by the interpolation method described by Reddy and Cho [8], see 2.3. Absorption profiles were obtained by plotting $\log_{10}[I_1(\nu)/I_2(\nu)]$ versus $\nu(cm^{-1})$. The areas of the

enhancement absorption profiles give the integrated absorption $\int \alpha_{en}(\nu)d\nu$ for the band. For binary gas mixtures, the absorption coefficient $\alpha_{en}(\nu)$ and the dimensionless absorption coefficient $\widetilde{\alpha}_{en}(\nu)$ are given by equations (3.3.3) and (3.3.7) respectively.

The average value of $\overline{\nu}$ for D_2-Ar, D_2-Kr and D_2-Xe overtone bands were determined to be 6100 ± 9 cm^{-1}, 6079 ± 6 cm^{-1} and 6065 ± 5 cm^{-1}, respectively. Since the corresponding matrix elements for Ar, Kr and Xe were not available, the isotropic polarizability values for Ar/Kr/Xe were set to 11.1/16.8/27.4 a_0^3, respectively [25]. The term Y_{LM} in equation (3.4.2) is equal to zero, and the $\langle|Q|\rangle$ matrix element is zero for each of Ar, Kr and Xe, hence the quantity X_{LM} is given by

$$\begin{aligned} X_{Lm} = P_{J_1}P_{J_2}C(J_1\ L\ J_1';00)^2 < v_1J_1 \mid Q_{L_1} \mid v_1'J_1' >^2 \\ \times C(J_2\ 0\ J_2';00)^2 < v_2J_2 \mid \alpha_2 \mid v_2'J_2' >^2 . \end{aligned} \tag{7.1.1}$$

7.2 Analysis of the absorption profiles

In the present investigation the CIA spectra of the transitions of D_2 ($v = 2 \longleftarrow 0$) + Ar, Kr and Xe ($\Delta v = 0$) in their binary mixtures were recorded at 298 K in the spectral region 5500 - 6750 cm^{-1}. Figure 7.1 shows a plot of $\log_{10}(I_1(\nu)/I_2(\nu))$ versus the wavenumber $\nu(cm^{-1})$, for three absorption profiles of the first overtone band of D_2 in the D_2-Ar mixtures at 298 K. The base density of D_2 is 214 amagat with partial densities of 137, 184 and 241 amagat for Ar. The positions of the transitions $O_2(2)$, $Q_2(5)$ to $Q_2(1)$ and $S_2(0)$ to $S_2(5)$ are shown along the wavenumber axis. The profiles exhibit no dip in the Q branch, unlike in the fundamental band of pure D_2, also there are a number of pronounced peaks at $O_2(2)$ and $S_2(J)$, $J = 0$ to 4, the peak at $Q_2(J)$ is a sum of all the Q transition lines. Similarly, Figs. 7.2 and 7.3 show three profiles for D_2-Kr and D_2-Xe mixtures, and again there is no evidence of

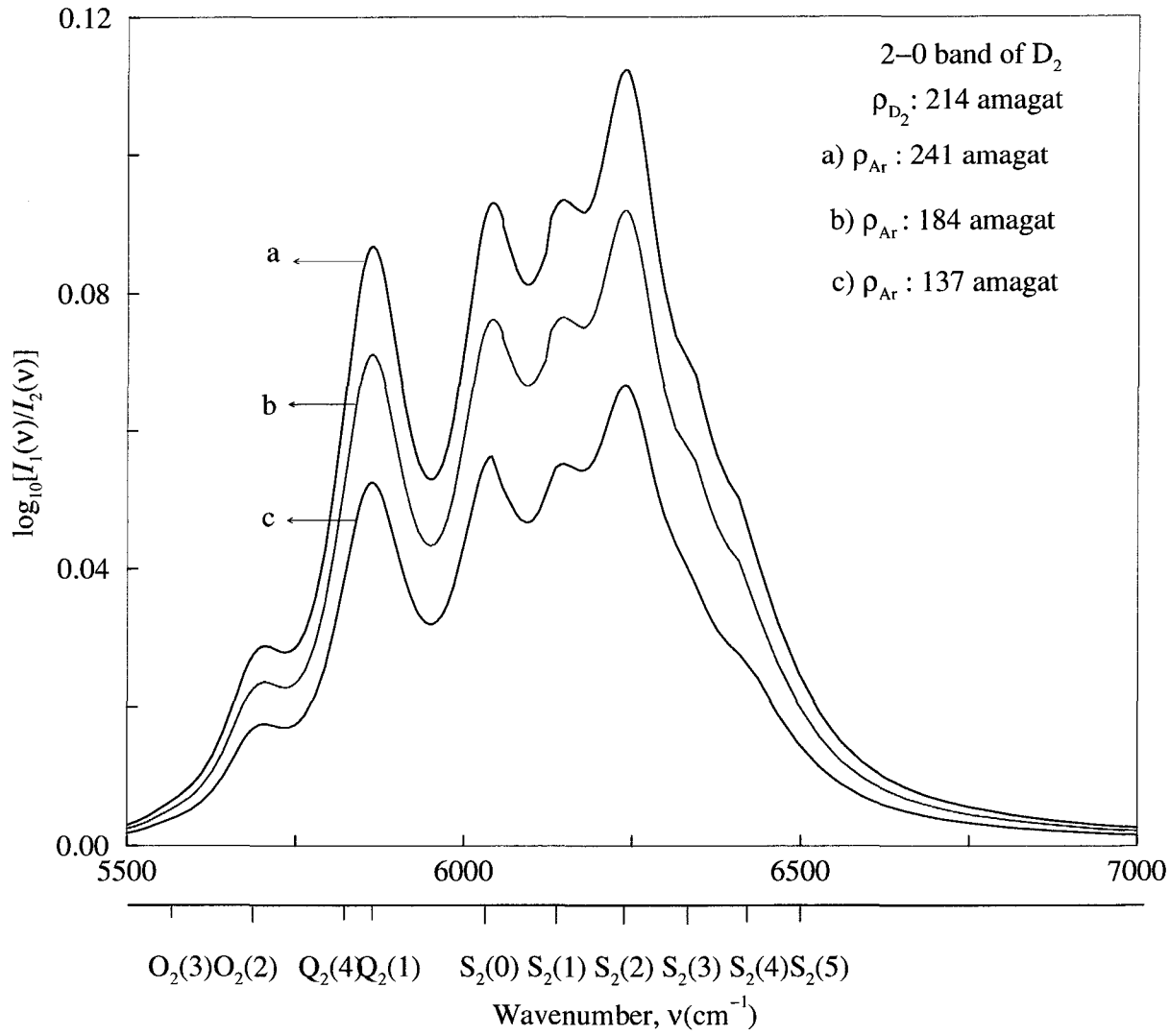

Figure 7.1: Three typical enhancement absorption profiles of the first overtone band of D_2 in D_2-Ar mixtures at 298 K.

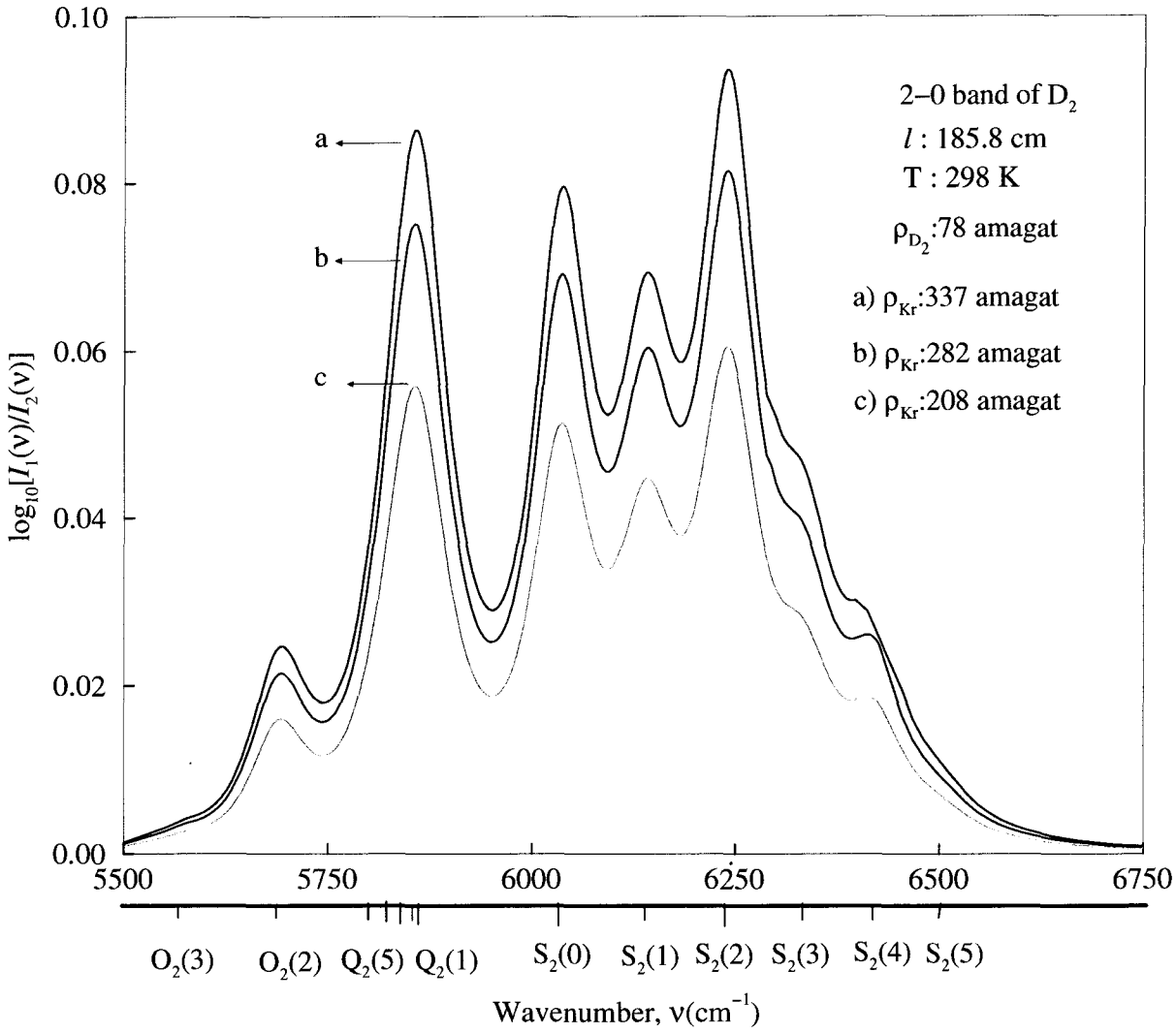

Figure 7.2: Three typical enhancement absorption profiles of the first overtone band of D_2 in D_2-Kr mixtures at 298 K.

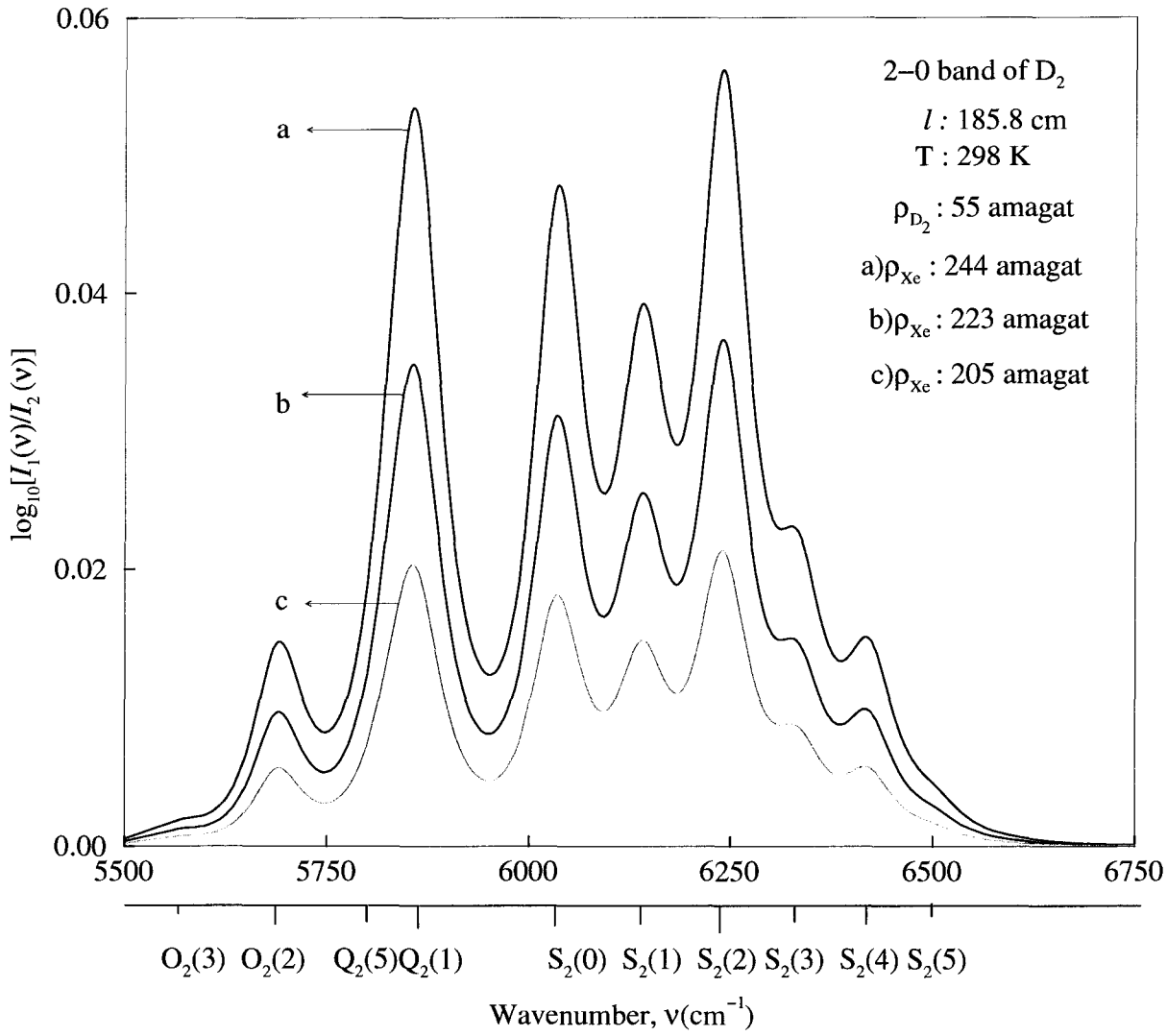

Figure 7.3: Three typical enhancement absorption profiles of the first overtone band of D_2 in D_2-Xe mixtures at 298 K.

any dip in the Q region because of the absence of isotropic overlap induction; the main feature of these curves is the similarity in the peaks, but it is clear that the line width decreases with increasing polarizabilty of the noble gas. Figure 7.4 shows a plot of the calculated values of $(1/\rho_a\rho_b)\int_{band}\alpha_{en}(\nu)d\nu$ versus ρ_b for D_2-Ar, D_2-Kr and D_2-Xe mixtures for different base densities of each. The plots give straight lines in both cases, while in the D_2-Xe mixture gives a quadratic curve. This result is similar to the result obtained by Prasad et al. [57] for the binary mixture H_2-Xe. From equation (3.3.5) the intercept is $\alpha_{ab}+\alpha_{2ab}\rho_a + \alpha_{3ab}\rho_a^2 + \cdots$, the ρ_b factor is $\alpha_{a2b}+ \alpha_{2a2b} + \cdots$ and the ρ_b^2 factor is $\alpha_{a3b} + \cdots$. These coefficients α_{ab}, α_{2ab} and α_{a2b} were determined and listed in Table 7.2; the calculated values compared well with previous results in Ref. [11], for D_2-Ar and D_2-N_2 $\alpha_{ab} = 1.33 \times 10^{-5}$ ($cm^{-2}amagat^{-2}$) and 1.81×10^{-5} ($cm^{-2}amagat^{-2}$), respectively. It is clear from the determined values of the coefficients that the ternary coefficients are very small compared to the binary coefficients. The calculated values of the Boltzmann factor using equation (3.4.7) for D_2 are given in Appendix B.2. The transition intensities for D_2-Ar, D_2-Kr and D_2-Xe for the different lines were calculated using equation (3.4.1) and are listed in Appendix C.1. These values were used in the BC line function to calculate the synthetic profiles which were compared with the experimental profiles in the three cases studied and are given in Figs. 7.5, 7.6 and 7.7. Figure 7.5 shows an enhancement absorption profile of the first overtone band of D_2 in a D_2-Ar mixture at 298 K. The solid curve is the experimental profile, the dashed curves represent the computed individual double-transition quadrupolar components and the dashed-dot curve is the summation of these, i.e. the total synthetic profile. The individual double-transition quadrupolar components used to calculate the theoretical profiles are $O_2(J)$ (J=2 and 3), $Q_2(J)$

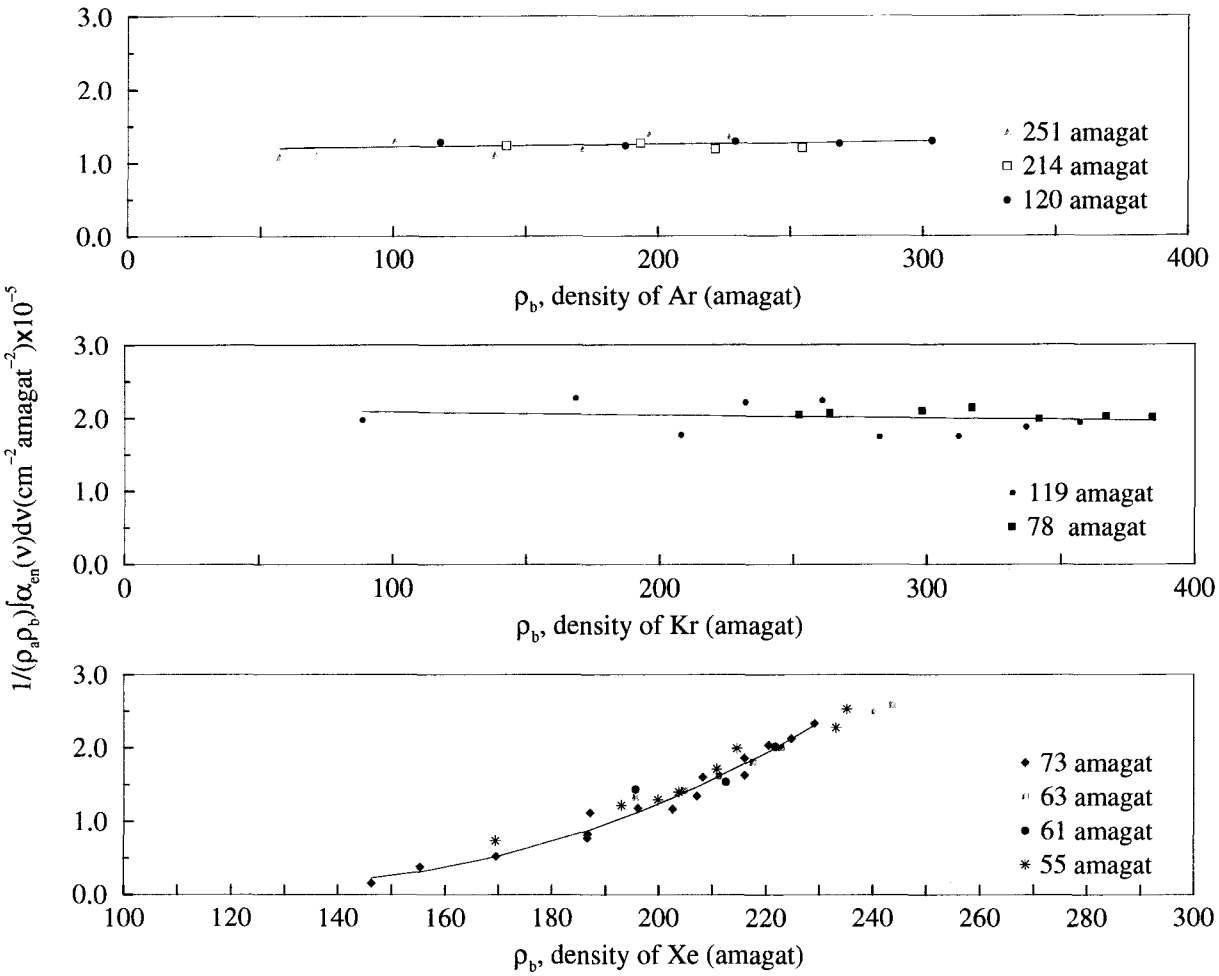

Figure 7.4: Plots of $(1/\rho_a\rho_b)\int \alpha_{en}(\nu)d\nu$ against ρ_b for the first overtone band of D_2 at 298 K in binary mixtures (a) D_2-Ar (b) D_2-Kr and (c) D_2-Xe.

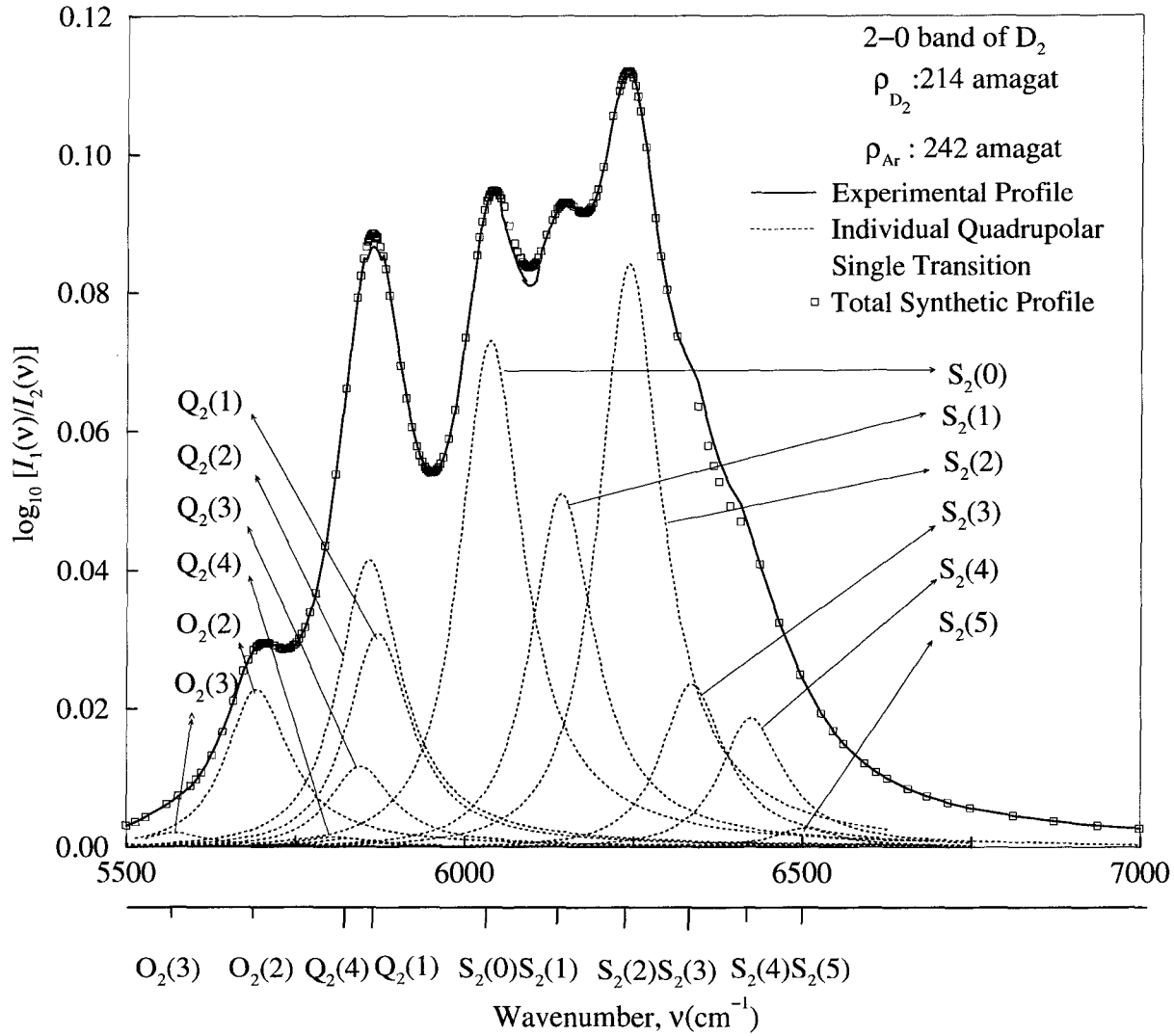

Figure 7.5: Analysis of an enhancement absorption profile of the first overtone band of D_2 in a D_2-Ar mixture at 298 K. The solid curve is the experimental profile, the dashed curves represent the computed individual double-transition quadrupolar components and the dashed-dot curve is the summation of these.

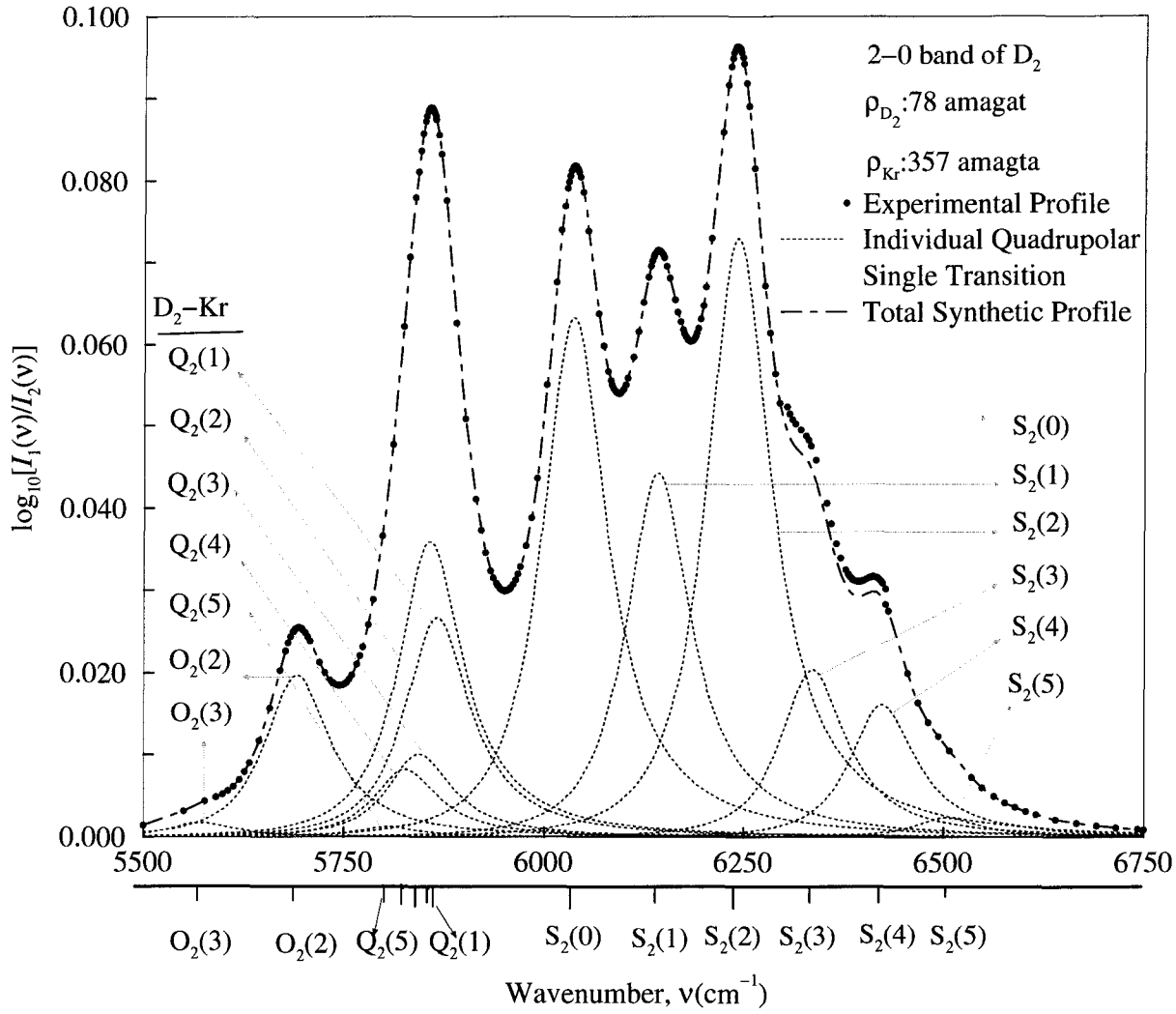

Figure 7.6: Analysis of an enhancement absorption profile of the first overtone band of D_2 in a D_2-Kr mixture at 298 K.

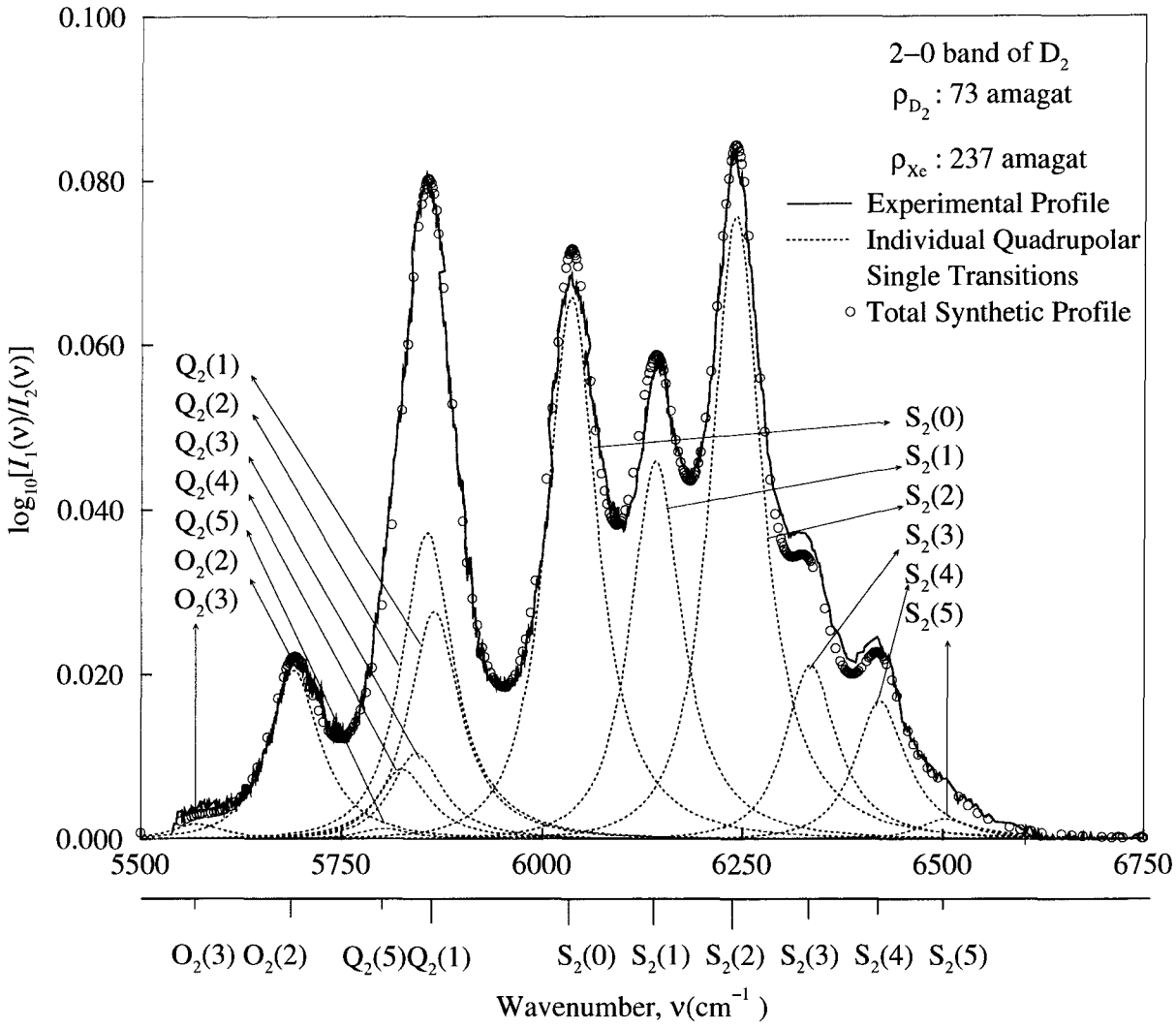

Figure 7.7: Analysis of an enhancement absorption profile of the first overtone band of D_2 in a D_2-Xe mixture at 298 K.

(J=1 to 5)and $S_2(J)$ (J= 0 to 5). It can be seen that the theoretical profiles agree well with the experimental profiles in all the cases studied. The average values of the parameters δ_1, δ_2, τ_1 and τ_2 of the line shape function for the best fits for profiles were determined and listed in Table 7.3, it is clear that δ_i decreases with increasing mass of the colliding molecule.

7.3 Conclusions

The observed spectra arise from quadrupolar transitions in all cases of the binary mixtures D_2-Ar, D_2-Kr and D_2-Xe. The synthetic profiles agree well with the observed profiles; the areas agree within 96%. The line shape fitting parameters δ_1, δ_2, τ_1 and τ_2 were determined and the absorption coefficients were calculated.

Table 7.2: Absorption coefficients of the first overtone band of D_2 in D_2-Ar, D_2-Kr and D_2-Xe binary mixtures at room temperature.

Mixture	α_{ab} ($cm^{-2}amagat^{-2}$) $\times 10^{-5}$	$\widetilde{\alpha}_{ab}$ ($cm^6 s^{-1}$) $\times 10^{-38}$	α_{2ab} ($cm^{-2}amagat^{-3}$) $\times 10^{-9}$	$\widetilde{\alpha}_{2ab}$ ($cm^9 s^{-1}$) $\times 10^{-60}$	α_{a2b} ($cm^{-2}amagat^{-3}$) $\times 10^{-9}$	$\widetilde{\alpha}_{a2b}$ ($cm^9 s^{-1}$) $\times 10^{-60}$
D_2-Ar	1.27 ± 0.13[a]	8.65 ± 0.10	-8.4 ± 0.5	- 2.13 ± 0.06	-4.1± 0.4	-1.04 ± 0.10
D_2-Kr	2.25 ± .11	15.4 ± 0.5	-4.88 ± 0.5	-1.24 ± 0.10	-4.5 ± 0.4	-1.14 ± 0.09
D_2-Xe	4.1 ± 0.4	28.1 ± 1.0	-4.65 ± 0.4	- 1.39 ± 0.08	-5.47 ± 0.45	-1.18 ± 0.09
D_2-N_2	1.9 ± 0.2	1.34 ± 0.11	–	–	17 ± 2	4.45 ± 0.12
H_2-Kr[b]	14.1 ± 1.2	68.9 ± 6	-28.7 ± 4.4	- 52.6 ± 8	-39.6± 7.4	-72.5 ± 1.4
H_2-Xe[b]	15.1 ± 1	74.3 ± 4.7	-22.1 ± 4	-40.5 ± 7.4	-106 ± 7	-194 ± 13

[a]Errors listed are standard deviations.
[b]From Ref. [57]

Table 7.3: Birnbaum-Cohen line shape parameters for the first overtone band of D_2 in D_2-Ar, D_2-Kr and D_2-Xe binary mixtures[a].

Mixture	Number of mixtures	δ_1 (cm^{-1})	δ_2 (cm^{-1})	τ_1^b (10^{-14}s)	τ_2^b (10^{-14}s)
D_2-Ar	15	59 ± 3	268 ± 58	9.0 ± 0.5	2.0 ± 0.4
D_2-Kr	15	46 ± 2	215 ± 33	11.5 ± 5	2.5 ± 0.4
D_2-Xe	35	40 ± 1	101 ± 10	13.3 ± 0.3	5.3 ± 0.5
D_2-N_2	16	74 ± 2	178 ± 9	7.2 ± 0.2	3.0 ± 0.2
H_2-Kr[c]	-	75 ± 4	214.3 ± 0.8	7.1 ± 0.4	2.477 ± 0.9
H_2-Xe[c]	-	72 ± 3	200 ± 3	7.4 ± 0.3	2.65 ± 0.4

[a]Errors listed are standard deviations.
[b]$\tau_i = 1/2\pi c\delta_i$.
[c]From Ref. [57]

Chapter 8

Summary of conclusions

1. The observed spectra confirm that the isotropic overlap induction mechanism is absent in the first overtone band of H_2 and D_2, unlike the CIA spectra of the fundamental bands of these molecules.

2. A total number of 434 quadrupolar transitions contribute to the CIA of the first overtone band of H_2 in each of H_2-N_2 and H_2-CO. Also, the present analysis does not indicate any detectable contribution of the permanent dipole of CO to the electric dipolar induction mechanism in H_2-CO mixtures. The observed spectra of D_2-N_2 binary mixtures were modeled with 1176 components of double vibrational transitions. This number decreases in the case of D_2-D_2 to 267, 214 and 92 for the observed profiles at 298, 201 and 77 K respectively. The binary mixtures D_2-Ar, D_2-Kr and D_2-Xe show only 13 components. Absorption coefficients of the first overtone band of the different mixtures are listed in Table 8.1.

3. The absorption profiles were analyzed using Birnbaum-Cohen line shape function for all the double transitions arising exclusively from the quadrupolar-induction mechanism. The line shape parameters δ_1, δ_2 and the characteristic

Table 8.1: Absorption coefficients of the first overtone band of different mixtures

Mixture	Temperature K	α_{ab} ($cm^{-2}amagat^{-2}$) $\times 10^{-5}$	$\widetilde{\alpha}_{ab}$ ($cm^6 s^{-1}$) $\times 10^{-37}$	α_{2ab} ($cm^{-2}amagat^{-3}$) $\times 10^{-8}$	$\widetilde{\alpha}_{2ab}$ ($cm^9 s^{-1}$) $\times 10^{-60}$	α_{a2b} ($cm^{-2}amagat^{-3}$) $\times 10^{-8}$	$\widetilde{\alpha}_{a2b}$ ($cm^9 s^{-1}$) $\times 10^{-60}$
H_2-N_2	298	6.6 ± 0.3	3.3 ± 0.1	1.9 ± 0.1	3.5 ± 0.1	1.5 ± 0.1	2.8 ± 0.1
H_2-CO	298	9.2 ± 0.5	4.6 ± 0.1	-8.1 ± 0.1	-15.1 ± 0.1	-2.9 ± 0.3	-5.4 ± 0.1
D_2-D_2	77	1.50 ± 0.05	1.02 ± 0.03	0.73 ± 0.20	0.18 ± 0.09		
D_2-D_2	201	1.88 ± 0.05	1.28 ± 0.03	3.6 ± 1.4	0.91 ± 0.04		
D_2-D_2	298	1.93 ± 0.03	1.31 ± 0.02	9 ± 1	2.2 ± 0.1		
D_2-N_2	298	1.9 ± 0.2	1.34 ± 0.11			17 ± 2	4.45 ± 0.12
D_2-Ar	298	1.27 ± 0.13	8.6 ± 0.1	-8.4 ± 0.5	-2.13 ± 0.06	-4.1 ± 0.4	-1.04 ± 0.10
D_2-Kr	298	2.25 ± 0.11	15.4 ± 0.5	-4.88 ± 0.5	-1.24 ± 0.10	-4.5 ± 0.4	-1.14 ± 0.09
D_2-Xe	298	4.1 ± 0.4	28.1 ± 1.0	-4.65 ± 0.4	-1.39 ± 0.08	-5.47 ± 0.45	-1.18 ± 0.09

time τ_1 and τ_2 were determined and are listed in Table 8.2.

Table 8.2: Birnbaum-Cohen line shape parameters for the first overtone band.

Mixture	Temperature K	δ_1 (cm^{-1})	δ_2 (cm^{-1})	τ_1 (10^{-14}s)	τ_2 (10^{-14}s)
H_2-N_2	298	92 ± 4	298 ± 13	5.8 ± 0.3	1.78 ± 0.08
H_2-CO	298	94 ± 3	188 ± 5	5.6 ± 0.2	2.82 ± 0.08
D_2-D_2	77	34 ± 1	88± 5	15.8 ± 0.4	6.0 ± 0.3
D_2-D_2	201	61 ± 1	150 ± 7	8.7 ± 0.1	3.5 ± 0.2
D_2-D_2	298	83 ± 2	170 ± 10	6.4 ± 0.2	3.1 ± 0.2
D_2-N_2	298	74 ± 2	178 ± 9	7.2 ± 0.2	3.0 ± 0.2
D_2-Ar	298	59 ± 3	268 ± 58	9.0 ± 0.5	2.0 ± 0.4
D_2-Kr	298	46 ± 2	215 ± 33	11.5 ± 5	2.5 ± 0.4
D_2-Xe	298	40 ± 1	101 ± 10	13.3 ± 0.3	5.3 ± 0.5

4. It was found that the ternary absorption coefficients are three or four orders of magnitude smaller than the binary absorption coefficients so that their contribution to the absorption band is very small at the densities investigated here.

5. In all the cases studied, the fits between the experimental profiles and the synthetic profiles were in good agreement in the first overtone region.

Appendix A

- Molecular constants

Table A.1: The vibrational constants of H_2, D_2, N_2 and CO respectively.

Constant (cm^{-1})	D_2 [76]	H_2	N_2	CO
ω_e	3115.5	4403.2	2358.57	2169.81358
$\omega_e x_e$	61.82	121.336	14.328	13.28831
$\omega_e y_e$	0.562	0.8129	-0.00226	0.010511
$\omega_e z_e$	-0.02286	-0.00024	5.74×10^{-5}	

Table A.2: Molecular constants used in the calculation of the energy levels of D_2, H_2, N_2 and CO. The constants B_2, D_2 and H_2 in the third line were calculated from the known constants.

v	(cm^{-1})	D_2	H_2	N_2	CO
	B_0	29.9132	59.33451	1.989574	1.92253006
0	D_0	0.01151	4.5651×10^{-2}	0.5764488×10^{-7}	0.612094×10^{-7}
	H_0	6.89×10^{-6}	4.5600×10^{-5}		5.7431×10^{-12}
	B_1	28.8583	56.37420	1.972192	1.90503001
1	D_1	0.01126	4.4050×10^{-2}	0.5573464×10^{-7}	0.612015×10^{-7}
	H_1	6.40×10^{-6}	4.3200×10^{-5}		5.5693×10^{-12}
	B_2	27.7057	53.48200	1.95486	1.88751996
2	D_2	0.01041	4.2800×10^{-2}	0.538294×10^{-7}	0.611972×10^{-7}
	H_2	5.9×10^{-6}	4.0000×10^{-5}		5.3955×10^{-12}

Appendix B

- Vibrational and rotational energies of H_2, D_2, N_2 and CO

Table B.1: The rotational energy levels of H_2 and D_2.

Vibrational Energy Term (cm^{-1})			Rotational energy Term (cm^{-1})		
$G_0(v)$	H_2	D_2	$F_v(J)$	H_2	D_2
$G_0(0)$	0	0	$F_0(1)$	0118.4868	59.7804
			$F_0(2)$	0354.3734	179.066
			$F_0(3)$	0705.5192	357.313
			$F_0(4)$	1168.7948	593.715
			$F_0(5)$	1740.1812	887.223
			$F_0(6)$	2414.9009	1236.56
			$F_0(7)$	3187.5815	1640.26
$G_0(1)$	4161.1685	2993.57	$F_1(1)$	0112.5725	57.6716
			$F_1(2)$	0172.746	336.6687
			$F_1(3)$	0670.2219	344.689
			$F_1(4)$	1110.2096	572.713
			$F_1(5)$	1652.7473	855.788
			$F_1(6)$	2293.2126	1192.66
			$F_1(7)$	3026.4009	1581.88
$G_0(2)$	8087.0049	5867.9	$F_2(1)$	0106.7931	55.3698
			$F_2(2)$	0319.3598	165.861
			$F_2(3)$	0635.6899	330.980
			$F_2(4)$	1052.8400	549.997
			$F_2(5)$	1567.0199	821.961
			$F_2(6)$	2173.7083	1145.71
			$F_2(7)$	2867.7957	1519.91

Table B.2: The possible transitions in the fundamental bands of H_2 and D_2.

Transition	Transition energy (cm^{-1})	
	H_2	D_2
$O_1(2)$	3806.7949	2814.5037
$O_1(3)$	3568.2219	2693.9287
$O_1(4)$	3329.0425	2572.6006
$O_1(5)$	3091.2092	2451.0361
$Q_1(0)$	4161.1685	2993.5701
$Q_1(1)$	4155.2544	2991.4612
$Q_1(2)$	4143.4639	2987.2495
$Q_1(3)$	4125.8711	2980.9463
$Q_1(4)$	4102.5830	2972.5679
$Q_1(5)$	4073.7346	2962.1348
$S_1(0)$	4497.8374	3166.3159
$S_1(1)$	4712.9033	3278.4788
$S_1(2)$	4917.0044	3387.2168
$S_1(3)$	5108.3965	3492.0449
$S_1(4)$	5285.5864	3592.5146
$S_1(5)$	5447.3882	3688.2241

Table B.3: The possible transitions in the first overtone bands of H_2 and D_2.

Transition	Transition energy (cm^{-1})	
	H_2	D_2
$O_2(2)$	7732.6313	5688.8335
$O_2(3)$	7494.0581	5568.2583
$O_2(4)$	7254.8789	5446.9302
$O_2(5)$	7017.0454	5325.3657
$Q_2(0)$	8087.0049	5867.8999
$Q_2(1)$	8075.3110	5863.4893
$Q_2(2)$	8051.9912	5854.6943
$Q_2(3)$	8017.1758	5841.5664
$Q_2(4)$	7971.0498	5824.1816
$Q_2(5)$	7913.8438	5802.6382
$S_2(0)$	8406.3643	6033.7607
$S_2(1)$	8604.2080	6139.0991
$S_2(2)$	8785.4717	6238.8306
$S_2(3)$	8948.5059	6332.5483
$S_2(4)$	9091.9180	6419.8979
$S_2(5)$	9214.6191	6500.5864

Table B.4: The rotational term values (cm^{-1}) in the first and the second vibrational levels of N_2.

$F_{v=0}(J)$	(cm^{-1})	$F_{v=1}(J)$	(cm^{-1})
$F_0(\ 0)$	0.0000	$F_1(\ 0)$	0.0000
$F_0(\ 1)$	3.9791	$F_1(\ 1)$	3.9444
$F_0(\ 2)$	11.9374	$F_1(\ 2)$	11.8331
$F_0(\ 3)$	23.8749	$F_1(\ 3)$	23.6663
$F_0(\ 4)$	39.7915	$F_1(\ 4)$	39.4438
$F_0(\ 5)$	59.6872	$F_1(\ 5)$	59.1657
$F_0(\ 6)$	83.5620	$F_1(\ 6)$	82.8320
$F_0(\ 7)$	111.4160	$F_1(\ 7)$	110.4426
$F_0(\ 8)$	143.2490	$F_1(\ 8)$	141.9975
$F_0(\ 9)$	179.0612	$F_1(\ 9)$	177.4968
$F_0(\ 10)$	218.8524	$F_1(\ 10)$	216.9404
$F_0(\ 11)$	262.6228	$F_1(\ 11)$	260.3284
$F_0(\ 12)$	310.3721	$F_1(\ 12)$	307.6606
$F_0(\ 13)$	362.1006	$F_1(\ 13)$	358.9371
$F_0(\ 14)$	417.8080	$F_1(\ 14)$	414.1579
$F_0(\ 15)$	477.4944	$F_1(\ 15)$	473.3229
$F_0(\ 16)$	541.1599	$F_1(\ 16)$	536.4321
$F_0(\ 17)$	608.8043	$F_1(\ 17)$	603.4855
$F_0(\ 18)$	680.4276	$F_1(\ 18)$	674.4832
$F_0(\ 19)$	756.0298	$F_1(\ 19)$	749.4249
$F_0(\ 20)$	835.6109	$F_1(\ 20)$	828.3109
$F_0(\ 21)$	919.1708	$F_1(\ 21)$	911.1408
$F_0(\ 22)$	1006.7097	$F_1(\ 22)$	997.9149
$F_0(\ 23)$	1098.2273	$F_1(\ 23)$	1088.6331
$F_0(\ 24)$	1193.7236	$F_1(\ 24)$	1183.2952
$F_0(\ 25)$	1293.1987	$F_1(\ 25)$	1281.9012
$F_0(\ 26)$	1396.6525	$F_1(\ 26)$	1384.4513
$F_0(\ 27)$	1504.0850	$F_1(\ 27)$	1490.9453
$F_0(\ 28)$	1615.4961	$F_1(\ 28)$	1601.3832
$F_0(\ 29)$	1730.8857	$F_1(\ 29)$	1715.7649
$F_0(\ 30)$	1850.2539	$F_1(\ 30)$	1834.0905
$F_0(\ 31)$	1973.6006	$F_1(\ 31)$	1956.3596

Table B.5: The rotational term values (cm^{-1}) in the first and the second vibrational levels of CO.

$F_{v=0}(J)$	(cm^{-1})	$F_{v=1}(J)$	(cm^{-1})
$F_0(0)$	0.0000	$F_1(0)$	0.0000
$F_0(1)$	3.8450	$F_1(1)$	3.8100
$F_0(2)$	11.5350	$F_1(2)$	11.4300
$F_0(3)$	23.0695	$F_1(3)$	22.8595
$F_0(4)$	38.4482	$F_1(4)$	38.0982
$F_0(5)$	57.6704	$F_1(5)$	57.1454
$F_0(6)$	80.7355	$F_1(6)$	80.0005
$F_0(7)$	107.6425	$F_1(7)$	106.6625
$F_0(8)$	138.3904	$F_1(8)$	137.1304
$F_0(9)$	172.9781	$F_1(9)$	171.4031
$F_0(10)$	211.4043	$F_1(10)$	209.4793
$F_0(11)$	253.6673	$F_1(11)$	251.3573
$F_0(12)$	299.7658	$F_1(12)$	297.0358
$F_0(13)$	349.6978	$F_1(13)$	346.5128
$F_0(14)$	403.4615	$F_1(14)$	399.7865
$F_0(15)$	461.0548	$F_1(15)$	456.8548
$F_0(16)$	522.4755	$F_1(16)$	517.7155
$F_0(17)$	587.7213	$F_1(17)$	582.3663
$F_0(18)$	656.7897	$F_1(18)$	650.8047
$F_0(19)$	729.6780	$F_1(19)$	723.0280
$F_0(20)$	806.3835	$F_1(20)$	799.0334
$F_0(21)$	886.9032	$F_1(21)$	878.8181
$F_0(22)$	971.2340	$F_1(22)$	962.3790
$F_0(23)$	1059.3728	$F_1(23)$	1049.7128
$F_0(24)$	1151.3160	$F_1(24)$	1140.8160
$F_0(25)$	1247.0604	$F_1(25)$	1235.6853
$F_0(26)$	1346.6022	$F_1(26)$	1334.3170
$F_0(27)$	1449.9374	$F_1(27)$	1436.7073
$F_0(28)$	1557.0623	$F_1(28)$	1542.8522
$F_0(29)$	1667.9727	$F_1(29)$	1652.7476
$F_0(30)$	1782.6644	$F_1(30)$	1766.3892

Appendix C

- Boltzmann factors P_J for H_2, D_2, N_2 and CO

Table C.1: The Boltzmann factors for H_2 and D_2 at 298 K.

Boltzmann factor P_J	H_2	D_2
P_0	0.1296	0.1825
P_1	0.6581	0.2052
P_2	0.1171	0.3845
P_3	0.9022E-01	0.1138
P_4	0.4130E-02	0.9347E-01
P_5	0.9596E-03	0.1385E-01

Table C.2: The Boltzmann factors for D_2 at 77, 201 and 298 K.

P_J	77 K	201 K	298 K
P_0	0.5982	0.2649	0.1825
P_1	0.2937	0.2590	0.2052
P_2	0.1054	0.3676	0.3845
P_3	0.2638E-2	0.7184E-1	0.1138
P_4	0.8186E-4	0.3401E-1	0.9347E-1
P_5	0.2077E-6	0.2543E-2	0.1385E-1

Table C.3: The Boltzmann factors for N_2 and CO at 298 K.

Boltzmann factor P_J	N_2	CO
P_0	0.9570E-02	0.9247E-02
P_1	0.2816E-01	0.2723E-01
P_2	0.4517E-01	0.4373E-01
P_3	0.5969E-01	0.5791E-01
P_4	0.7107E-01	0.6913E-01
P_5	0.7891E-01	0.7700E-01
P_6	0.8311E-01	0.8141E-01
P_7	0.8383E-01	0.8249E-01
P_8	0.8148E-01	0.8059E-01
P_9	0.7661E-01	0.7622E-01
P_{10}	0.6988E-01	0.6998E-01
P_{11}	0.6197E-01	0.6249E-01
P_{12}	0.5350E-01	0.5437E-01
P_{13}	0.4502E-01	0.4614E-01
P_{14}	0.3696E-01	0.3823E-01
P_{15}	0.2963E-01	0.3095E-01
P_{16}	0.2320E-01	0.2449E-01
P_{17}	0.1776E-01	0.1895E-01
P_{18}	0.1330E-01	0.1436E-01
P_{19}	0.9736E-02	0.1064E-01
P_{20}	0.6976E-02	0.7726E-02
P_{21}	0.4893E-02	0.5493E-02
P_{22}	0.3359E-02	0.3826E-02
P_{23}	0.2258E-02	0.2611E-02
P_{24}	0.1487E-02	0.1746E-02
P_{25}	0.9591E-03	0.1145E-02

Appendix D

- Calculated wavenumbers (cm^{-1}) and the corresponding intensities for D_2-X, where X=Ar, Kr and Xe at 298 K

Table D.1: The calculated wavenumbers (cm^{-1}) and the corresponding intensities for D_2-Ar, D_2-Kr and D_2-Xe at 298 K.

Transition	wavenumber (cm^{-1})	D_2Ar	D_2Kr	D_2Xe
$O_2(2)$	688.8335	0.2014E-09	0.4665E-09	0.7746E-09
$O_2(3)$	5568.2588	0.1754E-10	0.4064E-10	0.6747E-10
$Q_2(1)$	5863.4893	0.2725E-09	0.6313E-09	0.1048E-08
$Q_2(2)$	5854.6943	0.3672E-09	0.8505E-09	0.1412E-08
$Q_2(3)$	5841.5664	0.1024E-09	0.2371E-09	0.3937E-09
$Q_2(4)$	5824.1816	0.8295E-10	0.1922E-09	0.3190E-09
$Q_2(5)$	5802.6377	0.1233E-10	0.2857E-10	0.4744E-10
$S_2(0)$	6033.7607	0.6471E-09	0.1499E-08	0.2489E-08
$S_2(1)$	6139.0991	0.4513E-09	0.1046E-08	0.1736E-08
$S_2(2)$	6238.8306	0.7448E-09	0.1725E-08	0.2865E-08
$S_2(3)$	6332.5483	0.2079E-09	0.4817E-09	0.7997E-09
$S_2(4)$	6419.8979	0.1646E-09	0.3813E-09	0.6330E-09
$S_2(5)$	6500.5859	0.2363E-10	0.5527E-10	0.9176E-10

Table D.2: to D.7 The calculated wavenumbers (cm^{-1}) and the corresponding intensities for pure D_2 at 77, 201 and 298 K.

Transition	wavenumber (cm^{-1})	298 K	201 K	77 K
$Q_1(0)+O_1(2)$	5808.0737	0.3036E-10	0.3902E-10	0.2512E-10
$Q_1(1)+O_1(2)$	5805.9648	0.3562E-10	0.3983E-10	0.1287E-10
$Q_1(2)+O_1(2)$	5801.7529	0.6617E-10	0.5603E-10	0.4577E-11
$Q_1(3)+O_1(2)$	5795.4502	0.1964E-10	0.1098E-10	0.1149E-12
$Q_1(4)+O_1(2)$	5787.0718	0.1621E-10	0.5222E-11	
$Q_1(5)+O_1(2)$	5776.6382	0.2417E-11	0.3931E-12	
$Q_1(0)+O_1(3)$	5687.4990	0.1260E-10	0.1069E-10	0.8815E-12
$Q_1(1)+O_1(3)$	5685.3896	0.1478E-10	0.1091E-10	0.4515E-12
$Q_1(2)+O_1(3)$	5681.1782	0.2745E-10	0.1534E-10	0.1606E-12
$Q_1(3)+O_1(3)$	5674.8750	0.8146E-11	0.3006E-11	
$Q_1(4)+O_1(3)$	5666.4971	0.6724E-11	0.1430E-11	
$Q_1(5)+O_1(3)$	5656.0635	0.1003E-11	0.1077E-12	
$Q_1(0)+O_1(4)$	5566.1709	0.1249E-10	0.6107E-11	
$Q_1(1)+O_1(4)$	5564.0615	0.1464E-10	0.6230E-11	
$Q_1(2)+O_1(4)$	5559.8501	0.2721E-10	0.8766E-11	
$Q_1(3)+O_1(4)$	5553.5469	0.8073E-11	0.1717E-11	
$Q_1(4)+O_1(4)$	5545.1689	0.6664E-11	0.8171E-12	
$Q_1(5)+O_1(4)$	5534.7354	0.9940E-12		
$Q_1(0)+O_1(5)$	5444.6060	0.2125E-11	0.5243E-12	
$Q_1(1)+O_1(5)$	5442.4971	0.2491E-11	0.5348E-12	
$Q_1(2)+O_1(5)$	5438.2852	0.4628E-11	0.7525E-12	
$Q_1(3)+O_1(5)$	5431.9824	0.1373E-11	0.1474E-12	
$Q_1(4)+O_1(5)$	5423.6040	0.1134E-11	0.7014E-13	
$Q_1(5)+O_1(5)$	5413.1704	0.1691E-12		
$Q1(1)+Q_1(0)$	5985.0312	0.2325E-10	0.3945E-10	0.1004E-09
$Q_1(2)+Q_1(0)$	5980.8193	0.3120E-10	0.4010E-10	0.2581E-10
$Q_1(3)+Q_1(0)$	5974.5166	0.8644E-11	0.7333E-11	0.6048E-12
$Q_1(4)+Q_1(0)$	5966.1382	0.6933E-11	0.3391E-11	
$Q_1(5)+Q_1(0)$	5955.7046	0.1018E-11	.2512E-12	
$Q1(1)+Q1(1)$	5982.9224	0.5356E-10	0.3953E-10	0.0506E-09
$Q_1(2)+Q1(1)$	5978.7109	0.8594E-10	0.9608E-10	0.3105E-10
$Q_1(3)+Q1(1)$	5972.4072	0.2481E-10	0.1831E-10	0.7580E-12
$Q_1(4)+Q1(1)$	5964.0293	0.2025E-10	0.8614E-11	
$Q_1(5)+Q1(1)$	5953.5957	0.3002E-11	0.6445E-12	

Table D.3:

Transition	wavenumber (cm^{-1}	298 K	201 K	77 K
$Q_1(2)+Q_1(2)$	5974.4990	0.1342E-09	0.05680E-9	0.4642E-11
$Q_1(3)+Q_1(2)$	5968.1958	0.3852E-10	0.2153E-10	0.2254E-12
$Q_1(4)+Q_1(2)$	5959.8174	0.3137E-10	0.1011E-10	
$Q_1(5)+Q_1(2)$	5949.3838	0.4644E-11	0.7552E-12	
$Q_1(3)+Q_1(3)$	5961.8926	0.1104E-10	0.2038E-11	
$Q_1(4)+Q_1(3)$	5953.5146	0.8988E-11	0.1912E-11	
$Q_1(5)+Q_1(3)$	5943.0811	0.1330E-11	0.1428E-12	
$Q_1(4)+Q_1(4)$	5945.1362	0.7313E-11	0.4484E-12	
$Q_1(5)+Q_1(4)$	5934.7026	0.1082E-11		
$Q_1(5)+Q_1(5)$	5924.2690	0.1602E-12		
$S_1(0)+Q_1(0)$	6159.8857	0.4417E-10	0.8615E-10	0.4369E-09
$S_1(1)+Q_1(0)$	6272.0488	0.2669E-10	0.4528E-10	0.1153E-09
$S_1(2)+Q_1(0)$	6380.7871	0.3816E-10	0.4904E-10	0.3157E-10
$S_1(3)+Q_1(0)$	6485.6152	0.9262E-11	0.7857E-11	0.6480E-12
$S_1(4)+Q_1(0)$	6586.0850	0.6379E-11	0.3119E-11	
$S_1(5)+Q_1(0)$	6681.7939	0.7974E-12	0.1968E-12	
$S_1(0)+Q1(1)$	6157.7773	0.5212E-10	0.8844E-10	0.2252E-09
$S_1(1)+Q1(1)$	6269.9399	0.3153E-10	0.4655E-10	0.5949E-10
$S_1(2)+Q1(1)$	6378.6782	0.4516E-10	0.5049E-10	0.1632E-10
$S_1(3)+Q1(1)$	6483.5059	0.1098E-10	0.8105E-11	0.3356E-12
$S_1(4)+Q1(1)$	6583.9761	0.7582E-11	0.3226E-11	
$S_1(5)+Q1(1)$	6679.6855	0.9508E-12	0.2041E-12	
$S_1(0)+Q_1(2)$	6153.5654		0.1242E-09	0.7996E-10
$S_1(1)+Q_1(2)$	6265.7285	0.5846E-10	0.6536E-10	0.2112E-10
$S_1(2)+Q_1(2)$	6374.4668	0.8369E-10	0.7086E-10	0.5789E-11
$S_1(3)+Q_1(2)$	6479.2944	0.2034E-10	0.1137E-10	0.1190E-12
$S_1(4)+Q_1(2)$	6579.7646	0.1403E-10	0.4522E-11	
$S_1(5)+Q_1(2)$	6675.4736		0.2859E-12	
$S_1(0)+Q_1(3)$	6147.2622	0.2868E-10	0.2433E-10	0.2006E-11
$S_1(1)+Q_1(3)$	6259.4248	0.1734E-10	0.1280E-10	0.5299E-12
$S_1(2)+Q_1(3)$	6368.1631	0.2482E-10	0.1387E-10	0.1452E-12
$S_1(3)+Q_1(3)$	6472.9912	0.6033E-11	0.2226E-11	
$S_1(4)+Q_1(3)$	6573.4609	0.4161E-11	0.8852E-12	
$S_1(5)+Q_1(3)$	6669.1704	0.5213E-12		

Table D.4:

Transition	wavenumber (cm^{-1})	298 K	201 K	77 K
$S_1(0)+Q_1(4)$	6138.8838	0.2367E-10	0.1157E-10	
$S_1(1)+Q_1(4)$	6251.0469	0.1431E-10	0.6089E-11	
$S_1(2)+Q_1(4)$	6359.7852	0.2049E-10	0.6601E-11	
$S_1(3)+Q_1(4)$	6464.6133	0.4978E-11	0.1059E-11	
$S_1(4)+Q_1(4)$	6565.0830	0.3434E-11	0.4211E-12	
$S_1(5)+Q_1(4)$	6660.7920	0.4301E-12		
$S_1(0)+Q_1(5)$	6128.4560	0.3529E-11	0.8711E-12	
$S_1(1)+Q_1(5)$	6240.6100	0.2134E-11	0.4582E-12	
$S_1(2)+Q_1(5)$	6349.3515	0.3055E-11	0.4968E-12	
$S_1(3)+Q_1(5)$	6454.1894	0.7424E-12		
$S_1(4)+Q_1(5)$	6554.6594	0.5121E-12		
$S_1(0)+S_1(0)$	6332.6318	0.4713E-11	0.4596E-11	0.2331E-10
$S_1(1)+S_1(0)$	6444.7949	0.2920E-11	0.4955E-11	0.1262E-10
$S_1(2)+S_1(0)$	6553.5332	0.4306E-11	0.5534E-11	0.3562E-11
$S_1(3)+S_1(0)$	6658.3608	0.1084E-11	0.9196E-12	
$S_1(4)+S_1(0)$	6758.8311	0.7806E-12	0.3818E-12	
$S_1(5)+S_1(0)$	6854.5400	0.1031E-12		
$S_1(1)+S_1(1)$	6556.9575	0.1807E-11	0.1334E-11	0.1704E-11
$S_1(2)+S_1(1)$	6665.6958	0.2660E-11	0.2973E-11	0.9608E-12
$S_1(3)+S_1(1)$	6770.5234	0.6682E-12	0.4932E-12	0.1352E-12
$S_1(4)+S_1(1)$	6870.9937	0.4802E-12	0.2043E-12	
$S_1(2)+S_1(2)$	6774.4341	0.3908E-11	0.1655E-11	
$S_1(3)+S_1(2)$	6879.2617	0.9797E-12	0.5476E-12	
$S_1(4)+S_1(2)$	6979.7319	0.7023E-12	0.2263E-12	
$S_1(3)+S_1(3)$	6984.0898	0.2450E-12		
$S_1(4)+S_1(3)$	7084.5596	0.1752E-12		
$S_1(4)+S_1(4)$	7185.0298	0.1248E-12		
$S_1(0)+O_1(2)$	5980.8193	0.2867E-11	0.3685E-11	0.9591E-10
$S_1(1)+O_1(2)$	6092.9824	0.1792E-11	0.2004E-11	0.2533E-10
$S_1(2)+O_1(2)$	6201.7207	0.2670E-11	0.2261E-11	0.6943E-11
$S_1(3)+O_1(2)$	6306.5488	0.6795E-12	0.3798E-12	0.1427E-12
$S_1(4)+O_1(2)$	6407.0186	0.4952E-12	0.1596E-12	

Table D.5:

Transition	wavenumbers (cm^{-1})	298 K	201 K	77 K
$S_1(0)+O_1(3)$	5860.2446	0.1181E-11	0.1002E-11	0.2729E-11
$S_1(1)+O_1(3)$	5972.4072	0.7389E-12	0.5454E-12	0.7210E-12
$S_1(2)+O_1(3)$	6081.1455	0.1101E-11	0.6157E-12	0.1977E-12
$S_1(3)+O_1(3)$	6185.9736	0.2805E-12	0.1035E-12	
$S_1(4)+O_1(3)$	6286.4434	0.2046E-12		
$S_1(0)+O_1(4)$	5617.3516	0.1165E-11	0.5698E-12	
$S_1(1)+O_1(4)$	5851.0791	0.7291E-12	0.3102E-12	
$S_1(2)+O_1(4)$	5959.8174	0.1087E-11		
$S_1(3)+O_1(4)$	6064.6455	0.2771E-12		
$S_1(4)+O_1(4)$	6165.1152	0.2023E-12		
$S_1(0)+O_1(5)$	5617.3516	0.1975E-12		
$S_1(1)+O_1(5)$	5729.5146	0.1236E-12		
$S_1(2)+O_1(5)$	5838.2529	0.1844E-12		
$O_1(2)+O_1(2)$	5801.7529	0.1616E-11	0.0699E-11	0.0571E-12
$O_1(3)+O_1(2)$	5508.4326		0.3785E-12	
$O_1(4)+O_1(2)$	5387.1045		0.2145E-12	
$O_1(3)+O_1(3)$	5387.8574		0.1025E-12	
$O_2(2)+Q_0(J)$	5688.8335	0.1397E-10	0.6850E-10	0.1937E-11
$O_2(3)+Q_0(J)$	5568.2588	0.4869E-11	0.99544E-11	0.5102E-12
$O_2(4)+Q_0(J)$	5446.9307	0.4024E-11	0.98625E-11	
$O_2(5)+Q_0(J)$	5325.3657		0.53501E-12	
$Q_0(J)+Q_2(0)$	5867.8999	1.79111E-11	0.23283E-10	0.3258E-10
$Q_0(J)+S_2(1)$	5863.4893	1.22329E-10	1.45379E-10	1.53394E-10
$Q_0(J)+Q_2(2)$	5854.6943	1.75815E-10	1.57753 E-10	0.41244E-10
$Q_0(J)+Q_2(3)$	5841.5664	4.9791E-11	0.29473E-10	0.9796E-12
$Q_0(J)+Q_2(4)$	5824.1816	4.0592E-11	1.38461E-11	
$Q_0(J)+Q_2(5)$	5802.6377	6.05251E-12	0.10418E-11	
$S_0(0)+Q_2(0)$	6046.9663	0.1300E-10	0.2591E-10	0.1314E-09
$S_0(1)+Q_2(0)$	6165.4326	0.8811E-11	0.1528E-10	0.3889E-10
$S_0(2)+Q_2(0)$	6282.5488	0.1425E-10	0.1871E-10	0.1204E-10
$S_0(3)+Q_2(0)$	6397.8105	0.3941E-11	0.3416E-11	0.2817E-12
$S_0(4)+Q_2(0)$	6510.7466	0.3123E-11	0.1560E-11	
$S_0(5)+Q_2(0)$	6620.9321	0.4542E-12	0.1145E-12	

Table D.6:

Transition	wavenumbers (cm^{-1})	298 K	201 K	77 K
$S_0(0)+S_2(1)$	6042.5557	0.1527E-10	0.2647E-10	0.6740E-10
$S_0(1)+S_2(1)$	6161.0215	0.1035E-10	0.1561E-10	0.1995E-10
$S_0(2)+S_2(1)$	6278.1382	0.1674E-10	0.1912E-10	0.6180E-11
$S_0(3)+S_2(1)$	6393.3994	0.4631E-11	0.3492E-11	0.1446E-12
$S_0(4)+S_2(1)$	6506.3359	0.3671E-11	0.1596E-11	
$S_0(5)+S_2(1)$	6616.5215	0.5340E-12	0.1171E-12	
$S_0(0)+Q_2(2)$	6033.7607	0.2856E-10	0.3749E-10	0.2413E-10
$S_0(1)+Q_2(2)$	6152.2266	0.1936E-10	0.2211E-10	0.7144E-11
$S_0(2)+Q_2(2)$	6269.3433	0.3131E-10	0.2708E-10	0.2213E-11
$S_0(3)+Q_2(2)$	6384.6045	0.8660E-11	0.4945E-11	
$S_0(4)+Q_2(2)$	6497.5410	0.6864E-11	0.2259E-11	
$S_0(5)+Q_2(2)$	6607.7266	0.9984E-12	0.1659E-12	
$S_0(0)+Q_2(3)$	6020.6328	0.8523E-11	0.7387E-11	0.6092E-12
$S_0(1)+Q_2(3)$	6139.0986	0.5777E-11	0.4356E-11	0.1803E-12
$S_0(2)+Q_2(3)$	6256.2153	0.9344E-11	0.5336E-11	
$S_0(3)+Q_2(3)$	6371.4766	0.2585E-11	0.9743E-12	
$S_0(4)+Q_2(3)$	6484.4131	0.2048E-11	0.4451E-12	
$S_0(5)+Q_2(3)$	6594.5986	0.2980E-12		
$S_0(0)+Q_2(4)$	6003.2480	0.7085E-11	0.3540E-11	
$S_0(1)+Q_2(4)$	6121.7139	0.4802E-11	0.2087E-11	
$S_0(2)+Q_2(4)$	6238.8306	0.7767E-11	0.2557E-11	
$S_0(3)+Q_2(4)$	6354.0918	0.2149E-11	0.4669E-12	
$S_0(4)+Q_2(4)$	6467.0283	0.1703E-11	0.2133E-12	
$S_0(5)+Q_2(4)$	6577.2139	0.2477E-12		
$S_0(0)+Q_2(5)$	5981.7041	0.1066E-11	0.2687E-12	
$S_0(1)+Q_2(5)$	6100.1699	0.7223E-12	0.1584E-12	
$S_0(2)+Q_2(5)$	6217.2866	0.1168E-11	0.1941E-12	
$S_0(3)+Q_2(5)$	6332.5479	0.3232E-12		
$S_0(4)+Q_2(5)$	6445.4844	0.2561E-12		
$S_2(0)+Q_0(J)$	6033.7607	2.41802E-10	0.34131E-9	0.74551E-9
$S_2(1)+Q_0(J)$	6139.0991	1.68608E-10	0.20232E-9	0.2271E-9
$S_2(2)+Q_0(J)$	6238.8306	2.7821E-10	0.25282E-9	0.71744E-10
$S_2(3)+Q_0(J)$	6332.5483	7.7656E-11	0.4659E-10	0.16889E-11
$S_2(4)+Q_0(J)$	6419.8979	6.14669E-11	0.21257E-11	
$S_2(5)+Q_0(J)$	6500.5859	8.91160E-12	0.15552E-11	

Table D.7:

Transition	wavenumbers (cm^{-1})	298 K	201 K	77 K
$Q_2(0) + O_0(2)$	5688.8335			0.7133E-11
$Q_2(0) + O_0(3)$	5570.3672			0.1800E-11
$S_2(1) + O_0(2)$	5684.4229			0.7433E-11
$S_2(1) + O_0(3)$	5565.9570			0.1873E-11
$Q_2(2) + O_0(2)$	5675.6279			0.1033E-11
$Q_2(2) + O_0(3)$	5557.1621			0.2633E-11
$Q_2(3) + O_0(2)$	5662.5000			0.2033E-11

Bibliography

[1] H. L. Welsh. Pressure induced absorption spectra of hydrogen. *MTP International Review of Science-Physical Chemistry (A. D. Buckingham and D. A. Ramsay, Eds), Butterworths, London*, 3(1):33–71, 1972.

[2] H. L. Welsh, M. F. Crawford, and J. L. Locke. Infra-red absorption of hydrogen and carbon dioxide induced by intermolecular forces. *Phys. Rev.*, 76:580, 1949.

[3] M. F. Crawford, H. L. Welsh, and J. L. Locke. Infra-red absorption of oxygen and nitrogen induced by intermolecular forces. *Phys. Rev.*, 75:1607, 1949.

[4] M. F. Crawford, H. L. Welsh, J. C. F. MacDonald, and J. L. Locke. Infra-red absorption of hydrogen induced by foreign gases. *Phys. Rev.*, 80:469–470, 1950.

[5] H. L. Welsh, P. E. Pashler, and A. F. Dunn. Influence of foreign gases at high pressures on the infra-red absorption band of methane at 3.3μ. *J. Chem. Phys.*. 19(3):340–343, 1951.

[6] H. L. Welsh, M. F. Crawford, and J. MacDonald. Infra-red absorption of H_2, N_2 and O_2 in the first overtone regions. *Phys. Rev.*, 84:1264, 1951.

[7] D. A. Chisholm and H. L. Welsh. Induced infrared absorption in hydrogen and hydrogen-foreign gas mixtures at pressures up to 1500 atmospheres. *Can. J. Phys.*, 32:291–312, 1954.

[8] S. P. Reddy and C. W. Cho. Induced infrared absorption of nitrogen and nitrogen - foreign gas mixtures. *Can. J. Phys.*, 43:2331–2343, 1965.

[9] S. T. Pai, S. P. Reddy, and C. W. Cho. Induced infrared absorption of deuterium in deuterium-foreign gas mixtures. *Can. J. Phys.*, 44:2893—2903, 1966.

[10] A. Watanabe and H. L. Welsh. Pressure-induced infrared absorption of gaseous hydrogen and deuterium at low temperatures. *Can. J. Phys.*, 45:2859–2871, 1967.

[11] S. P. Reddy and C. Z. Kuo. Collision-induced 1st overtone infrared absorption band of deuterium. *J. Mol. Spectr.*, 37:327–345, 1971.

[12] W. E. Russell, S. P. Reddy, and C. W. Cho. Collision-induced fundamental band of D_2 in D_2-He and D_2-Ne mixtures at different temperatures. *J. Mol. Spectr.*. 52:72–81, 1974.

[13] P. W. Gibbs, C. G. Gray, and J. L. Hunt. New rotational transition in hydrogen molecule. *Phys. Rev. Letters*, 33(5):256–258, 1974.

[14] R. D. G. Prasad, M. J. Clouter, and S. P. Reddy. Observation of U-branch transitions in the infrared fundamental band of solid hydrogen. *Phys. Rev. A*, 17(5):1690–1693, 1978.

[15] R. J. Penney, R. D. G. Prasad, and S. P. Reddy. Collision - induced absorption spectra of the fundamental band of gaseous deuterium: overlap parameters of D_2-D_2 collision pairs. *J. Chem. Phys.*, 77(1):131–141, 1982.

[16] G. Varghese, R. D. G. Prasad, and S. P. Reddy. Absorption spectra of solid para and normal hydrogen in the first overtone region. *Phys. Rev. A*, 35(2):701–707, 1987.

[17] W. F. Hare, E. J. Allin, and H. L. Welsh. Infrared absorption of liquid and solid hydrogen with various ortho-para ratios. *Phys. Rev. Letters*, 99:1887–1888. 1955.

[18] E. J. Allin, W. F. J. Hare, R. E. Jakobsson, and S. MacDonald. Infrared absorption of liquid and solid hydrogen. *Phys. Rev. Letters*, 98:554–555, 1955.

[19] M. L. Oxholm and D. Williams. Infra-red absorption by homonuclear diatomic molecules. *Phys. Rev.*, 76:151–152, 1949.

[20] A. Crane and H. P. Gush. The induced infrared absorption spectrum of solid deuterium and solid hydrogen deuteride. *Can. J. of Phys.*, 44:373–398, 1966.

[21] A R. W. McKellar and M. J. Clouter. Infrared spectra of liquid hydrogen and deuterium. *Can. J. Phys.*, 72:51–55, 1994.

[22] J. van Kranendonk and R. Byron Bird. Pressure-induced absorption i. *Physica*, XVII(11-12):953–967, 1951.

[23] J. van Kranendonk and R. Byron Bird. Pressure-induced absorption ii. *Physica*, XVII(11-12):968–975, 1951.

[24] J. van Kranendonk. Theory of induced infra-red absorption. *Physica*, 23:825–837, 1957.

[25] J. van Kranendonk. Induced infra-red absorption in gases. *Physica*, 24:347–362, 1958.

[26] J. van Kranendonk. Induced infrared absorption in gases. *Physica*, 25:337–342, 1959.

[27] J. van Kranendonk. Intermolecular spectroscopy. *Physica*, 73:156–173, 1974.

[28] J. D. Poll and J. L. Hunt. On the moments of the pressure-induced spectra of gases. *Can. J. Phys.*, 54(5):461–470, 1976.

[29] J. D. Poll. Intermolecular spectroscopy of gases. *in Intermolecular Spectroscopy and Dynamical Properties of Dense Systems, (Proceedings of the International*

School of Physics, Enrico Fermi, Course 75, edited by J. van Kranendonk (North-Holand, New York), pages 45–76, 1980.

[30] G. Birnbaum and E. R.Cohen. Theory of lineshape in pressure induced absorption. *Can. J. Phys.*, 54:593–602, 1976.

[31] G. Birnbaum, B. Guillot, and S. Bratos. Theory of collision-induced line shapes-absorption and light scattering at low density. *Adv. Chem. Phys.*, 51:49–112, 1982.

[32] J. C. Lewis. Intercollisional interference - theory and experiment. *In Phenomena induced by intermolecular interactions, edited by G. Birnbaum*, pages 215–257, 1985.

[33] L. Frommhold. Collision induced absorption in gases. *Cambridge University Press*, 1993.

[34] G. C. Tabisz and M.N. Neuman. Collision- and interacton-induced spectroscopy. *(Kluwer Academic Publishers, Dordrecht)*, 452(NATO ASI Series), 1995.

[35] S. P. Reddy. Induced vibrational absorption in the hydrogens. *In Phenomena induced by intermolecular interactions, edited by G. Birnbaum*, pages 129–167, 1985.

[36] A. Borysow. Collision-induced molecular absorption in stellar atmospheres. *Collision- and interacton-induced spectroscopy Edited by G. C. Tabisz and M.N. Neuman(Kluwer Academic Publishers, Dordrecht)*, 452(Section H. Astrophysics):529–539, 1995.

[37] A. Borysow, U. G. Jorgensen, and C. Zheng. Model atmospheres of cool, low-metallicity stars: the importance of collision-induced absorption. *Astron. Astrophys.*, 324(1):185–195, 1997.

[38] A. Borysow, J. Borysow, and Y. Fu. Semi-emperical model of collision-induced absorption spectra of H_2- H_2 complexes in the second overtone band of hydrogen at temperatures from 50 to 500 K. *Icarus*, 145(2):601–608, 2000.

[39] Y. Fu, C. Zheng, and A. Borysow. First quantum mechanical computations of collision-induced absorption in the second overtone band of hydrogen. *J. Quant. Spect. and Rad. Trans.*, 67(4):303–321, 2000.

[40] A. Borysow. Collision induced absorption coefficients of H_2 pairs at temperatures from 60 K to 1000 K. *Astron. Astrphys.*, 390(2):779–782, 2002.

[41] L. M. Trafton. Induced spectra in planetary atmospheres. *Collision- and interacton-induced spectroscopy Edited by G. C. Tabisz and M.N. Neuman(Kluwer Academic Publishers, Dordrecht)*, 452(Section H. Astrophysics):517–528, 1995.

[42] L. M. Trafton. Planetary atmospheres: The role of collision-induced absorption. *Molecular Complexes in Earth's Planetary, Cometary, and Interstellar Atmospheres, Edited by A. A. Vigasin and Z. P. Slanina (World Scientific, Singapore)*, Chap. 6:177–193, 1998.

[43] C. Brodbeck, J-P. Bouanich, van Thanh Nguyen, Y. Fu, and A. Borysow. Gas phase dynamics and structure: spectroscopy, molecular interactions, scattering, and photochemistry - collision-induced absorption by H_2 pairs in the second overtone band at 298 and 77.5 K: Comparison between experimental and theoretical results. *J. of Chem. Phys.*, 110(10):4750–4757, 1999.

[44] C. Brodbeck, J-P. Bouanich, van Thanh Nguyen, and A. Borysow. The binary collision-induced second overtone band of gaseous hydrogen: modelling and laboratory measurements. *Planetary and Space Science*, 47(10):1285–1291, 1999.

[45] M. Gustafsson, L. Frommhold, D. Bailly, J. Bouanich, and C. Brodbeck. Infrared spectra of liquid hydrogen and deuterium. *J. Chem. Phys.*, 119(23):12264–1227, 2003.

[46] A R. W. McKellar. High resolution infrared spectra of H_2-Kr and D_2-Kr van der Waals complexes. *J. Chem. Phys.*, 122:84320_1–84320_5, 2005.

[47] A R. W. McKellar. Infrared spectra of CO_2-H_2 complexes. *J. Chem. Phys.*, 122:174313_1–174313_6, 2005.

[48] W. F. Hare and H. L. Welsh. Pressure-induced infrared absorption of hydrogen and hydrogen-foreign gas mixtures in the range 1500-5000 atmospheres. *Can. J. Phys.*, 36:88–103, 1958.

[49] A. R. W. McKellar and H. L. Welsh. Collsion-induced absorption spectra of hydrogen in the first and second overtone regions with applications to planetary atmospheres. *Proc. Roy. Soc. Lond. A.*, 322:421–434, 1971.

[50] A. Watanabe, J. L. Hunt, and H. L. Welsh. Structure of the pressure-induced infrared spectrum of hydrogen in the first overtone region. *Can. J. Phys.*, 49:860–863, 1971.

[51] A. Watanabe. Pressure-induced infrared absorption of gaseous hydrogen and deuterium at low temperatures. iii. further analysis of the fundamental and first overtone bands of hydrogen. *Can. J. Phys.*, 49:1320–1326, 1971.

[52] P. M. Silvaggio, D. Goorvitch, and R. W. Boese. Investigation of the 2-0 pressure-induced vibrational absorption spectrum of hydrogen at temperatures below ambient. *J. Qauntum Spectrosc. Radiat. Transfer*, 26:103, 1981.

[53] S. P. Reddy, G. Varghese, and R. D. G. Prasad. Overlap parameters of $H_2 - H_2$, molecular pairs from the absorption spectra of the collision - induced fundamental band of H_2,. *Phys. Rev. A*, 15(3):975–984, 1977.

[54] A. Sen, R. D. G. Prasad, and S. P. Reddy. Quadrupole double transitions $S_1(J)+S_0(J)$ in the infrared fundamental band of molecular hydrogen at 77 K. *J. Chem. Phys.*, 72(3):1716–1721, 1979.

[55] P. G. Gillard. Ph.D. Thesis. *Memorial Unversity of Newfoundland*, 1983.

[56] S. Paddi Reddy and Fan Xiang an G. Varghese. Observations of the new triple transitions $Q_1(J_1)+Q_1(J_2)+Q_1(J_3)$ in molecular hydrogen in its second overtone region. *Phys. Rev. Letters*, 74(3):367–370, 1995.

[57] R. D. G. Prasad, P. G. Gillard, and S. P. Reddy. Collision-induced first overtone band of H_2 in H_2-Kr and H_2-Xe mixtures. *J. Chem. Phys.*, 107(13):4906–4910, 1997.

[58] C. Stamp and S. Paddi Reddy. Collision-induced first overtone band of hydrogen at 77 K, 201 K and 295 K. *Private Communication*, 2005.

[59] A. R. W. McKellar. The collision-induced first-overtone band of hydrogen at low temperature. *Can. J. Phys.*, 66(000):155–158, 1987.

[60] A R. W. McKellar. High resolution infrared spectra of H_2-Ar, HD-Ar, and D_2-Ar van der Waals complexes between 160 and 8620 cm^{-1}. *J. Chem. Phys.*, 105(7):2628–2638, 1996.

[61] A. Watanabe and H. L. Welsh. Pressure-induced infrared absorption of gaseous hydrogen and deuterium at low temperatures. *Can. J. Phys.*, 43:818–828, 1965.

[62] G. Varghese, C. Stamp, and S. P. Reddy. Collision-induced fundamental band of D_2 in D_2 and D_2-CO mixtures. *J. Quant. Spect. Rad. Transfer*, 87:387–397, 2004.

[63] M. Abu-Kharma, G. Varghese, and S. P. Reddy. Analysis of the CIA spectra of the first overtone band of D_2 in D_2-N_2. *J. Mol. Spect.*, 232(2):369–375, 2005.

[64] A. Michels, W. De Graff, T. Wassenaar, J. N. H. Levett, and P. Louwerse. Compressibility isotherms of hydrogen and deuterium at temperatures between -175°C and 150°C (at densities up to 960 amagat). *Physica*, 25(1):25–42, 1959.

[65] A. Michels and M. Goudeket. Compressibility of deuterium between 0°C and 150°C up to 3000 atmospheres. *Physica*, VIII(3):353–360, 1941.

[66] W. F. J. Hare. Ph. D. Thesis. *University of Toronto*, page 13, 1955.

[67] A. Michels, R. J. Lunbeck, and G. J. Wolkers. Thermodynamical properties of nitrogen as function of density and temperatures between -125°C and 150°C and densities up to 760 amagat. *Physica*, 17(9):801–816, 1951.

[68] J. G. Hust and R. B. Stewart. Thermodynamic property values for gaseous and liquid carbon monoxide from 70 to 300 K with pressures to 300 atmospheres. *NBS, Technical Note*, 202(30):1–109, 1963.

[69] A. Michels, R. J. Lunbeck, and G. J. Wolkers. Thermodynamical properties of argon as function of density and temperature between 0 and 150°C and densities to 640 amagat. *Physica*, 15(8-9):689–695, 1949.

[70] N. J. Trappeniers, T. Wassenaar, and G. J. Wolkers. Isotherms and thermodynamic properties of krypton at temperatures between 0° and 150°C and at densities up to 620 amagat. *Physica*, 32:1503–1520, 1966.

[71] A. Michels, T. Wassenaar, and P. Louwerse. Isotherms of xenon at temperatures between 0°C, and 150°C, and at densities up to 515 amagats. *Physica*, 20:99–106, 1954.

[72] A. N. Zaidel, V. K. Prokofer, S. M. Raisku, V. A. Slavnyi, and E. Ya. Shreider. Tables of spectral lines. *(IFI/Plenum, New York-London)*, 1970.

[73] E. K. Plyler, N. M. Gailer, and T. A. Wiggins. The calibration of infrared prism spectrometers. *J. Res. Natl Bur. Standards*, 48(3):221–227, 1952.

[74] A. R. Downie, M. C. Magoon, T. Purcell, and B. Crawford. The calibration of infrared prism spectrometers. *J. Opt. Soc.*, 43(11):941–951, 1953.

[75] C. Stamp. M. Sc. Thesis. *Memorial Unversity of Newfoundland*, 1999.

[76] A. R. W. McKellar and T. Oka. A study of the electric quadrupole fundamental band of D_2 using an infrared difference frequency laser system. *Can. J. Phys.*, 56:1315–1320, 1978.

[77] K. P. Huber and G. Herzberg. Molecular spectra and molecular structure. *Constants of Diatomic Molecules, van Nostrand Reinhold Company*, 4:240–253, 1979.

[78] M. Mizushima. A theory of pressure absorption. *Phys. Rev.*, 76:1268–1269, 1949.

[79] M. Mizushima. On the infra-red absorption of the hydrogen molecule. *Phys. Rev.*, 77:150–151, 1950.

[80] F. R. Britton and M. F. Crawford. The theory of collision-induced absorption in hydrogen and deuterium. *Can. J. Phys.*, 36:825–837, 1958.

[81] J. D. Poll and J. L. Hunt. On the moments of the pressure-induced spectra of gases. *Can. J. Phys.*, 39:189–204, 1961.

[82] G. Karl, J. D. Poll, and L. Wolniewicz. Multipole moments of the hydrogen molecule. *Can. J. Phys.*, 53(19):1781–1790, 1975.

[83] J. D. Poll, J. L. Hunt, and J. W. Mactaggart. Intercollisional interference in the S lines of H_2-He mixtures. *Can. J. Phys.*, 53:954–961, 1975.

[84] J. L. Hunt, J. D. Poll, and L. Wolniewicz. Ab initio calculation of properties of the neutral diatomic hydrogen molecules H_2, HD, D_2, DT, and T_2. *Can. J. Phys.*, 62:1719–1723, 1984.

[85] R. M. Hill and W. V. Smith. Microwave collision diameters and associated quadrupole moments. *Phys. Rev.*, 82:451, 1951.

[86] A. J. Bridge and A. D. Buckingham. Polaization of laser light scattered by gases. *J. Chem. Phys.*, 40:2733–2734, 1964.

[87] J. O. Hirschfelder, C. F. Curtiss, and R. B. Bird. Molecular theory of gases and liquids. *John Wiley and Sons Inc., New York*, 1954.

[88] P. Dore, A. Borysow, and L. Frommhold. Roto-translational far-infrared absorption spectra of H_2 - N_2 pairs. *J. Chem.Phys.*, 84(9):5211–5213, 1986.

[89] P. Codastefano and P. Dore. Far-infrared absorption of N_2 - H_2 gaseous mixtures. *J. Quant. Spect.. Rad. Trans.*, 36(5):445–452, 1986.

[90] A R. W. McKellar. Low-temperature infrared absorption of gaseous N_2 and N_2 + H_2 in the 2.0-2.5μm region: Application to the atmospheres of Titan and Triton,. *ICARUS*, 80:361–369, 1989.

[91] C. Stamp, R. D. G. Prasad, P. G. Gillard, and S. P. Reddy. Analysis of the collision-induced absorption spectra of double vibrational transitions in H_2-N_2. *(CP467, Spectral Line Shapes: 14 ICSLS, edited by R. M. Herman)*, 10:453–456, 1998.

[92] J. Boissoles, C. Boulet, R. H. Tipping, and Q. Ma. New experimental measurements and theoretical analysis of the collision induced absorption in N_2 - H_2 pairs. *J. Quant. Spect. Rad. Transfer*, 95(4):489–498, 2005.

[93] S. L. Bragg, J. W. Brault, and W. H. Smith. Line positions and strengths in the H_2 quadrupole spectrum. *Astrophysical J.*, 263:999–1004, 1982.

[94] A. Lofthus and P. Krupenie. The spectrum of molecular nitrogen. *J. Phy. Chem. Ref. Data*, 6:113–307, 1977.

[95] R. D. McCarty, J. Hord, and H. M. Roder. Selected properties of hydrogen. *Natl. Bur. Standards Monograph*, 168:0, 1981.

[96] E. van Nostrand. M. Sc. Thesis,. *Memorial Unversity of Newfound Land*, 1983.

[97] U. Buontempo, P. Codastefano, S. Cunsolo, P. Dore, and P. Maselli. New analysis of the density effects observed on the rotational line profile of induced spectra of H_2 and D_2 dissolved in argon. *Can. J. Phys.*, 61:156–163, 1983.

[98] U. Buontempo, P. Codastefano, S. Cunsolo, P. Dore, and P. Maselli. Density effects on the rotational lines of D_2 in D_2-Ar, mixtures. *Can. J. Phys.*, 59:1495–1498, 1981.

[99] U. Buontempo and P. Maselli. Far infrared spectra of the D_2 and the D_2-He systems. *J. Mol. Liquids*, 32:161–172, 1986.